The copyright of this thesis vests in the author. No quotation from it or information derived from it is to be published without full acknowledgement of the source. The thesis is to be used for private study or non-commercial research purposes only.

Published by the University of Cape Town (UCT) in terms of the non-exclusive license granted to UCT by the author.

University of Cape Town

Multivariable Controller Design Using Pareto Front

Thesis presented for the degree of Master of Science
in the Department of Electrical Engineering
University of Cape Town
South Africa

by

Ka Wing Ho
August, 2011

University of Cape Town

DECLARATION

I, Ka Wing Ho (HxxKAx002) hereby declare that all the work that is presented in this thesis is my own.

Any information that was gathered from alternative sources has been referenced accordingly.

_____
Ka Wing Ho (HxxKAx002)
31 August 2011

University of Cape Town

Acknowledgments

I would like to acknowledge the following people who have guided and supported me through this thesis:

• To Professor Martin Braae for all his guidance, positive criticism and always inspiring me to do my best.

• To my best friends Chris Cecchini and Thabo Koetje who has helped and supported me to complete this thesis.

University of Cape Town

Abstract

An existing multivariable, thermal system with two inputs and two outputs is investigated. Its inputs are a pair of heaters controlled by a computer while its outputs are temperatures measured by two sensors.

A lumped parameter model is used to approximate the thermal system adequately. The system is multivariable and fully interactive so two different controlling structures can be used to ensure that the temperatures track their respective set-points. Both are multivariable controllers though one has a diagonal structure while the other has a triangular structure, namely a SISO controller and a MIMO controller respectively.

In order to analyze the two controllers, six different cost functions are used to compare either the performance or the interaction against the cost of inputs in order to quantify the efficiency of the controller under evaluation.

The overall cost function of the MIMO controller is consistently better than that of the SISO controller so the conclusion from the multi-objective optimization, based on priori decision-making, indicates that the MIMO system is best.

Multi-objective optimization with a posteriori decision-making is critical for producing effective engineering designs since it provides the engineer with invaluable insight into the problem under investigation and its proposed solutions. For high dimensional problems it becomes difficult to overcome this problem Pareto efficiency, level diagrams, binary hyper volumes and other performance indices are used to compare quantitatively the two controller structures, when applied to a highly interactive multivariable system based at this thermal plant.

The result of using binary hyper volumes makes it difficult to interpret or compare the system. To overcome this, the concept of Centroid is proposed and demonstrated. It is recommended to explore Centroid further.

University of Cape Town

Table of Contents

University of Cape Town

University of Cape Town

List of Figures

List of Tables

Nomenclature

$J_{u_i r_j}$ - The cost function of the input u_i of loop i due to a change of the setpoint r_j in loop j.

$J_{e_i r_j}$ - The cost function of the error e_i of loop i due to a change of the setpoint r_j in loop j.

$e(t)_{i_{r_j}}$ - The error $e(t)_i$ of loop i due to a change of the setpoint r_j in loop j.

$u(t)_{i_{r_j}}$ - The input $u(t)_i$ of loop i due to a change of the setpoint r_j in loop j.

$u_{0_{i_{r_j}}}$ - The initial value of the input $u(0)_i$ of loop i due to a change of the setpoint r_j in loop j.

J_e - The cost function of the error.

J_u - The cost function of the cost of input.

$e(s)$ - Errors of the system.

$u(s)$ - Inputs of the system.

$y(s)$ - Outputs of the system.

θ - The input or decision vector.

Ω - The decision space.

$J(\theta)$ - The cost or objective vector.

A_{ij} - The gain of loop i due to a change of the setpoint r_j in loop j.

ΔY_i - Changes of output of loop i.

ΔU_j - Changes of input of loop i.

T_{ij} - The time constant of loop i due to a change of the setpoint r_j in loop j.

University of Cape Town

Chapter 1
Introduction

1.1 SUBJECT OF THIS INVESTIGATION

Many methods have been developed over decades to design control systems for a wide variety of dynamic processes. Generally each new method addresses a need or difficulty with the existing methods. As a simple example, the frequency response method, like Nyquist plots, can address dead-time systems with ease while pole-zero methods like the Root Locus diagram resort to Pade approximations that may or may not be adequate. Often comparisons of different control systems found in the literature make use of visual inspection of the step response data leading to a qualitative rather than a quantitative conclusion as to whether and by how much a given method improves on another [Moore 2010] [Graebe 1994].

This thesis investigates ways of using Pareto efficiency to determine if one controller works better than another one, when both controllers are applied to the same system.

1.2 BACKGROUND TO THE INVESTIGATION

Systems with many inputs, u(t), and many outputs, y(t), are classified as multivariable control systems. In some cases the interactions between loops are severe resulting in a truly multivariable problem (as compared to a multiple variable one). In such instances the overall multivariable control problem cannot simply be split into a set of simpler, single-variable control problems without due attention being given to the degree of interaction present in the plant dynamics. The extent of the interaction can be gauged by Gershgorin bands based on Direct or Indirect Nyquist Plots that lead to one method for designing multivariable control systems [Rosenbrock 1974].

Such interactive multivariable plants can be modeled by transfer function matrices, as shown in Eq.(1.1) below:

$$y(s) = G(s)u(s) \tag{1.1}$$

where y(s) are the outputs, u(s) are the inputs and matrix G(s) contains the transfer function models.

University of Cape Town

A plant with two inputs and two outputs would have the form, shown in Eq.(1.2) below:

$$\begin{pmatrix} y_1(s) \\ y_2(s) \end{pmatrix} = \begin{pmatrix} g_{11}(s) & g_{12}(s) \\ g_{21}(s) & g_{22}(s) \end{pmatrix} \begin{pmatrix} u_1(s) \\ u_2(s) \end{pmatrix} \tag{1.2}$$

The individual matrix elements are Single Input and Single Output (SISO) transfer functions; consisting of the ratio of two polynomials which allow for a dead-time term, as shown in Eq.(1.3) below:

$$g_{ij} = \frac{b_0 + b_1 s + b_2 s^2 + \cdots + b_m s^m}{a_0 + a_1 s + a_2 s^2 + \cdots + a_n s^n} e^{-s\tau} \tag{1.3}$$

Control systems for multivariable systems with dynamics that are formulated as transfer function matrices can be produced by a number of design methods [Maciejowski 1989]. The method based on Nyquist arrays proposed by Rosenbrock [1974] splits the problem into two stages. First the interaction between the loops in the plant is minimized with the design of a decoupling precompensator $k_{21}(s)$. This results in a multiple variable compensated system that could then be controlled by individual SISO control laws, as shown in Fig 1.1 below where w_1 and w_2 are the inputs to the decoupling precompensator ($k_{21}(s)$):

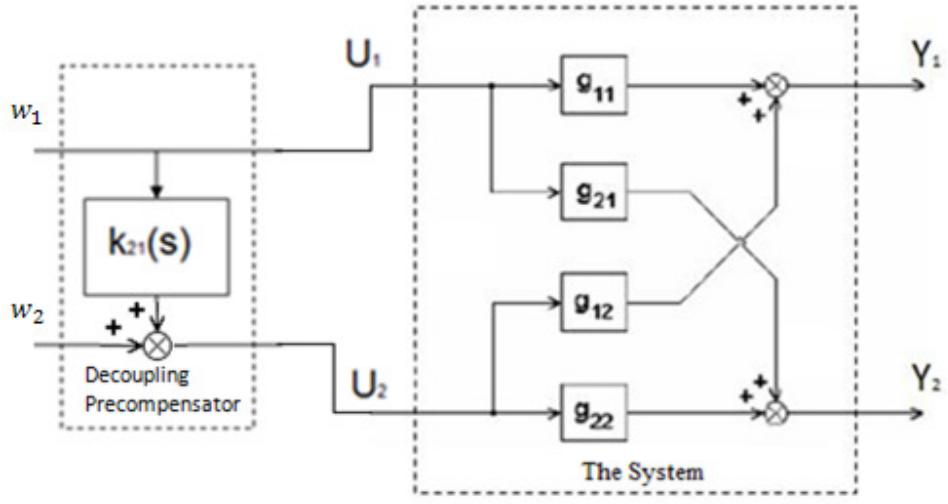

Fig 1.1 Block Diagram of the Compensated System

University of Cape Town

In essence the requirement that each output of the plant track and its individual setpoint with minimal interaction from adjustments to other setpoints necessitates the decoupled closed loop transfer function model. In Fig 1.2, e_1 and e_2 are the error signals derived from the setpoints and the outputs In a one-degree of freedom control loop as shown in Fig 1.2 this means that the open loop transfer function model Q(s) must be diagonally dominant and hence that the precompensator $k_{21}(s)$ must include a decoupling function.

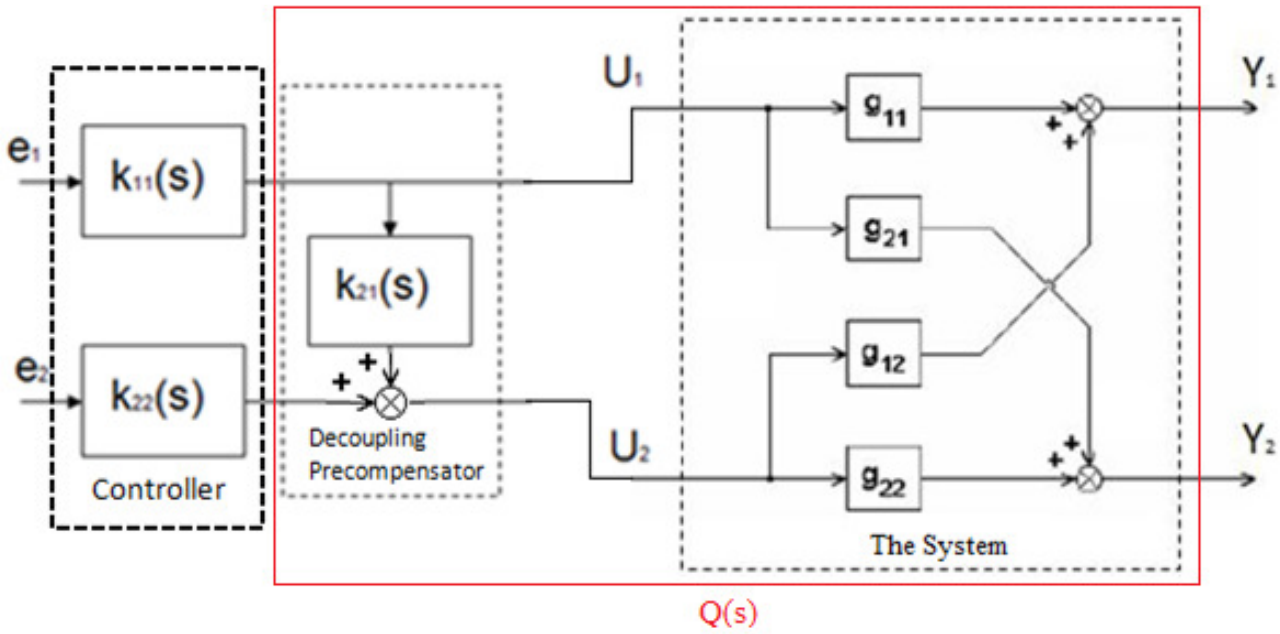

Fig 1.2 Block Diagram of the Plant Showing Q(s)

Even after thirty years of use, this approach is still applied [Hamane et al. 2010] and it was noted that the necessary decoupling provided by the precompensator leads to reduced gains in the subsequent SISO control laws and hence, by extrapolation, to the sub-optimal performance of such loops.

The main focus of this thesis is to use the modern methods of multi-objective optimization (MOO) with a posteriori decision making, to quantify the degradation in performance when a decoupling compensator is included in a Multi input and Multi output (MIMO) control loop. Specifically Pareto fronts based on well known cost functions are used to evaluate the relative performance of a decoupled or MIMO control law and a simpler coupled or SISO control law.

In this thesis a MIMO fan heating system will be used, as shown in Fig 1.3:

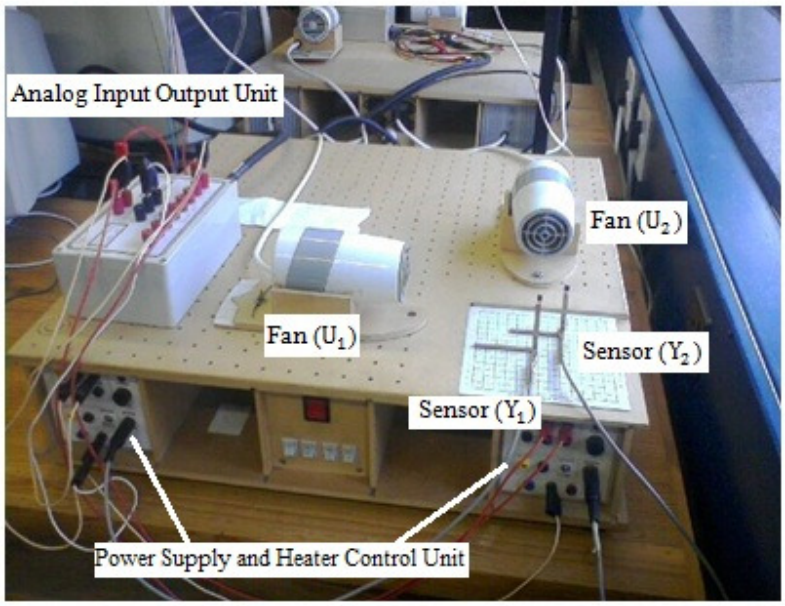

Fig 1.3 The MIMO Fan Heating System

The position of the sensors and the heaters are shown in Fig 1.4 below:

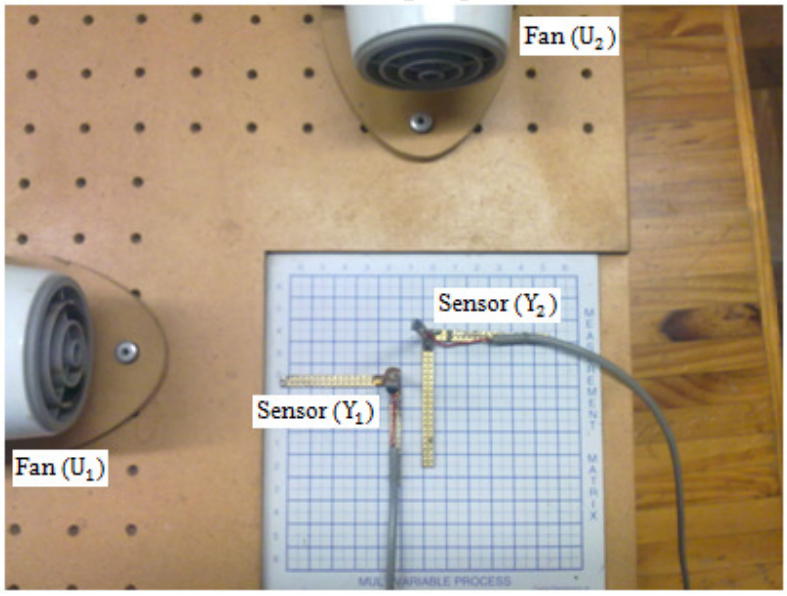

Fig 1.4 Position of Sensors and Heaters

This system has a block diagram as shown below in Fig 1.5:

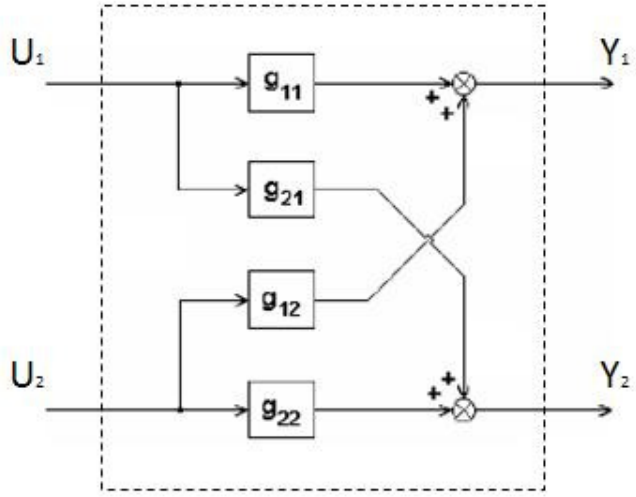

Fig 1.5 Block Diagram of the System

Where the MIMO transfer functions are in the following format, as shown in Eq. (1.4) below:

$$G(s) = \begin{pmatrix} g_{11} & g_{12} \\ g_{21} & g_{22} \end{pmatrix} = \begin{pmatrix} \frac{A_{11}}{1+sT_{11}} & \frac{A_{12}}{1+sT_{12}} \\ \frac{A_{21}}{1+sT_{21}} & \frac{A_{22}}{1+sT_{22}} \end{pmatrix} \quad (1.4)$$

Two types of controllers are applied to this system, one with a decoupling precompensator and one without. In both cases two SISO controllers of PI form will be used since these are commonly encountered in industrial applications. These have two changing variables, K_{ij} and I_{ij}, in each of the elements of the matrix.

The transfer function of the SISO controller is given in Eq.(1.5) below:

$$K(s) = \begin{pmatrix} k_{11} & 0 \\ 0 & k_{22} \end{pmatrix} = \begin{pmatrix} \frac{K_{11}(1+sI_{11})}{sI_{11}} & 0 \\ 0 & \frac{K_{22}(1+sI_{22})}{sI_{22}} \end{pmatrix} \quad (1.5)$$

University of Cape Town

The block diagram of the SISO controller is shown in Fig 1.6 below:

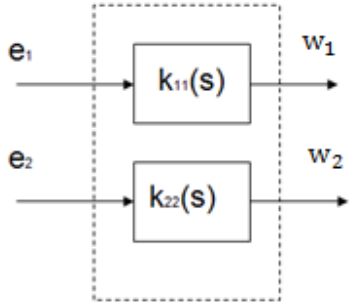

Fig 1.6 Block Diagram of the SISO Controller

The transfer function matrix for the decoupling precompensator is given, as shown in Eq.(1.6) below:

$$\begin{pmatrix} 1 & 0 \\ k_{21} & 1 \end{pmatrix} = \begin{pmatrix} 1 & 0 \\ -\frac{g_{21}}{g_{22}} & 1 \end{pmatrix} \tag{1.6}$$

The block diagram for the decoupling precompensator is shown in Fig 1.7:

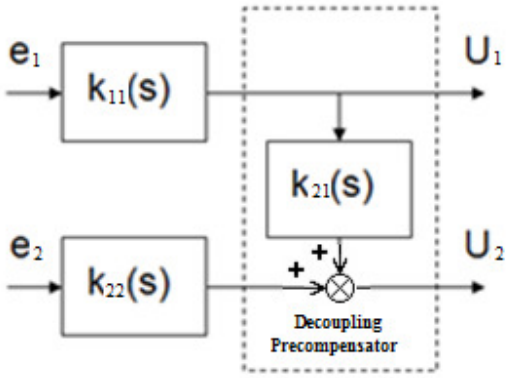

Fig 1.7 Block Diagram of the Decoupling Precompensator

where the error signals, e_1 and e_2, are the differences between the desired temperature, r_1 and r_2, and the measured temperature, y_1 and y_2.

University of Cape Town

The transfer function of the MIMO controller is given by:

$$K(s) = \begin{pmatrix} 1 & 0 \\ k_{21} & 1 \end{pmatrix} \begin{pmatrix} k_{11} & 0 \\ 0 & k_{22} \end{pmatrix} = \begin{pmatrix} \frac{K_{11}(1+sI_{11})}{sI_{11}} & 0 \\ \frac{-A_{21}K_{11}[1+(T_{22}+I_{11})s+T_{22}I_{11}s^2]}{A_{22}I_{11}(s+T_{21}s^2)} & \frac{K_{22}(1+sI_{22})}{sI_{22}} \end{pmatrix} \quad (1.7)$$

The block diagrams of the MIMO controllers are shown below in Fig 1.8:

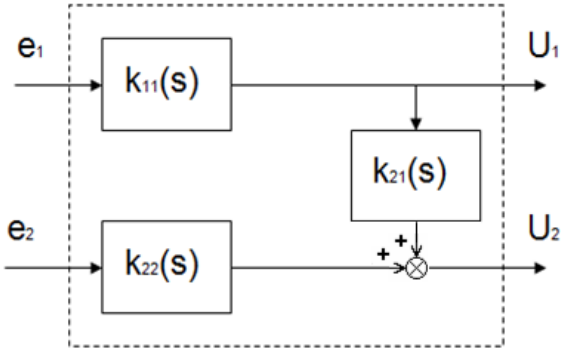

Fig 1.8 Block Diagram of the MIMO Controller

The SISO and MIMO controllers will be applied to the system, and suitable cost functions will need to be determined. Then the concept of Pareto fronts will be used to quantify which controller works better on the system.

Since it is difficult to visualize costs in four or more dimensions, level diagrams and hyper volume will be used to provide a clearer representation of the Pareto front for the two control systems in the required six dimensional space.

University of Strathclyde

1.3 OBJECTIVES OF THIS THESIS

The specific objectives of this thesis are to:

• Verify suitable cost functions for a MIMO system

• Use these cost functions to determine the Pareto fronts of the two controllers adopting approach of the MOO with the a posteriori decision making

• Determine which controller works better on the system under investigation, by using recent concepts of level diagrams [Blasco et al. 2008], hyper volumes [Emmerich et al. 2005], coverage indices [Zitzler 1999] and centroids based on binary hyper volumes.

• Draw conclusions on the applied method and make recommendations for future work.

1.4 LIMITATIONS AND SCOPE OF THESIS

This project used well established methods of designing controllers, for example, the Inverse Nyquist Array, written in MATLAB. The investigation was based on articles researched from the University of Cape Town library including its internet resources like the on-line IEEE publications and search engines, such as www.scholar.google.com.

An important aspect of a posteriori decision making in multi-objective optimization is the presentation of set of optimal costs to the designer. In practice this can be difficult as shown by a three dimensional visualization of datasets that was done in [Rapson et al. 2007]. This thesis used a method which simplifies the comparing of such multi-dimensional costs for controllers based on Level Diagrams. For systems with a large number of loops and cost functions, like the thermal plant, this method was found to result in many graphs that needed to be compared simultaneously even though it improved significantly on the method of [Rapson et al. 2007]. This led to the proposal of a centroid method based on binary hyper volumes that makes it easier to deal with high dimensional datasets.

The controllers were compared by Pareto fronts and binary hyper volumes and the validity of these analytical predictions was tested by a digital simulation of a number of cases derived from the Pareto Fronts.

University of Cape Town

1.5 PLAN OF DEVELOPMENT

This thesis starts with a brief introduction to the project. This is followed in chapter two by a literature review. Chapter three explains the tools to be used in the thesis. The modeling of the thermal plant is discussed in chapter four and the method used to obtain the results in chapter five. A detailed discussion of the results follows in chapter six. Lastly, a conclusion will be drawn and recommendations of future works will be discussed.

University of Cape Town

Chapter 2
Literature Review

This chapter will describe the basics of Pareto Fronts and how they can be applied to Multi-Objective Optimal control.

2.1 MULTI-OBJECTIVE OPTIMIZATION DESIGN

Both the SISO controller with its diagonal multivariable structure (Fig 1.6) and the MIMO controller with its triangular multivariable structure (Fig 1.8) have a few parameters that can be altered. In an attempt to find the best possible controllers, Multi-Objective Optimization was used to optimize the given parameters for each controller. Many possible solutions exist for each of the parameters in a given problem. Some of these parameter values are better than others. It is well known that Multi-Objective Optimization attempts to find the most optimal of such solutions in terms of the criteria defined by its cost functions [Gambier 2008] .

Multi-Objective Optimization aims to optimize two or more objectives simultaneously, and both concepts of cost functions and Pareto Efficiency are take into account. It can be formalized mathematically as shown in Eq.(2.1) below [Moore 2010]:

$$\theta = [\theta_1, \cdots, \theta_i] \in \Omega,$$

$$J(\theta) = [J_1(\theta), \ldots, J_k(\theta)],$$

$$\min_{\theta \in \Omega} J(\theta) \qquad (2.1)$$

where θ is the input or decision vector, Ω is the decision space and $J(\theta)$ is the cost or objective vector.

Many methods have already been developed to solve MOO, and Pareto Efficiency has been identified as a suitable method to solve Multi-Objective Optimization problems in this thesis [Liu et al. 2002]. State that MOO is a concept where when one individual is improved but the other individuals' performance will not be affected or may become worse. To achieve this, each variable within the

University of Cape Town

controllers will be treated as a parameter, each error and input in the controller that would need to be optimized is seen as contributing to a cost function or an objective. The idea is to find the best possible controllers, by optimizing the cost functions. The cost functions will be plotted against each other, and in this way the Pareto front is formed. The concept of a Pareto front will be discussed latter in this section.

In [Moore 2010], the mathematical formulations of the cost functions are defined and shown below, where J_e is the cost function of the error and J_u is the cost function of the input as shown in Eq.(2.2) and Eq.(2.3) below:

$$J_e = \frac{1}{Tmax}\int_0^{Tmax} e(t)^2 \, dt \tag{2.2}$$

$$J_u = \frac{1}{Tmax}\int_0^{Tmax} (U(t) - U_\infty)^2 \, dt \tag{2.3}$$

where, e(t) is the error signal at the time equal to t, U(t) is the input at the time equal to t and U_∞ is the input at the time equal to Tmax.

The Pareto Front and dominance are both part of Pareto Efficiency. The combination of the two allows one cost function to be rated against another cost function in terms of performance. A cost function point is (Pareto) dominated if another cost function point can be found that has smaller cost function values in all of its cost components.

When a series of non-dominated cost functions are combined together, a Pareto Front is formed. This Pareto Front represents a series of optimal solutions of the changing variables within the controller. Fig 2.1 shows the point-approximation to a typical Pareto Front in 2-Dimensions:

University of Cape Town

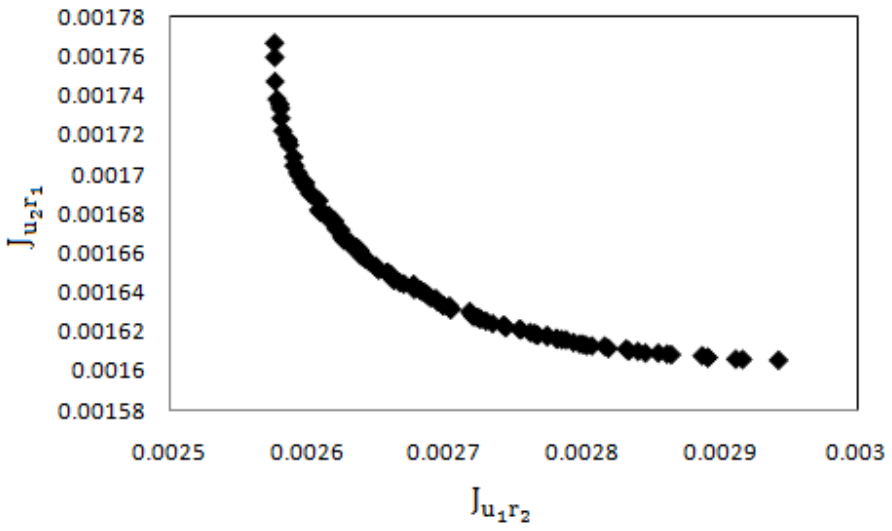

Fig 2.1 Pareto Front

Fig 2.1 represents a series of optimal solutions for the control system. These are computed by Differential Evolution algorithms like the one defined in [Abbass 2001] and form an approximation of the actual Pareto Front for the system.

2.2 COST FUNCTIONS FOR MULTIVARIABLE CONTROL SYSTEMS

There are many definitions for cost functions, starting with the simple but well-known example as shown in Eq.(2.4) below:

$$J = \int_0^\infty [x^T(t)Qx(t) + u^T(t)Ru(t)]dt \tag{2.4}$$

from optimal control [Belanger 1995].

The Linear Matrix Inequality Based Approach for MPC Economic Performance Assessment (LMIPA) is one way to verify the performance of MPC [Lee et al. 2010]. LMIPA combines all the cost functions together into one specific cost function, and by minimizing that specific cost function the optimal operation is done. This is an example of a priori decision making. A Pareto Front on the other hand allows for a posteriori decision making and this implies the use of visualization, meaning that each cost function can be visualized or analyzed individually while retaining an overview of the trade-offs between costs.

University of Cape Tow

As an example of a very complicated cost function consider a plant G(s) which has p outputs (y_i) and m inputs (u_j), with the mathematical expression of LMIPA [Lee et al. 2010] is shown below in Eq.(2.5):

$$J = \sum_{i=1}^{p} \left[b_{y,i} \times \bar{y}_i + a_{y,i}^2 \left(\bar{y}_i - y_{s,i} \right)^2 \right] + \sum_{j=1}^{m} \left[b_{u,j} \times \bar{u}_j + a_{u,j}^2 \left(\bar{u}_j - u_{s,j} \right)^2 \right] \quad (2.5)$$

where, $b_{y,i}$ and $a_{y,i}$ are the linear and quadratic coefficients for the i-th input variable, $b_{u,j}$ and $a_{u,j}$ are the linear and quadratic coefficients for the j-th output variable, $y_{s,i}$ and $u_{s,j}$ are the target values for the i-th controlled variable and the j-th manipulated variable respectively [Lee et al. 2010].

The research wants to use a cost function based on that used for Model Predictive Control, which weights the tracking error and the input. But Pareto front does not require the a priori definition of such coefficients or weightings.

In this project there are error matrices and input matrices, e(s) and u(s) respectively, which will be examined in order to determine which elements in the matrices are suitable for determining the cost functions, in order to analyze the two controllers being investigated. The error and input vectors are defined below in Eq.(2.6) and Eq.(2.7) respectively:

$$e_{r_i}(s) = \begin{pmatrix} e_1 \\ e_2 \end{pmatrix} \quad (2.6)$$

$$u_{r_i}(s) = \begin{pmatrix} u_1 \\ u_2 \end{pmatrix} \quad (2.7)$$

where $\begin{pmatrix} e_1 \\ e_2 \end{pmatrix}$ represents the error signals e_1 and e_2 in the two loops due to the change of setpoint r_1 and r_2, and $\begin{pmatrix} u_1 \\ u_2 \end{pmatrix}$ represents the resulting inputs u_1 and u_2 due to the same setpoint changes.

Thus after one experiment in which the two setpoints are changed sequentially, the cost functions used to judge the system become the cost function matrices below in Eq.(2.8) and Eq.(2.9):

University of Cape Town

$$J_e = \begin{pmatrix} J_{e_1 r_1} & J_{e_1 r_2} \\ J_{e_2 r_1} & J_{e_2 r_2} \end{pmatrix} \tag{2.8}$$

$$J_u = \begin{pmatrix} J_{u_1 r_1} & J_{u_1 r_2} \\ J_{u_2 r_1} & J_{u_2 r_2} \end{pmatrix} \tag{2.9}$$

where the cost function elements for the errors and inputs are defined in Eq.(2.10) and Eq.(2.11) respectively:

$$J_{e_i r_j} = \frac{1}{Tmax} \int_0^{Tmax} (e(t)_{i_{r_j}})^2 \, dt \tag{2.10}$$

$$J_{u_i r_j} = \frac{1}{Tmax} \int_0^{Tmax} (u(t)_{i_{r_j}} - u_{0_{i_{r_j}}})^2 \, dt \tag{2.11}$$

In a closed loop MIMO system when a change in setpoint r_1 of loop 1 occurs; $J_{e_1 r_1}$ describes the performance of the system and $J_{e_2 r_1}$ represents the interactions. The same goes for Loop 2 when a change in setpoint r_2 of loop 2 occurs; $J_{e_2 r_2}$ describes the performance of the system and $J_{e_1 r_2}$ represents the interactions. The combination of $J_{u_1 r_1}$ and $J_{u_2 r_1}$ together represent the amount of input needed when a change in setpoint r_1 of loop 1 occurs. Similarly $J_{u_1 r_2}$ and $J_{u_2 r_2}$ are combined to represent the amount of input needed due to the change in setpoint r_2 of loop 2.

A change to the original J_u cost function equation from [Moore 2010] is made in that the mathematical expression of $J_{u_i r_j}$ in Eq.(2.11) is different compared to the mathematical expression of J_u shown in Eq.(2.3). More details of J_u is given in [Moore 2010], where in Eq.(2.11) u(t) is subtracted by its initial value (U_0) but in Eq.(2.3) u(t) is subtracted by its final value (U_∞).

University of Cape Town

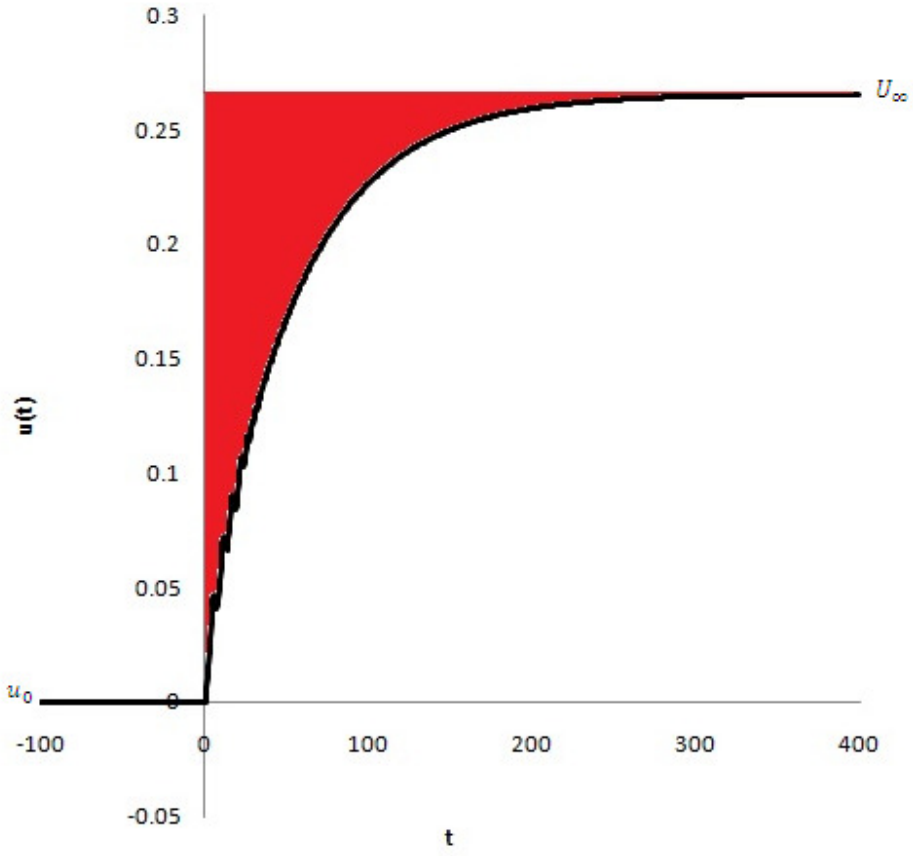

Fig 2.2 u(t) Subtracted by the final value (U_∞)

The shaded area in Fig 2.2 is the area that was used to calculate the original J_u cost function, the J_u cost function from [Moore 2010], and that corresponds to the J_u mathematical expression of Eq.(2.3) But the actual amount of input needed when the setpoint changes is the shaded area in Fig 2.3, and this corresponds to the mathematical expression of $J_{u_i r_j}$ in Eq.(2.11). Therefore, it is more appropriate to use the $J_{u_i r_j}$ mathematical expression of Eq.(2.11) to evaluate the input cost function, compared to the J_u mathematical expression of Eq.(2.3).

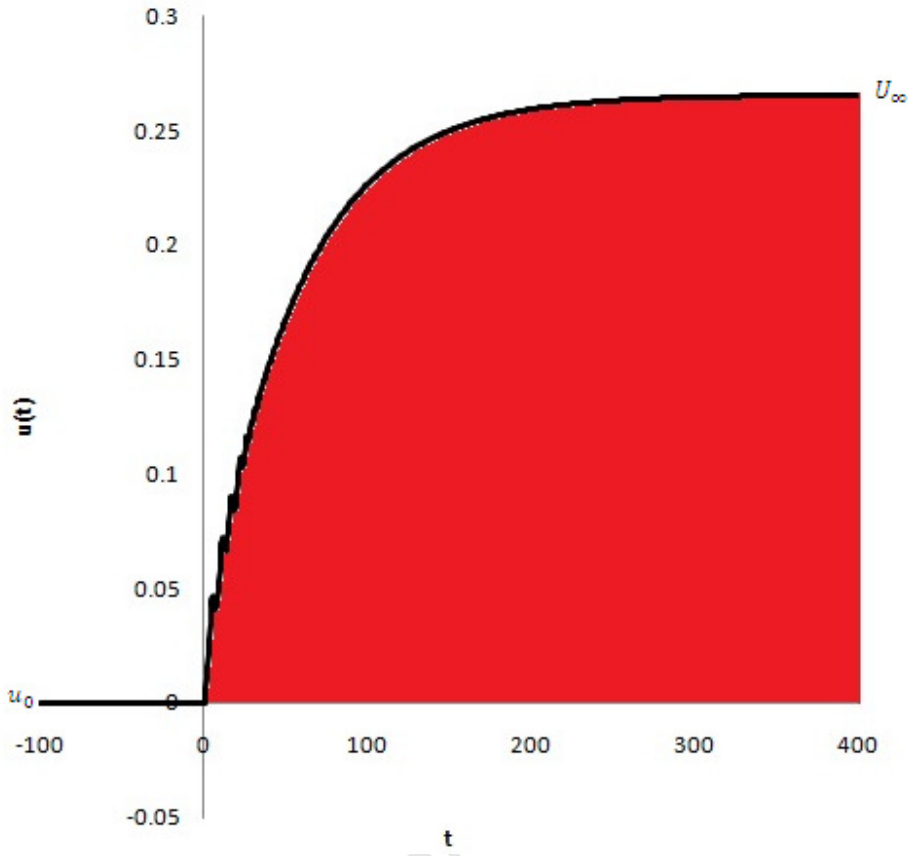

Fig 2.3 u(t) Subtracted by the initial value (u_0)

In order to analyze or optimize the controllers, comparing the performance against the cost of inputs can give an idea of how efficient the controller is. By comparing the interaction against the performance, the trade-offs between performance and interaction will be shown. Therefore, six different cost functions were picked to analyze the controllers. They are shown in Table 2.1:

Table 2.1 The six different cost functions

Cost Function No.	Description of the Cost Function
$J_{e_1r_1}$	Performance error of e_1 due to r_1
$J_{e_2r_1}$	Interaction error of e_2 due to r_1
$J_{e_1r_2}$	Interaction error of e_1 due to r_2
$J_{e_2r_2}$	Performance error of e_2 due to r_2
J_{ur_1}	Cost of input for change in r_1, uses Norm-2 to combine $J_{u_1r_1}$ and $J_{u_2r_1}$
J_{ur_2}	Cost of input for change in r_2, uses Norm-2 to combine $J_{u_1r_2}$ and $J_{u_2r_2}$

2.3 MULTIVARIABLE CONTROLLER DESIGN

In [Rosenbrock 1974], it indicates that the diagonal dominance of the Multi-input Multi-output (MIMO) system needs to be achieved before the actual multivariable controllers design process can begin. Once the condition of diagonal dominance is satisfied, the multivariable controller's elements can be obtained by simply using the single-loop controller design method to formulate single-loop controllers for each of the diagonal elements of the diagonal dominated MIMO system.

Assuming that an MIMO transfer function matrix model with two inputs and two outputs that is based on the laboratory thermal system, as shown in Eq. (2.12) below:

$$G(s) = \begin{pmatrix} g_{11} & g_{12} \\ g_{21} & g_{22} \end{pmatrix} = \begin{pmatrix} \frac{-0.405}{1+6.569s} & \frac{-0.4}{1+4.873s} \\ \frac{-0.4}{1+8.878s} & \frac{-0.435}{1+8.569s} \end{pmatrix} \tag{2.12}$$

University of Cape Town

Its Direct Nyquist Array is shown below in Fig 2.4 from which it can be seen that some of the Gershgorin circles encircle the origin of the g_{11} and g_{22} elements of the transfer function. This system is therefore not diagonally dominant [Maciejowski 1989].

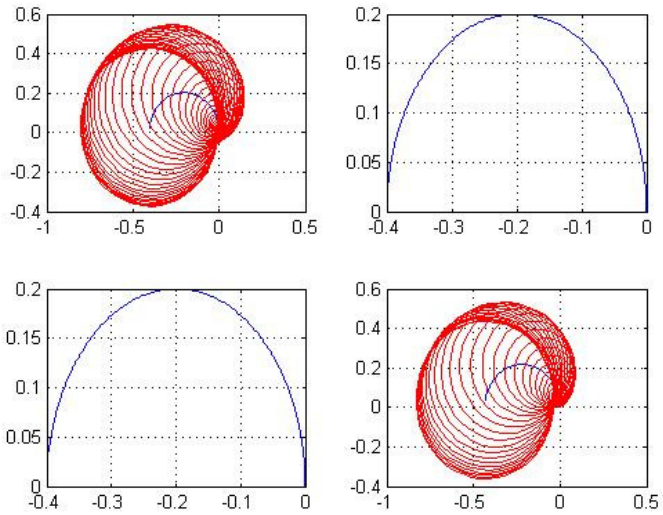

Fig 2.4 Direct Nyquist Array of the system G(s)

In order to make such a system diagonally dominant, a MIMO controller with a triangular structure (or decoupling MIMO controller) is used. Once diagonal dominance is achieved a SISO controller (a diagonal MIMO controller) is added to the loop to ensure infinite loop gain and hence setpoint tracking [Rosenbrock 1974]. Thus the structure of the final MIMO controller, as mentioned in Chapter 1, is shown below:

$$K(s) = \begin{pmatrix} 1 & 0 \\ k_{21} & 1 \end{pmatrix} \begin{pmatrix} k_{11} & 0 \\ 0 & k_{22} \end{pmatrix} = \begin{pmatrix} k_{11} & 0 \\ k_{11}k_{21} & k_{22} \end{pmatrix} \tag{2.13}$$

where, $\begin{pmatrix} 1 & 0 \\ k_{21} & 1 \end{pmatrix}$ is the precompensator and $\begin{pmatrix} k_{11} & 0 \\ 0 & k_{22} \end{pmatrix}$ is the diagonal MIMO controller.

When combined with the plant model G(s) this results in the open loop model Q(s), as shown in Eq. (2.14):

$$Q(s) = \begin{pmatrix} q_{11} & q_{12} \\ q_{21} & q_{22} \end{pmatrix} = \begin{pmatrix} g_{11} & g_{12} \\ g_{21} & g_{22} \end{pmatrix} \begin{pmatrix} 1 & 0 \\ k_{21} & 1 \end{pmatrix}$$

$$= \begin{pmatrix} g_{11} + g_{12}k_{21} & g_{12} \\ g_{21} + g_{22}k_{21} & g_{22} \end{pmatrix} = \begin{pmatrix} g_{11} + g_{12}k_{21} & g_{12} \\ 0 & g_{22} \end{pmatrix} \quad (2.14)$$

The selection of $k_{21} = -g_{21}/g_{22}$ was applied to produce the triangular structure. This Q(s) would be diagonally dominant as shown in Fig.2.5. By considering the resulting system, it can be seen that only the q_{21} element of Eq. (2.14) is zero. (Where, $k_{21} = \frac{-g_{21}}{g_{22}}$ [Maciejowski 1989]) Therefore, Q(s) is diagonally dominant as shown in Fig 2.5.

The Direct Nyquist Array of Q(s) is plotted in Fig 2.5, the Gershgorin bands on the DNA that show interaction in loop 1 can be made arbitrarily small (by scaling), and the stability of loop 1 can be determined from q_{11} itself [Braae 1994a] since the off-diagonal term, g12, is open loop stable. Hence the SISO controllers can be designed independently for loop 1 and loop 2 of the compensated plant model.

When attempting to design a controller for the q_{11} element the critical point needs to be sitting at anywhere greater than 0.03 on the Real axis, for the q_{11} element to be stable [Braae 1994b]. Therefore, controller gain will have to be small and the integral time constant will have to be large for such a critical point position [Hamane et al. 2010].

University of Cape Town

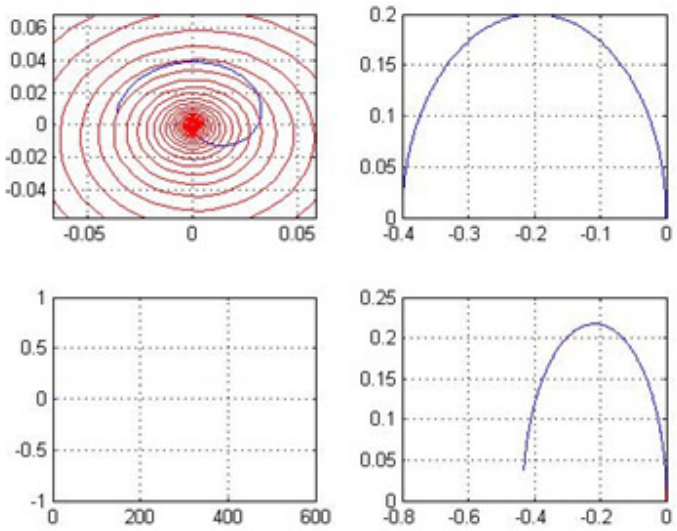

Fig 2.5 Direct Nyquist Array of Q(s)

Cost functions can take numerous forms; those of Eq.2.10 and Eq.2.11 are selected. Six cost functions were defined in Table 2.1 to provide specific metrics for performance, for interaction and for cost of input. The plant considered is fully interactive and a MIMO compensator that produces a triangular structure allows the SISO controllers to be designed for both loops in the compensated plant.

University of Cape Town

Chapter 3
Multi-Objective Tools

3.1 VISUALIZATION OF PARETO FRONT IN MULTI-DIMENSIONAL SPACE

In multi-objective optimization with a posteriori decision making, visualization of the cost function space (and possibly the decision space as well) is critical in guiding the engineer towards an acceptable design. In two or three dimensional space this is possible through graphical representations but to visualize the trade-offs in higher dimensions, other more sophisticated techniques are required.

Unfortunately in most realistic cases more than three dimensions will be involved in the designs. For example a simple SISO control problem in an industrial setting could contain a dozen cost functions (like setpoint tracking, settling time, the damping factor, disturbance rejection at the input and the output, sensor noise attenuation, sensitivity to model changes, and also the cost of input to achieve each of these).

In [Fleming et al. 1998], visualization of cost functions in seven dimensions is achieved using parallel processing technique in the way shown in Fig 3.1:

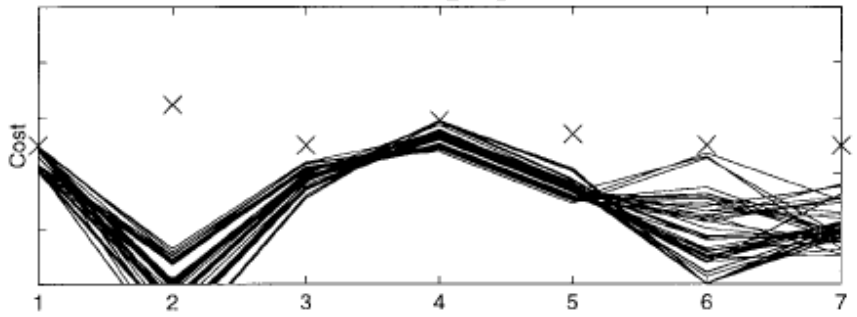

Fig 3.1 Pegasus NL governor design (8 params) [Fleming et al. 1998]

The crosses on Fig 3.1 indicate the maximum acceptable values of each cost function. The straight lines connect the actual values of the cost functions that are all on the Pareto front. If the positions of the cost functions on the x-axis are altered, the shapes of these plots will change.

Alternative methods include using the recently proposed Level Diagrams [Blasco et al. 2008] and Hyper Volumes [Moore 2010] which are methods to visualize and to quantitatively compare cost functions in more than 2-Dimensions [Moore 2010].

University of Cape Town

3.1.1 LEVEL DIAGRAM

The visualization obtained through level diagram [Blasco et al. 2008] provides the engineer with a set of diagrams that allow visualization of the trade-offs between cost functions in higher dimensions. In level diagrams, cost functions plot the overall norm of all the cost functions (on the y-axes) against each cost function (on the x-axes).

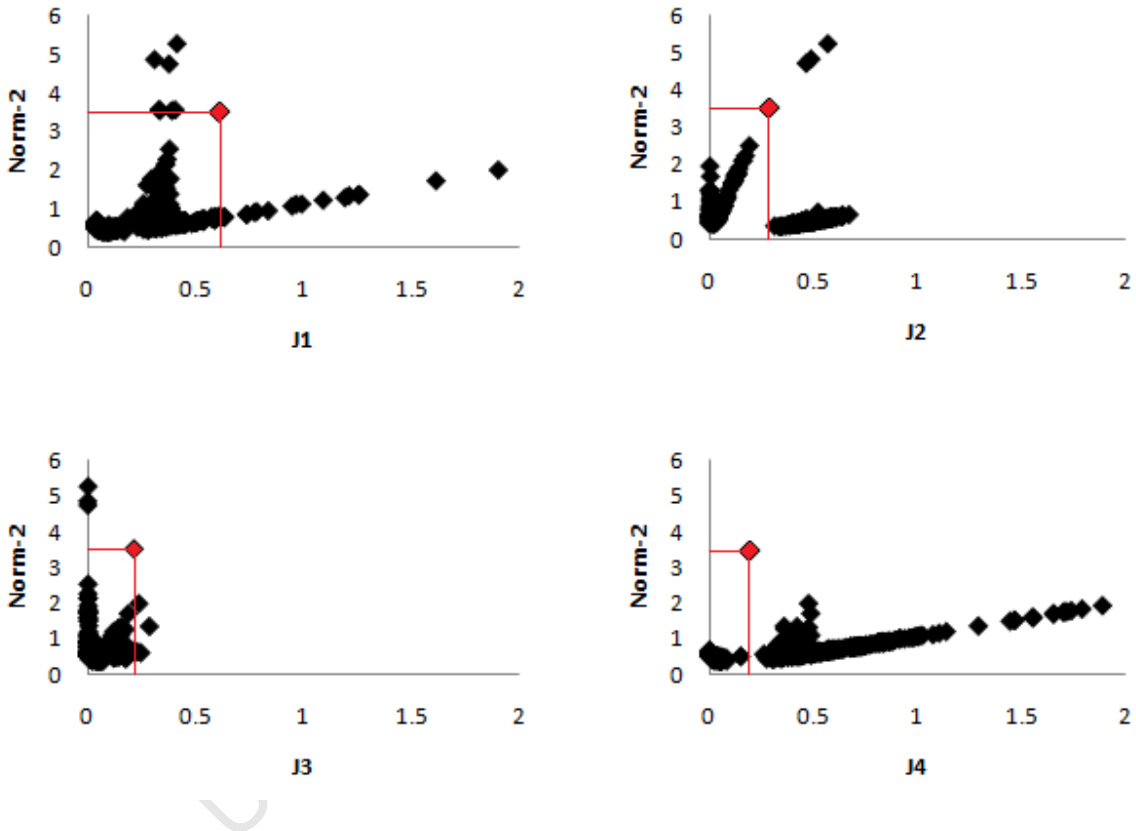

Fig 3.2 Level Diagrams of 4-Dimensional Space

Level Diagrams make visualizing the trade-offs between cost functions simpler. In Fig 3.2 an example of level diagrams involved in 4-Dimensions is shown; a point which corresponds to the same set of parameters will have the same Norm-2 value in all of the cost function plots, therefore the value of the different cost functions can be read from these plots. The overall cost function is given as a Norm-2 and is calculated by using the mathematical formulation shown in Eq. (3.1) below:

$$\mathbf{Norm - 2} = \sqrt{\mathbf{J_1}^2 + \mathbf{J_2}^2 + \mathbf{J_3}^2 + \ldots + \mathbf{J_n}^n} \quad (3.1)$$

3.1.2 HYPER VOLUME

When two Pareto Fronts of more than 2-Dimensions are computed to represent two controller structures, the Pareto fronts of the two controller designs need to be compared quantitatively to determine which one is performing best, perhaps in a sub-region of the global region of interest. In this situation the Pareto Front, which dominates more space or volume of the region of interest, may be regarded as the one performing better than the other. Estimation of the Hyper Volume in 2- or 3-Dimensions is relatively simple, but to estimate the Hyper Volume in 4-Dimensions or above is not an easy task.

There are many different methods [Brockho et al. 2007] [Bader et al. 2008] [While et al. 2006] that exist to calculate hyper volume. But Hyper Volumes is selected in this study.

3.1.3 REGION OF INTEREST

When visualizing Pareto fronts of more than three dimensions, the Pareto front is sitting in a multidimensional space which could be infinitely large. In most cases, it is only necessary to visualize and analyse a specific section of the multidimensional space which contains the Pareto front applicable to the engineering problem under investigation.

Experience with multiobjective optimization has shown [Purshouse et al. 2007] that a Region of Interest needs to be defined in order to focus the optimization when dealing with engineering problems. This adds an element of a priori decision making to a posterior decision making implied in the use of visualization but is important in practice. The focus is provided by a subset of the cost function space that contains the Pareto front. This sub-space is known as the Region of Interest and is selected to calculate the Hyper Volumes for the thermal controllers under investigation. As illustrated by Fig. 3.3, the shaded region is the Region of Interest and it is defined to translate and normalize the cost functions under consideration. Thus the resulting Region of Interest becomes a unit hypercube with unity side lengths and a Hyper Volume equal to 1.

University of Cape Town

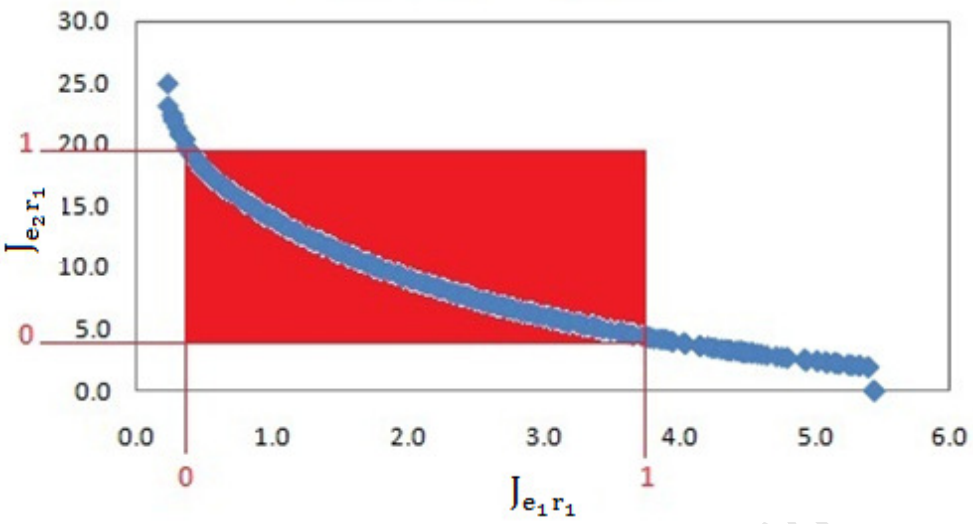

Fig 3.3 Region of Interest

3.1.4 THE UNARY HYPER VOLUME AND THE BINARY HYPER VOLUME

When two different systems produce respective Pareto fronts then a secondary indicator to the Hyper Volume becomes necessary. This leads to the Unary Hyper Volume indicator $I_H(B)$ (As shown in E.q.(3.2).) [Moore 2010] which is a useful method to calculate the "volume" of the cost function space that has been dominated by the Pareto front, B. It gives an indication of how optimal Pareto front B is.

Alternatively two different systems can be compared more directly by means of the Binary Hyper Volume indicator $I_{H2}(A,B)$ [Zitzler 1999] [Zitzler et al. 2003], and is referred to as the coverage difference indicator in [Zitzler 1999]. It determines the volume in cost function space that is dominated by Pareto front A but not by Pareto front B. Its mathematical expression is given in Eq. (3.2) [Moore 2010] .

$$I_{H2}(A, B) = I_H(A \cup B) - I_H(B) \tag{3.2}$$

As shown in Fig. 3.3, the upper region is the Hype Volume dominated by the Pareto front and this volume is estimated by filling the entire box with randomly distributed points and then determining the fraction of points that are eliminated as being dominated by the given Pareto front. This fraction yields the Unary Hyper Volume indicator $I_H(B)$ [Moore 2010].

University of Cape Town

The Binary Hyper Volume indicators of Pareto front A and Pareto front B are shown in Fig 3.4, where $I_{H2}(A,B)$ is the region which is dominated by Pareto front A only and $I_{H2}(B,A)$ is the region dominated by Pareto front B only.

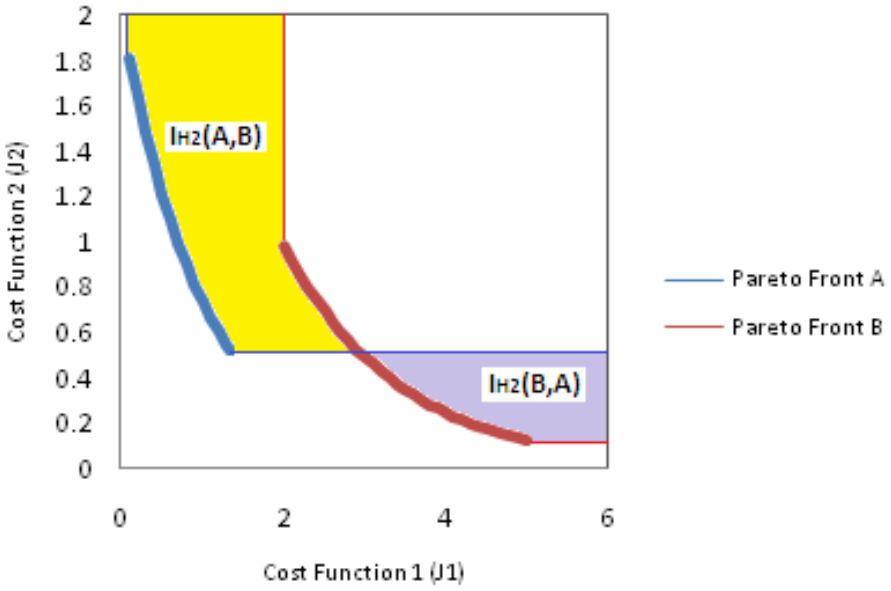

Fig 3.4 The Binary Hyper Volume Indicators

3.1.5 CENTROID

In addition to the coverage index derived from binary hyper-volumes, the centroid is the mean point within each binary Hyper Volume as computed from two Pareto Fronts representing two controller designs. It is assumed that the binary hyper volume of a Pareto front forms a single cluster of points in cost function space. The centroid is thus a point in the cost function space that can be applied to compare any two Pareto Fronts defined for any number of dimensions in cost space.

As a simple two-dimensional example, consider the two Pareto Fronts in Fig. 3.5, where centroid will be used to compare Cost Function 1 and Cost Function 2 of the two Pareto Fronts separately. The results of the centroid of $I_{H2}(A,B)$ and $I_{H2}(B,A)$ are shown in Fig 3.5 and Table 3.1 below:

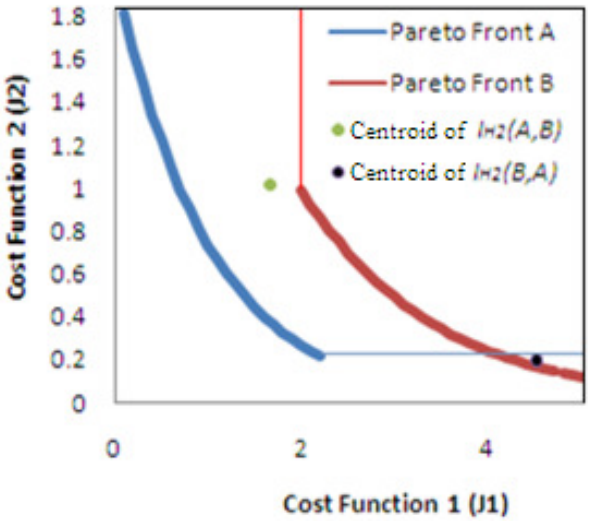

Fig 3.5 Two Pareto Fronts

Table 3.1 Centroid Results of Pareto Front A and Pareto Front B

	Cost Function 1 (J_1)	**Cost Function 2 (J_2)**
I_{H2}(A,B)	1.66160	1.01719
I_{H2}(B,A)	4.52230	0.198290

According to the Centroid in Table 3.1, I_{H2}(A,B) is performing better than I_{H2}(B,A) in term of Cost Function 1 (J_1), but I_{H2}(B,A) is performing better than I_{H2}(A,B) in term of Cost Function 2 (J_2). Centroids do not only show that a specific Pareto Front is better than another Pareto Front, but they also determine which cost functions within a Pareto Front, are performing better compared to the cost function of another Pareto Front. In Fig 3.6, these Centroids are plotted against the cost functions which make it easier to observe the performances as measured by each cost function:

University of Cape Town

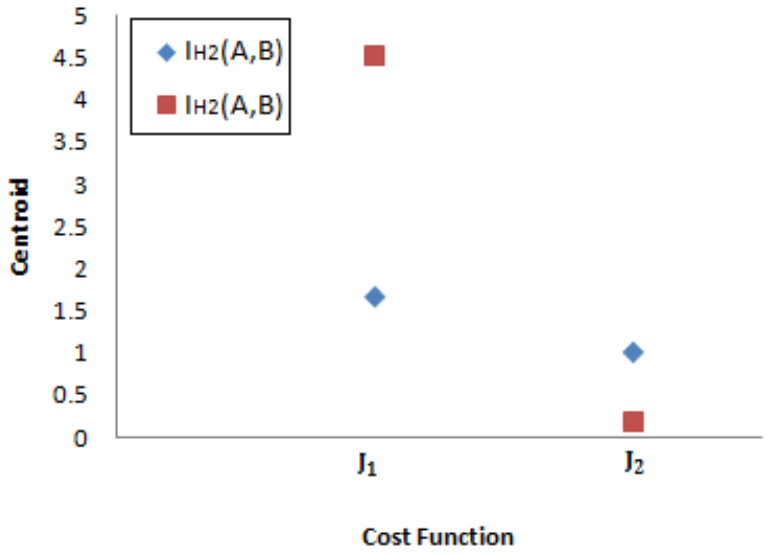

Fig 3.6 Centroid Plots

This Chapter has described all the tools that will be used in this project. This includes the level diagrams, the Hyper Volume, the Region of Interest, the Unary Hyper Volume, the Binary Hyper Volume and the centroids.

University of Cape To

Chapter 4
System Modeling

This chapter will explain the procedure of obtaining the simulation model, the transfer function (G(s)), obtained from the physical system.

4.1 OPEN LOOP STEP TEST ON THE THERMAL PLANT

The existing thermal fan heating system is the most interactive experimental equipment in the laboratory; with two inputs (U_i) and two outputs (Y_i). The system was designed and constructed during a previous project and its block diagram is shown in Fig 1.5.

Due to the behavior of the system, the transfer function model G(s) of such a system will be determined by stepping each input separately i.e. one at a time. By stepping the input U_1, the g_{11} and g_{21} elements of the system's transfer function matrix model G(s) could be obtained. By stepping the input U_2, the g_{12} and g_{22} elements of the system's transfer function G(s) could be obtained.

When a step of the input (U_1) is made at time t = 0[s], the corresponding input (U_1) is shown below in Fig 4.1:

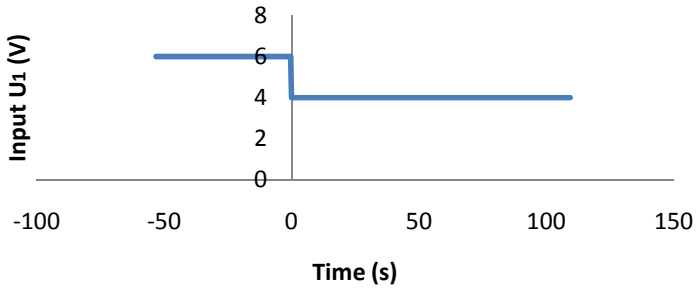

Fig 4.1 Step Input of (U_1)

The response in output (Y_1) graph is shown in Fig 4.2:

rsity of Cape Town

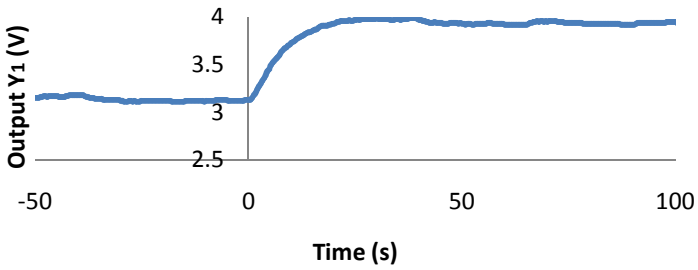

Fig 4.2 Output (Y_1) Graph when a Step of the Input (U_1) is Made

And in output (Y_2) graph is shown in Fig 4.3:

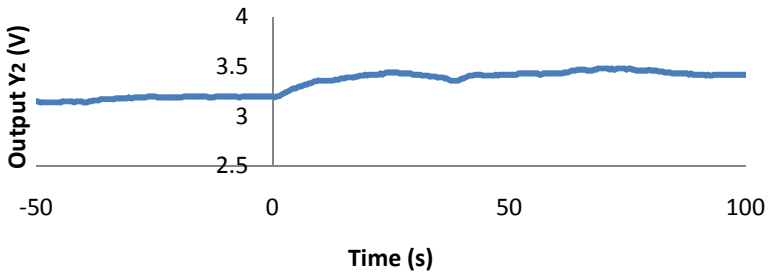

Fig 4.3 Output (Y_2) Graph when a Step of the Input (U_1) is Made

The same scales are used for the axes on the output signals to show that the first input (U_1) affects the first output (Y_1) the most, and affects the second output (Y_2) the least. Both sensors are affected by disturbances.

When a step of the input (U_2) is made as shown in Fig 4.4, the corresponding output (Y_1) is shown in Fig 4.5:

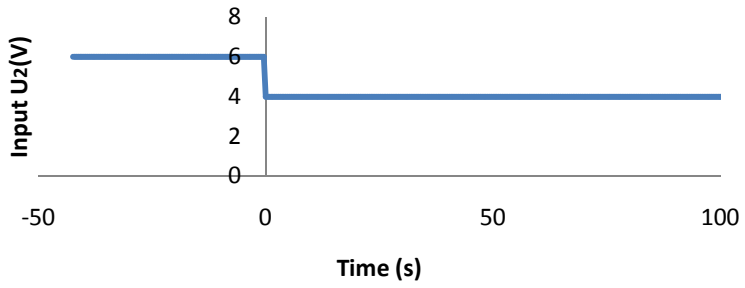

Fig 4.4 Step Input of (U_2)

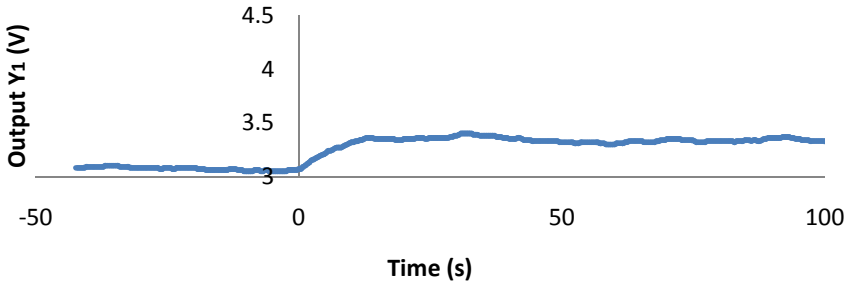

Fig 4.5 Output (Y_1) Graph when a Step of the Input (U_2) is Made

The output (Y_2) graphs are shown below in Fig 4.6:

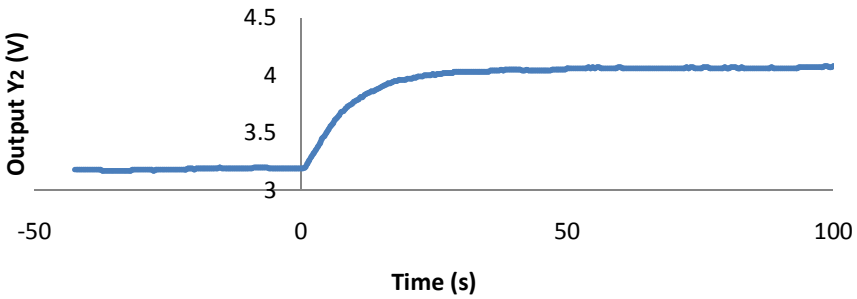

Fig 4.6 Output (Y_2) Graph when a Step of the Input (U_2) is Made

Clearly the second input (U_2) affects the second output (Y_2) the most and the first output (Y_1) the least. Both sensors are affected by disturbances that can be observed during the steady state operation of the plant.

The data file Number 1, listed in Appendix A, contains the detailed input and output data which are used to plot the above graphs.

By observing the input and output graphs above, it is clear that each element within the transfer function matrix G(s) of the system will be in the $\frac{A_{ij}}{1+sT_{ij}}$ format; therefore the transfer function elements $g_{ij}(s)$ of the system should have the mathematical expression as shown in Eq. (1.4). The two unknown variables, namely the gain (A_{ij} in [V]/[V] for the thermal system)and the time constant (T_{ij} in [s]) were estimated by using the following simple engineering methods:

$$g_{ij}(s) = \frac{A_{ij}}{1+sT_{ij}} \tag{4.1}$$

where the gain A_{ij} is estimated from Eq (4.2).

$$A_{ij} = \frac{\Delta Y_i}{\Delta U_j} \tag{4.2}$$

and the time constant T_{ij} could be computed as shown in Fig 4.7.

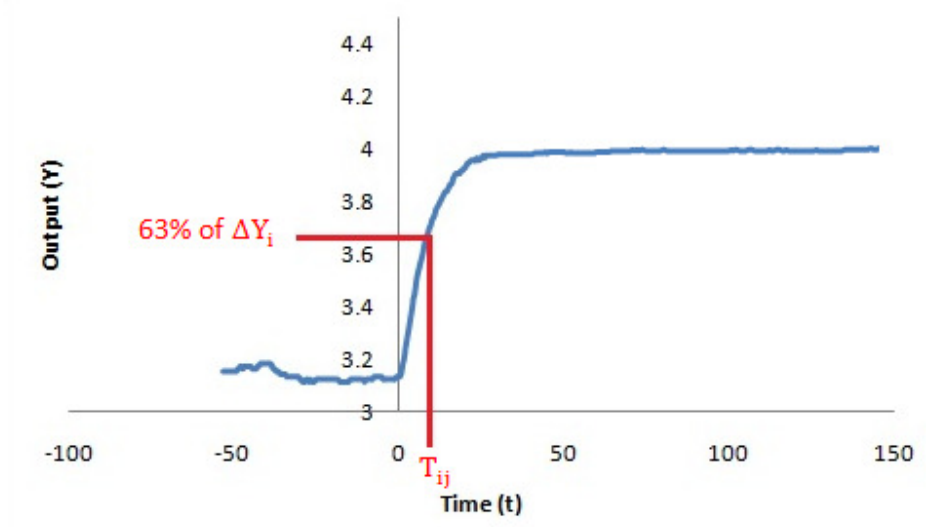

Fig 4.7 The time constant (T_{ij}) of each element of the transfer function G(s)

University of Cape Town

where T_{ij} is the time corresponding to 63% of ΔY_i.

The above responses are approximated with a 1st order system [Ibrahim 2006], because we want the precompensator (k_{21}) to be simple yet adequate.

The transfer function model obtained from the method mentioned above was:

$$G(s) = \begin{pmatrix} g_{11} & g_{12} \\ g_{21} & g_{22} \end{pmatrix} = \begin{pmatrix} \frac{A_{11}}{1+sT_{11}} & \frac{A_{12}}{1+sT_{12}} \\ \frac{A_{21}}{1+sT_{21}} & \frac{A_{22}}{1+sT_{22}} \end{pmatrix} = \begin{pmatrix} \frac{-0.405}{1+7.800s} & \frac{-0.145}{1+5.400s} \\ \frac{-0.110}{1+8.300s} & \frac{-0.430}{1+8.900s} \end{pmatrix} \quad (4.3)$$

Note that the response of g_{21} and g_{12} look like a second order since they contain overshoots of about 10%. Nevertheless it will not be a problem to estimate the system's transfer function G(s), because the format of each element $g_{ij}(s)$ within the transfer function will be defined as $\frac{A_{ij}}{1+sT_{ij}}$ which will ensure that the NELM [Moore 2010] approximates it as first order.

Thus the approximate estimates of the gain (A_{ij}) and time constant (T_{ij}) were refined by use of a nonlinear regression technique, NELM, based on the Nelder-Mead algorithm [Olsson et al. 1975] discussed in the next section.

4.2 USE OF NELM TO APPROXIMATE THE TRANSFER FUNCTION G(s)

There are two unknown variables in each of the elements $g_{ij}(s)$ of the assumed transfer function, namely the gain (A_{ij}) and the time constant (T_{ij}). In order to approximate the gain and the time constant (T_{ij} in [s]) as accurately as possible, the Nelder-Mead method (called NELM) is utilized. NELM is a non-linear regression program that minimizes the difference between the response data and that of the model.

The transfer function model obtained from the NELM method is shown in Eq (4.4).

$$G(s) = \begin{pmatrix} g_{11} & g_{12} \\ g_{21} & g_{22} \end{pmatrix} = \begin{pmatrix} \frac{A_{11}}{1+sT_{11}} & \frac{A_{12}}{1+sT_{12}} \\ \frac{A_{21}}{1+sT_{21}} & \frac{A_{22}}{1+sT_{22}} \end{pmatrix} = \begin{pmatrix} \frac{-0.405}{1+6.569s} & \frac{-0.142}{1+4.873s} \\ \frac{-0.116}{1+8.878s} & \frac{-0.435}{1+8.569s} \end{pmatrix} \quad (4.4)$$

University of Cape Town

4.3 VALIDATION OF THE TRANSFER FUNCTION G(s)

This was done on both the open loop and the closed systems.

4.3.1 OPEN LOOP STEP TEST

In order to verify that the transfer function models in Section 4.2 approximated the plant dynamics correctly, step tests were done on both loops of the physical system, compared to those obtained by digital simulation of the plant model in Eq. (4.4). The comparison was done by visual inspection of the two output signals y(t) of loop 1 and loop 2 superimposed on the plant data in the same plots.

In an open loop, when one step of the input (U_1) is made at time t = 0[s], the corresponding input (U_1) is shown in Fig 4.8 (The data used is given as Number 2 in the list in Appendix A):

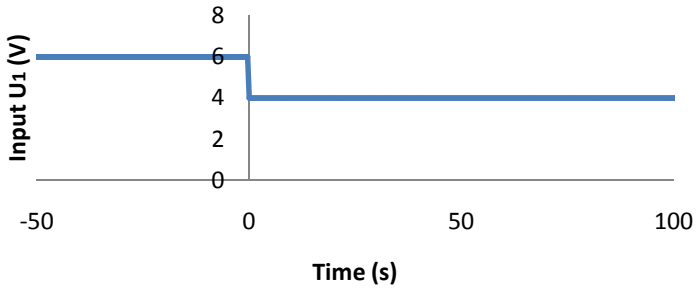

Fig 4.8 Step Input of (U_1)

The response in output (Y_1) graph is shown in Fig.4.9 below:

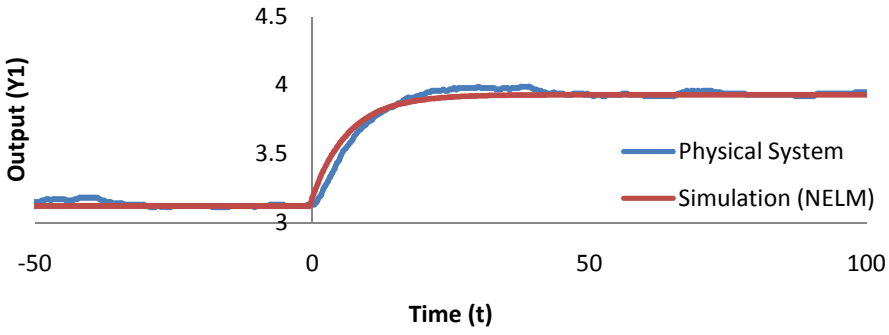

Fig 4.9 Output (Y_1) Graph when a Step of the Input (U_1) is Made

In Fig 4.9, there is clear indication of some dead time which is estimated to be 0.4s. This is not significant compared to time constant of 6.569s and thus was neglected to make the precompensator (K21) as simple as possible.

And in output (Y_2), the graph is shown in Fig 4.10:

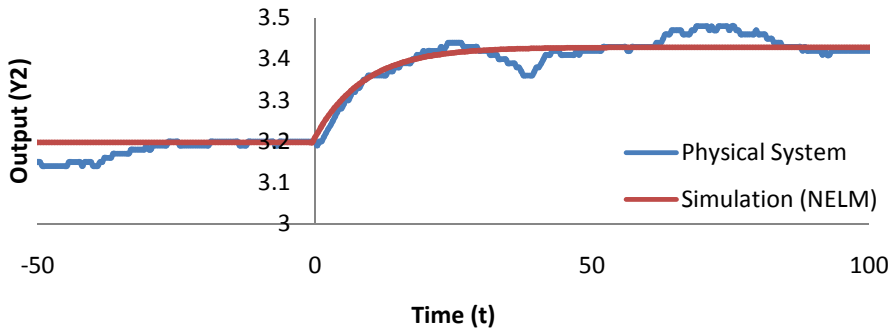

Fig 4.10 Output (Y_2) Graph when a Step of the Input (U_1) is Made

In Fig 4.10, there is a clear indication of some dead time which is estimated to be 1.2s. This is not significant compared to time constant of 8.878s and thus was neglected. The variation in plant data after steady state is reached is attributed to an output disturbance as it was also ob served before the application of the step change.

Alternatively, when a step of the input (U_2) is made as shown in Fig 4.11, the corresponding output (Y_1) and output (Y_2) graphs are shown in Fig 4.12 and Fig 4.13 respectively:

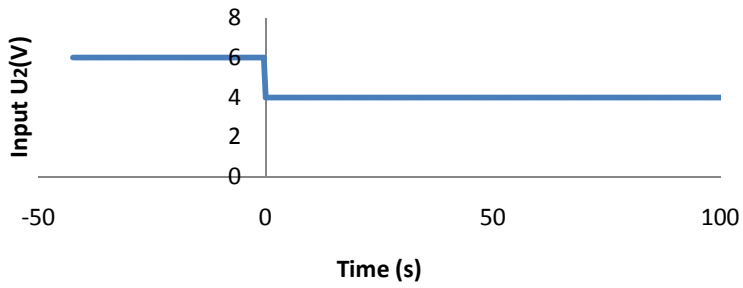

Fig 4.11 Step Input of (U_2)

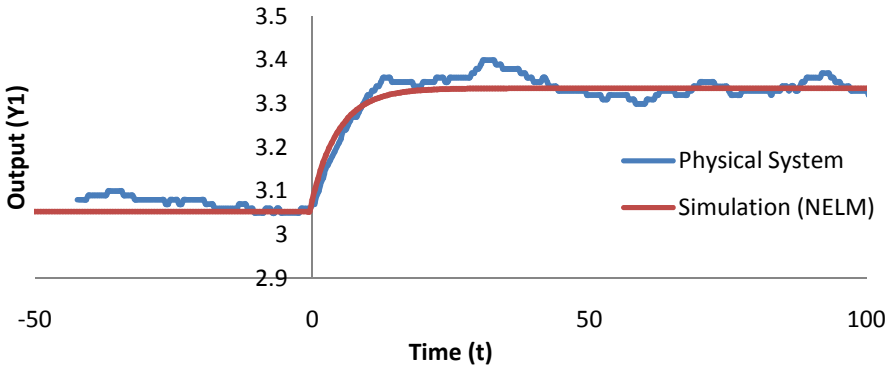

Fig 4.12 Output (Y_1) Graph when a Step of the Input (U_2) is Made

In Fig 4.12, there is a clear indication of some dead time which is estimated to be 0.4s. This is not significant compared to time constant of 4.873s and was thus neglected. Again there is consider disturbance to the output.

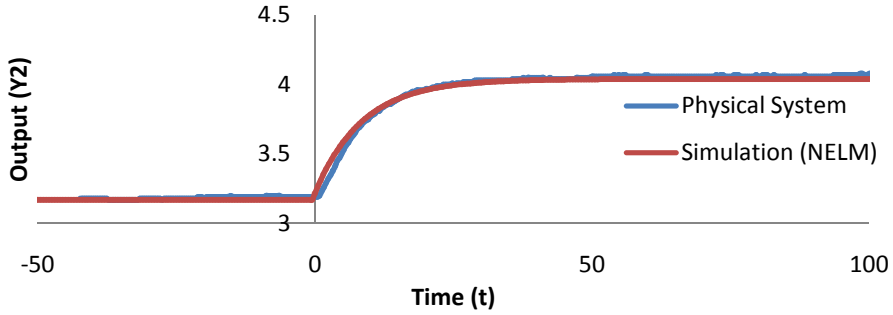

Fig 4.13 Output (Y_2) Graph when a Step of the Input (U_2) is Made

In Fig 4.13, Again a small dead-time is noted but at 0.4s is negligible compared to the dominant time constant of 8.569s.

4.3.2 CLOSED LOOP STEP AND DISTURBANCE TEST

The block diagram of the closed loop system with disturbance is shown in Fig 4.14 below:

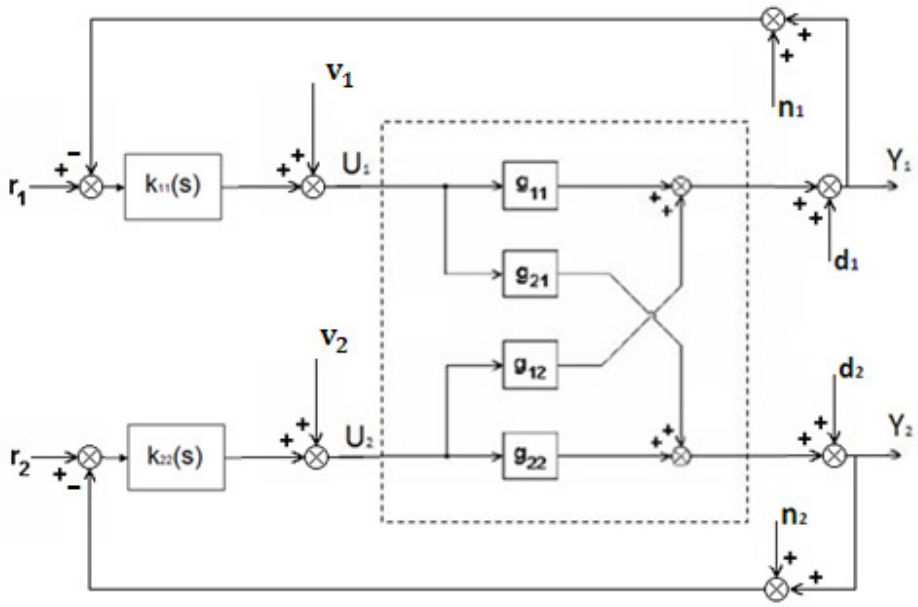

Fig 4.14 Block Diagram of the Closed Loop System with Disturbance

University of Cape

In the diagram given in Fig 4.14 the controllers are defined in Eq. (4.5) and Eq. (4.6).

$$k_{11}(s) = \frac{-0.1(1+s)}{s} \tag{4.5}$$

and

$$k_{22}(s) = \frac{-0.1(1+s)}{s} \tag{4.6}$$

Also, V_1 and V_2 represent the input disturbance of loop 1 and loop 2 respectively, d_1 and d_2 show the output disturbance of loop 1 and loop 2 respectively and n_1 and n_2 show the sensor noise in loop 1 and loop 2 respectively.

On both the physical system and the simulation, the setpoint r_1 of loop 1 is stepped at time equal to 0.0 sec and setpoint r_2 of loop 2 is stepped at time equal to 306.0 sec. The output of disturbance d_1 and d_2 will then be introduced at time equal to 604.5 sec and 872.5 sec respectively. The input disturbance V_1 and V_2 will be introduced at time equal to 1139.0 sec and 1401.5 sec respectively. Finally, the sensor noise n_1 and n_2 will be introduced at time equal to 1699.5 sec and 1941.0 sec.

Table 4.1 gives a summary of the experiments and the simulations:

Table 4.1 Changes Made on the Physical system and the Simulation

	r_1	r_2	d_1	d_2	v_1	v_2	n_1	n_2
Changes made	0.3	0.3	1.0	1.0	-0.1	0.1	-0.2	0.2
Time [s]	0.0	306.0	604.5	872.5	1139.0	1401.5	1699.5	1941.0

After running the physical system and the simulation according to the changes made in Table 4.1, the following results were found and are shown as time plots in Fig.4.15 to 4.20 and x-axes ranging from -50.0s to 2200.0s were used to retain in indication of the variations in the signals The details of which are given in Number 3 of Appendix A including the experimental and simulated data, the errors $e_1(t)$and $e_2(t)$ are shown below in Fig 4.15 and Fig 4.16 respectively:

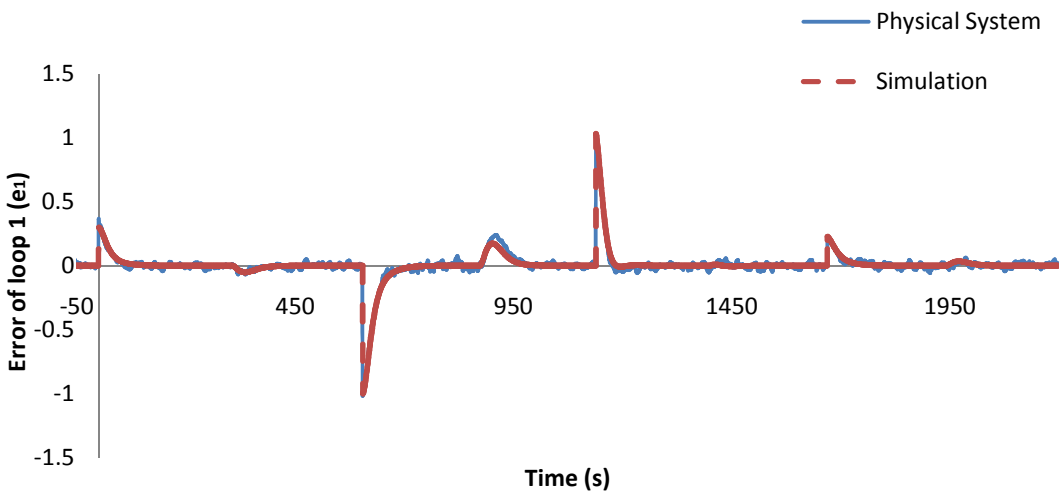

Fig 4.15 Error of Loop 1 (e_1) for All the Changes Listed in Table 4.1

of Cape Town

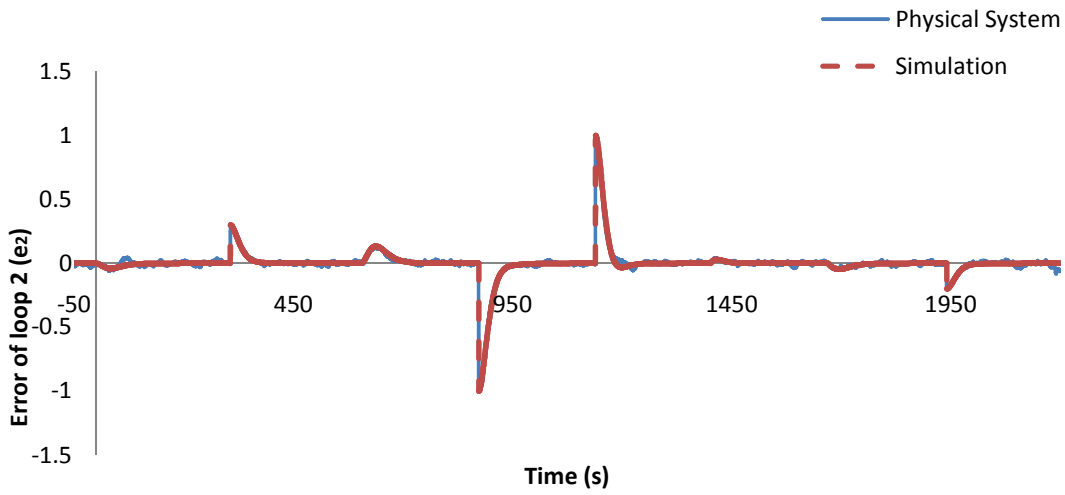

Fig 4.16 Error of Loop 2 (e_2) for All the Changes Listed in Table 4.1

The inputs $u_1(t)$and $u_2(t)$ are shown below in Fig 4.17 and Fig 4.18 respectively:

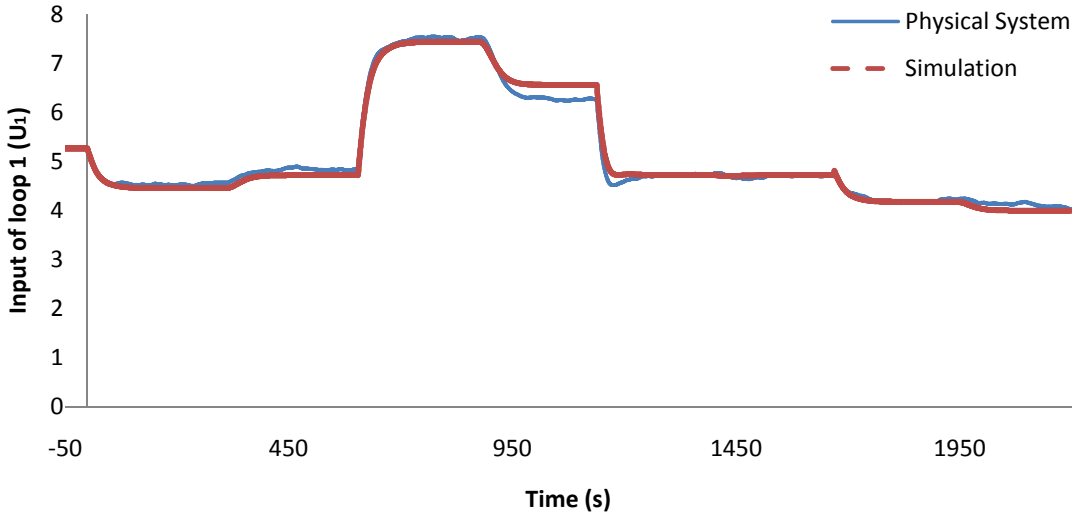

Fig 4.17 Input of Loop 1 (u_1) for All the Changes Listed in Table 4.1

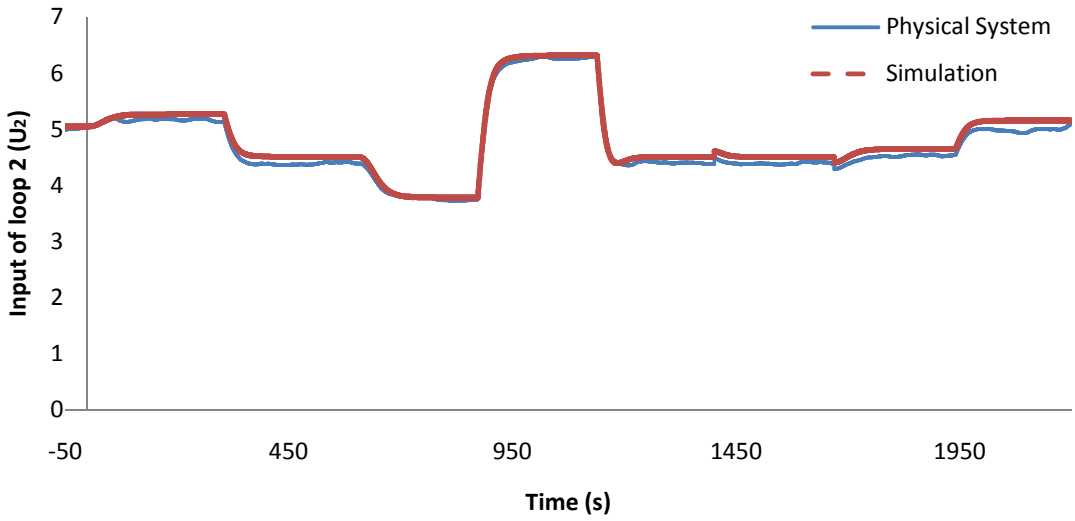

Fig 4.18 Input of Loop 2 (u_2) for All the Changes Listed in Table 4.1

Where the outputs $y_1(t)$and $y_2(t)$ are shown below in Fig 4.19 and Fig 4.20 respectively:

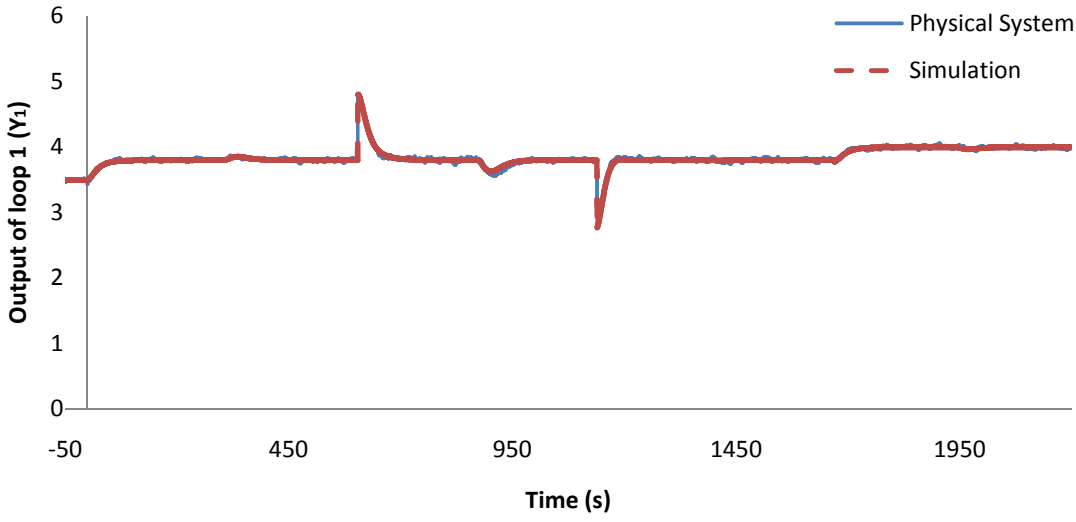

Fig 4.19 Output of Loop 1 (y_1) for All the Changes Listed in Table 4.1

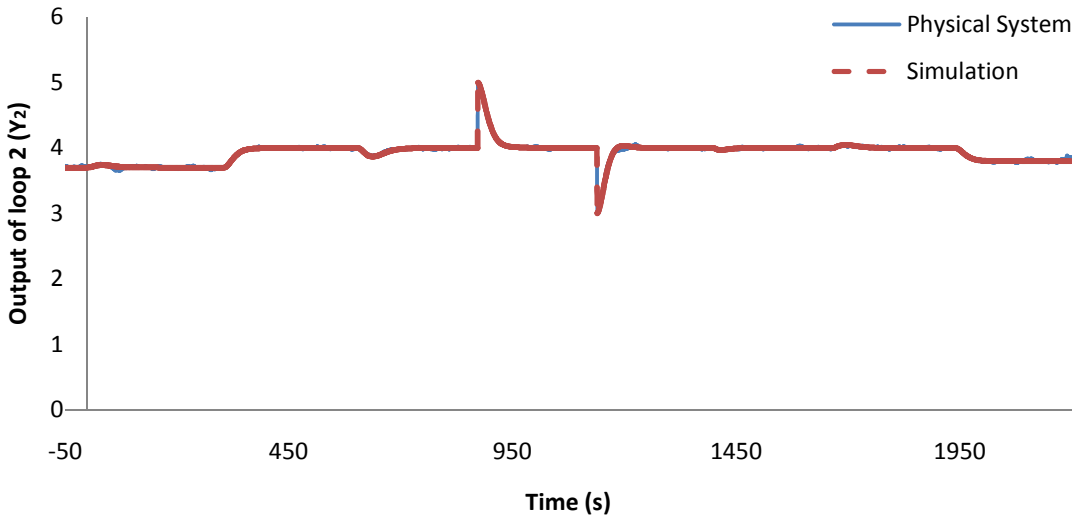

Fig 4.20 Output of Loop 2 (y_2) for All the Changes Listed in Table 4.1

By observing the above figures, the physical system appears to have small oscillations everywhere which the simulation does not have. It is apparent that the simulation matches the dominant responses of the physical system well.

4.3.2 COST FUNCTION TEST

The aim of this thesis is to analyze the cost functions of the system, so it is important to test if the cost functions of the physical system match the cost functions of the simulation. In Section 2.2, six different cost functions were defined. Hence the test of cost functions will focus on these six different cost functions.

In this test, an SISO controller with both k_{11} and k_{22} elements equal to $\frac{-0.1(1+s)}{s}$ were used.

The cost function results obtained from the experiment conducted are listed in Table 4.2.

University of Cape To

Table 4.2 Results Obtain from the Cost Function Test

	$J_{e_1r_1}$	$J_{e_2r_1}$	$J_{e_1r_2}$	$J_{e_2r_2}$	J_{ur_1}	J_{ur_2}
Physical System	1.494	0.133	0.177	1.463	130.256	134.348
Simulation	1.448	0.060	0.096	1.452	485.383	441.212

From Table 4.2, it is clear that only $J_{e_1r_1}$ and $J_{e_2r_2}$ represent a match between the physical system and the simulation; the other four cost functions did not match. In order to investigate the inconsistency of cost functions between the physical system and the simulation, a series of "cost function vs. time" graphs were plotted. The data for these plots are given in file Number 4 of the list in Appendix A.

The "$J_{e_1r_1}$ vs. time" and the "$J_{e_2r_2}$ vs. time" graphs are shown below in Fig 4.21 and Fig 4.22 respectively, where the cost function between the physical system and the simulation displays a relatively good fit:

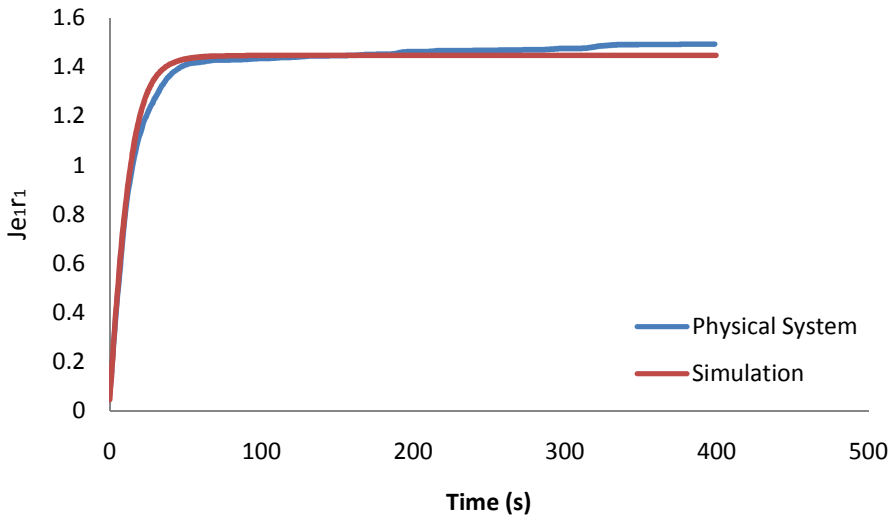

Fig 4.21 $J_{e_1r_1}$ vs. Time Graph

University of Cape Town

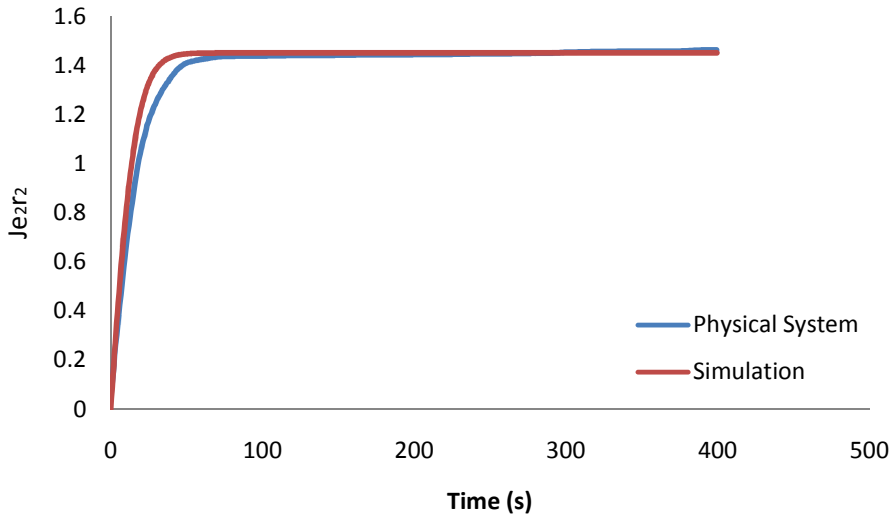

Fig 4.22 $J_{e_2r_2}$ vs. Time Graph

However the graphs of the other four cost functions displayed otherwise. Refer to Fig 4.23, Fig 4.24, Fig 4.25 and Fig 4.26 shown below:

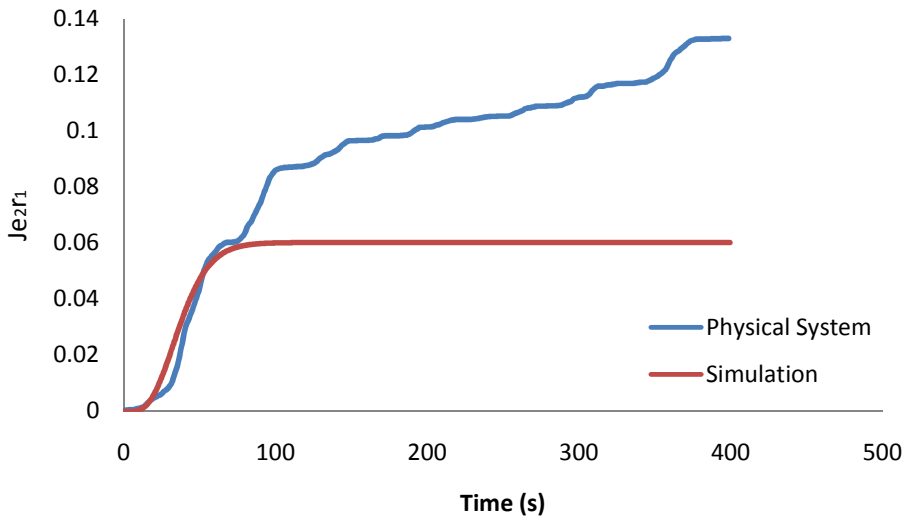

Fig 4.23 $J_{e_2r_1}$ vs. Time Graph

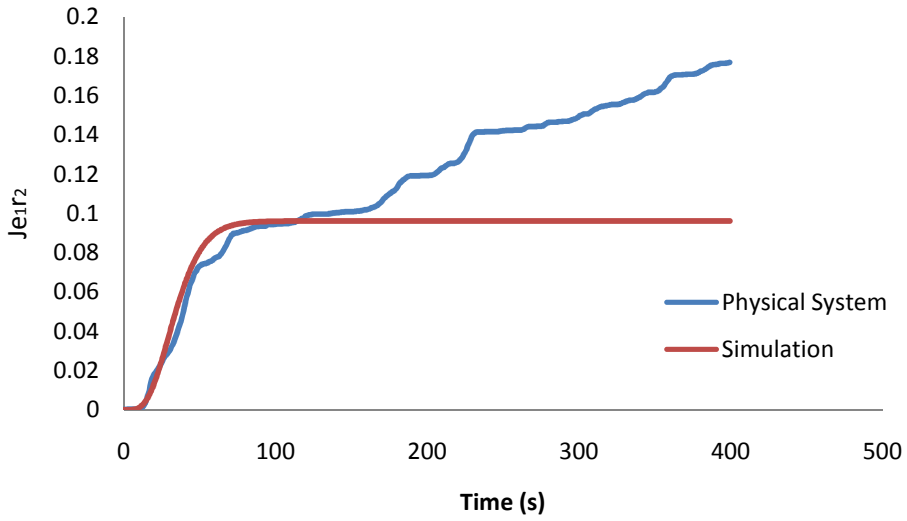

Fig 4.24 $J_{e_1r_2}$ vs. Time Graph

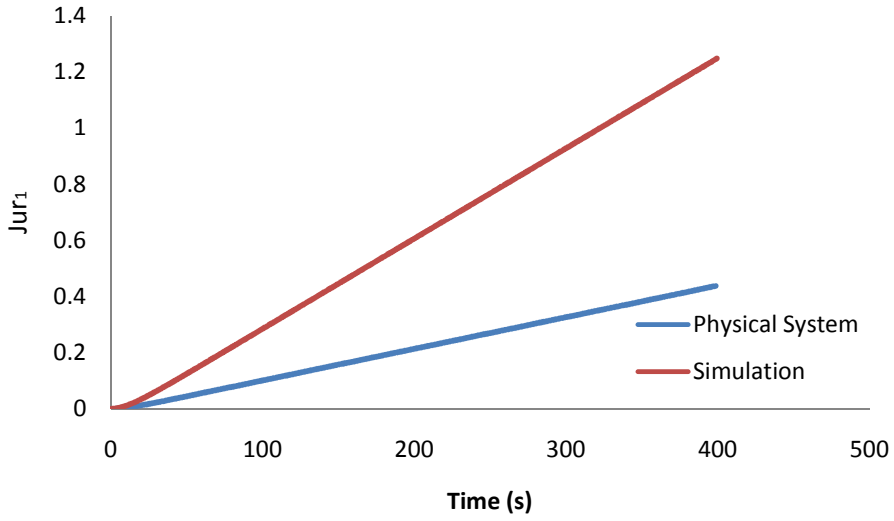

Fig 4.25 J_{ur_1} vs. Time Graph

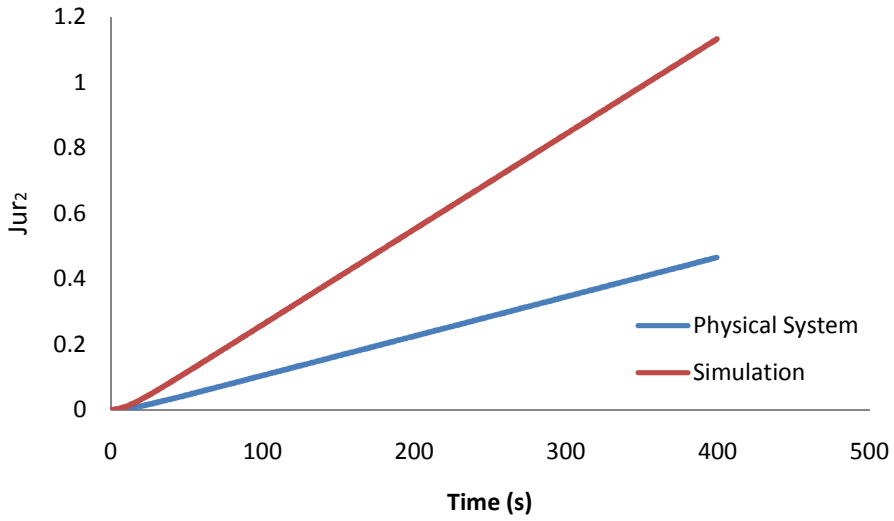

Fig 4.26 J_{ur_2} vs. Time Graph

There is a need to further investigate the reason(s) behind the inconsistency of the cost functions between the physical system and the simulation. This is achieved by referring to the cost function equations Eq.(2.10) and Eq.(2.11). These demonstrate the purpose of the integration of the cost function equations which is to calculate the area of the error e(t) square in Eq.(2.10) and the area of the input u(t) square in Eq.(2.11). Further investigation of this phenomenon includes breaking down the equation by looking only at the modified integrand in these equations. Specifically the integrand of each cost function equation of the error e(t) and the input u(t) was multiplied by the sampling time dt as shown below:

$$\text{Integrand } J_{e_i r_j} = \frac{(e(t)_{i_{r_j}})^2 \text{ x dt}}{\text{Tmax}} \tag{4.7}$$

$$\text{Integrand } J_{u_i r_j} = \frac{(u(t)_{i_{r_j}} - u_{0_{i_{r_j}}})^2 \text{ x dt}}{\text{Tmax}} \tag{4.8}$$

A series of Integrand time graphs showing the six different cost functions are plotted. (Refer to Number 5 of Appendix A for the data that was used.)

University of Cape To

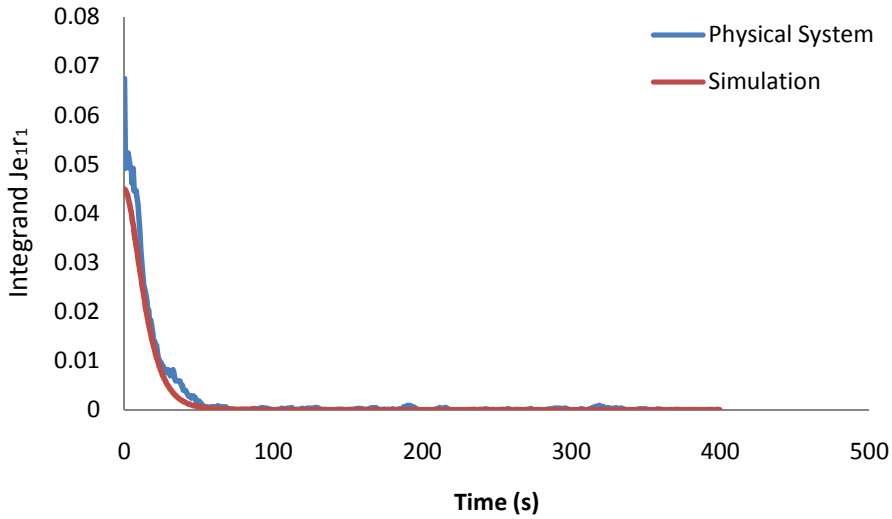

Fig 4.27 Integrand $J_{e_1r_1}$ vs. Time Graph

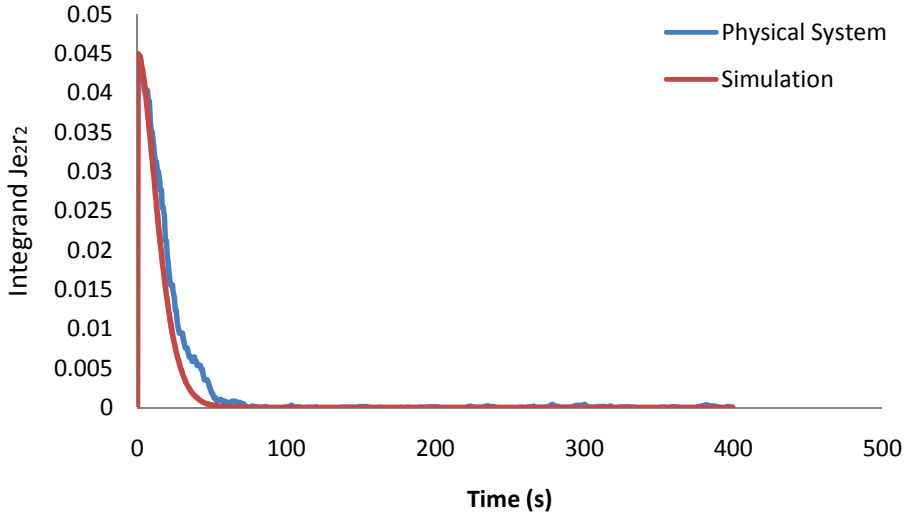

Fig 4.28 Integrand $J_{e_2r_2}$ vs. Time Graph

As shown in Fig 4.27 and Fig 4.28, the integrand of the cost function for the simulation matches that for the physical system suitably. Whereas in Fig 4.29 and Fig. 4.30, the integrand of the cost function of the simulation can match the shape of the integrand of the cost function of the physical system, but the simulation does not have any oscillation which was observed for the physical system. With reference to the small scales on the y-axes this kind of oscillation is attributed to the sensor noise and inaccuracy of

the physical system. However the integrand of the cost function of the simulation matches the shape of the integrand of the cost function of the physical system, therefore $J_{e_2r_1}$ and $J_{e_1r_2}$ of the simulation in Table 4.2 do correspond to $J_{e_2r_1}$ and $J_{e_1r_2}$ of the physical system. Thus one can conclude that $J_{e_2r_1}$ and $J_{e_1r_2}$ of the simulation do approximate the $J_{e_2r_1}$ and $J_{e_1r_2}$ of the physical system correctly and the discrepancies are therefore attributed to sensor noise.

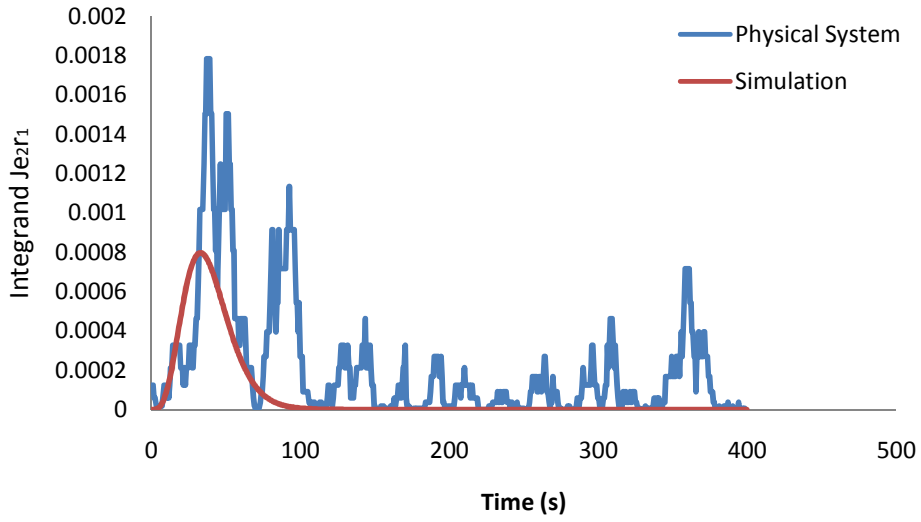

Fig 4.29 Integrand $J_{e_2r_1}$ vs. Time Graph

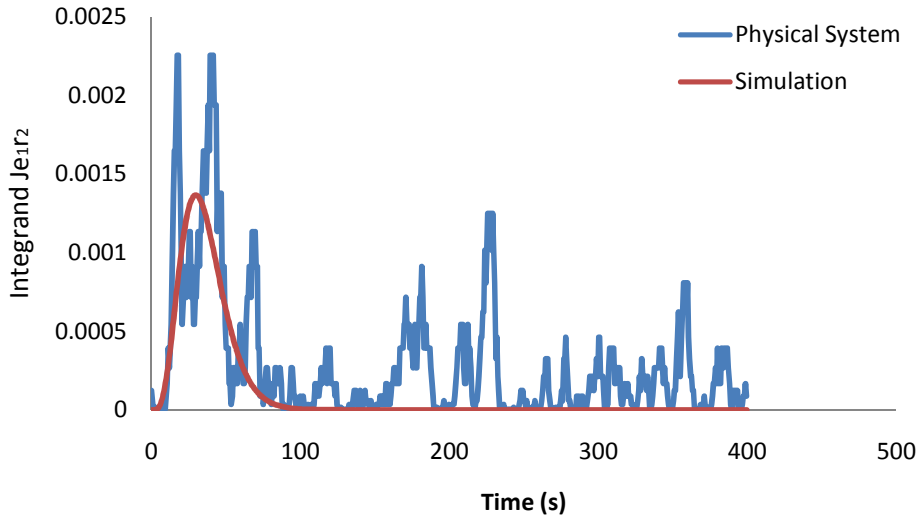

Fig 4.30 Integrand $J_{e_1r_2}$ vs. Time Graph

The Integrand cost function J_{ur_1} and J_{ur_2} are shown below in Fig 4.31 and Fig 4.32 respectively:

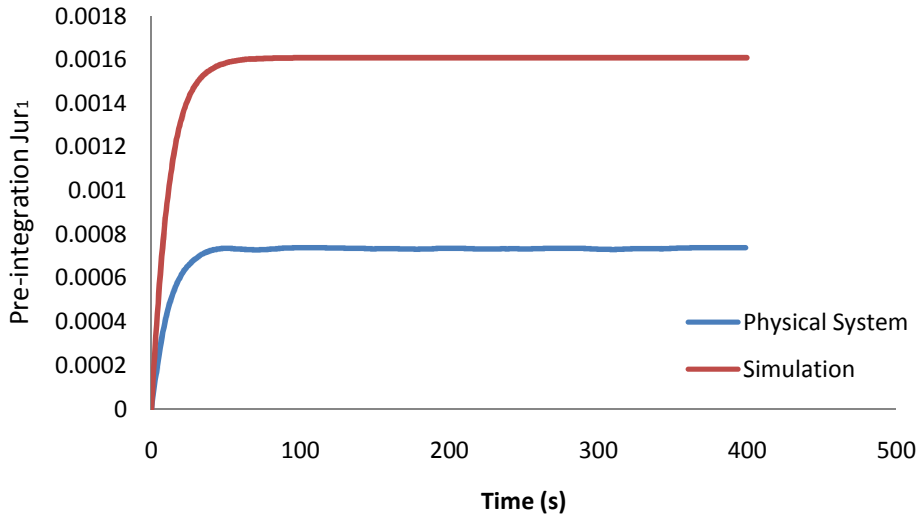

Fig 4.31 Integrand J_{ur_1} vs. Time Graph

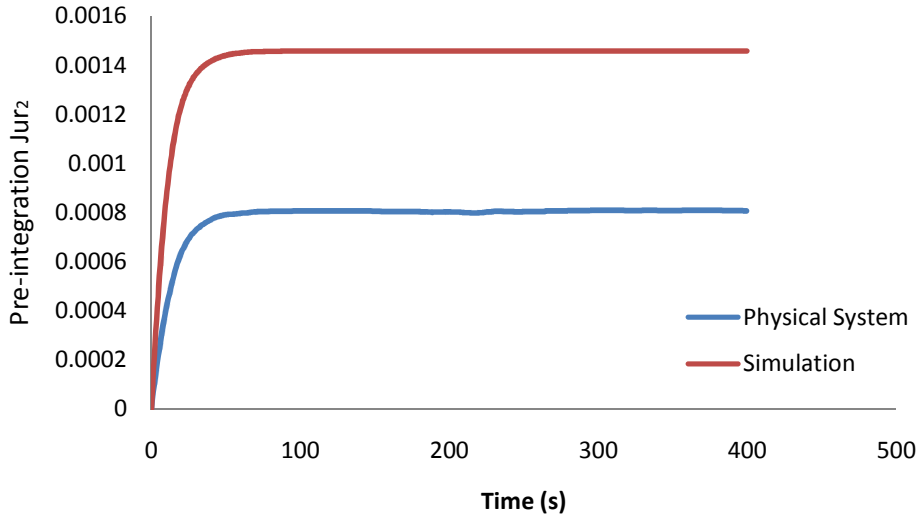

Fig 4.32 Integrand J_{ur_2} vs. Time Graph

As shown in Fig 4.31 and Fig 4.32, the final values of the integrand J_{ur_1} and the integrand J_{ur_2} for the simulation greatly exceeded the final value for the physical system. J_{ur_1} and J_{ur_2} represent the amount of input that is needed to ensure that the system's output value reaches the setpoint's value. The gain of each element g(s) of the system's transfer function G(s) is the most significant source that will affect the amount of inputs needed. Therefore a more in depth investigation on the gain will need to be done.

Consider the closed loop system shown in Fig 4.33 below:

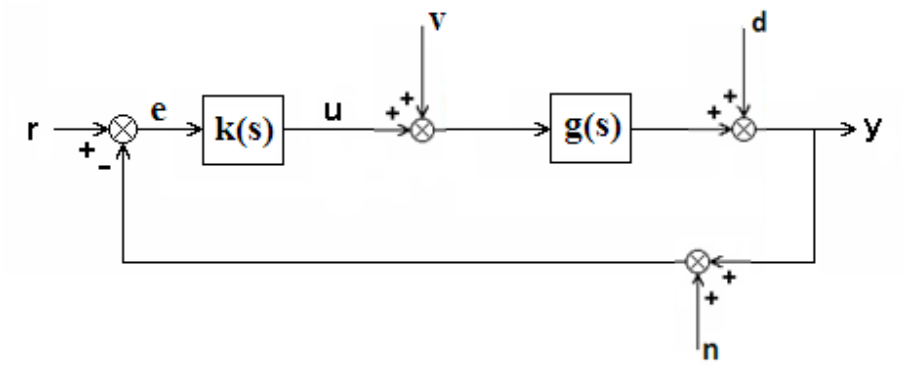

Fig 4.33 Block Diagram of a Closed Loop System

where,

$g(s) = \frac{Ae^{-s\tau}}{1+sT}$; $k(s) = \frac{K(1+s)}{s}$; $v = \frac{V}{s}$; $d = \frac{D}{s}$; $r = \frac{R}{s}$ and n is zero-mean Gaussian noise with a small initial value n_0.

By block diagram algebra it can readily be deduced to Eq. (4.9):

$$U = \frac{kr-kn-kd-kgv}{1+kg} \tag{4.9}$$

Apply initial value theorem to Eq. (4.9) it can be shown in Eq. (4.10) that:

$$U_0 = \lim_{s\to\infty} sU(s) = RK - Kn_0 - DK \tag{4.10}$$

University of Ca

And using the final value theorem it can be shown in Eq. (4.11) that:

$$U_{\infty} = \lim_{s \to 0} sU(s) = \frac{R}{A} - \frac{D}{A} - V \tag{4.11}$$

All the disturbance (d(t), v(t) and n(t)) were zero during the test. Therefore, changes in U were entirely due to the changes in $\frac{R}{A}$. Since the gain A of g(s) is not constant in practice due to changes in ambient temperature, it could be the cause of inconsistencies between the time plots of the physical system and those of the simulation. This could be the main cause of the inconsistencies between the physical system and the simulation's J_{ur_1} and J_{ur_2}. In order to verify if the gain A of g(s) did change, a detailed investigation was carried out.

Since the physical system has two inputs and two outputs, the output voltage of the system was measured when the two heating fans were off. This gave the output voltages for both sensors that corresponded to the room temperature and is called the offset output (y-offset). The test began with both setpoints being equal and set to 2V then the setpoint of loop 1 (r_1) only was stepped up by 1V at a time until it reached 8V. (The setpoint of loop 2 (r_2) was kept constant for this test.) The test was repeated for the second loop: The setpoint of loop 2 (r_2) was stepped up by 1V at a time until it reached 8V while keeping the setpoint of loop 1 (r_1) constant. This kind of test was done twice, each time at different room temperature or offset output (y-offset).

The results of the two tests are shown in Fig 4.34, Fig 4.35, Fig 4.36 and Fig 4.37; the data used to plot the following graphs is given in Number 6 of Appendix A:

University of Cape Town

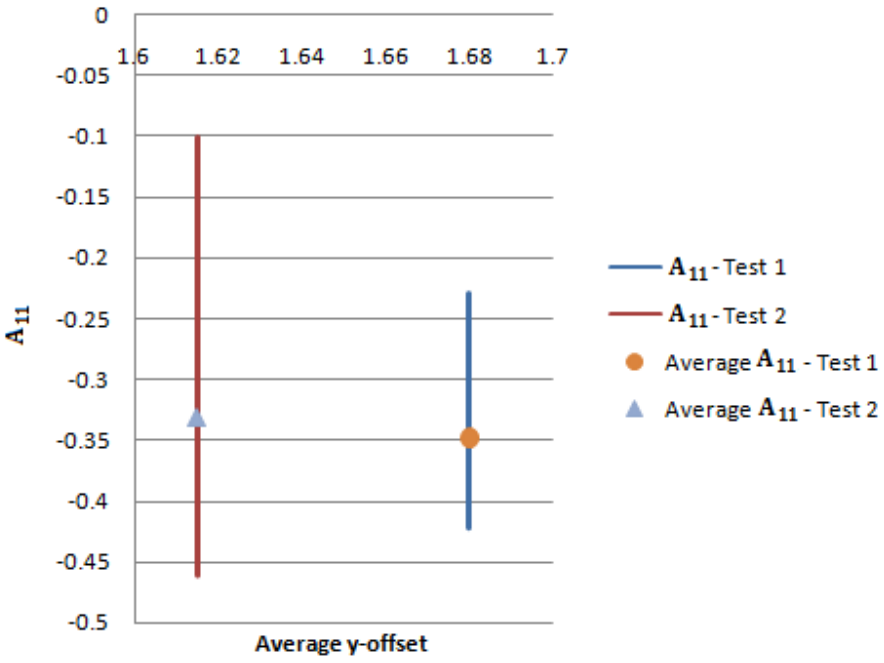

Fig 4.34 A_{11} vs. Average y-offset Graph

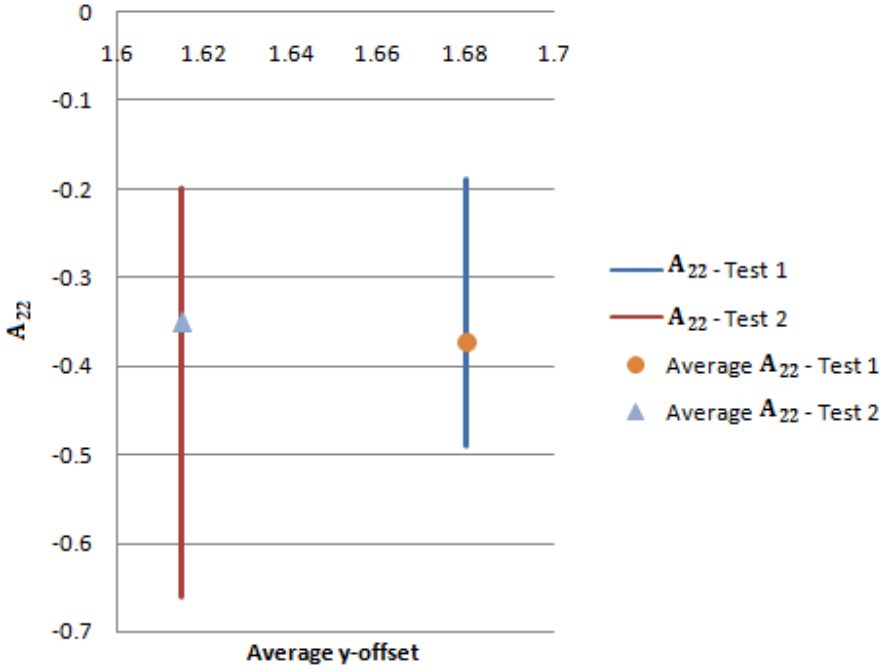

Fig 4.35 A_{22} vs. Average y-offset Graph

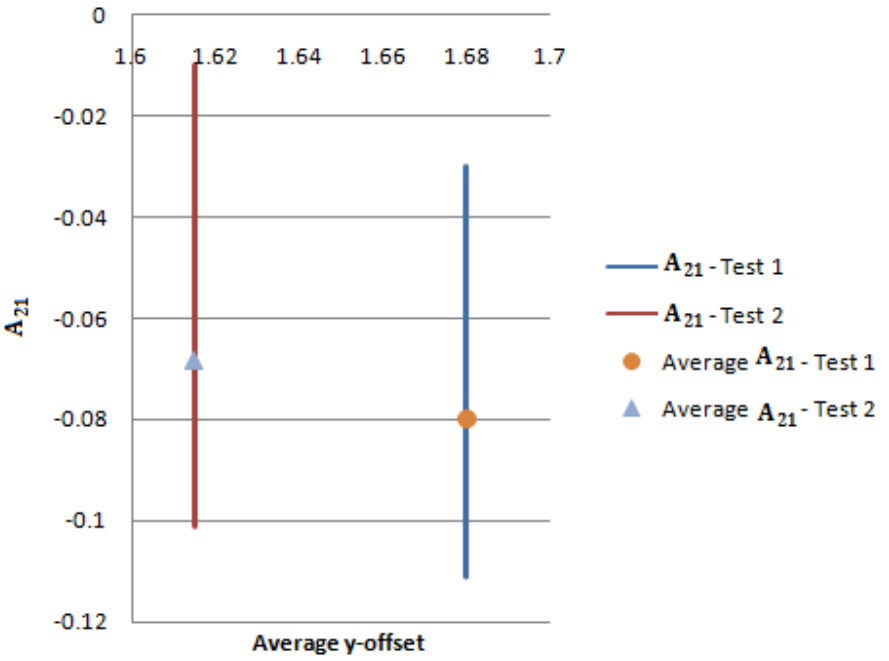

Fig 4.36 A_{21} vs. Average y-offset Graph

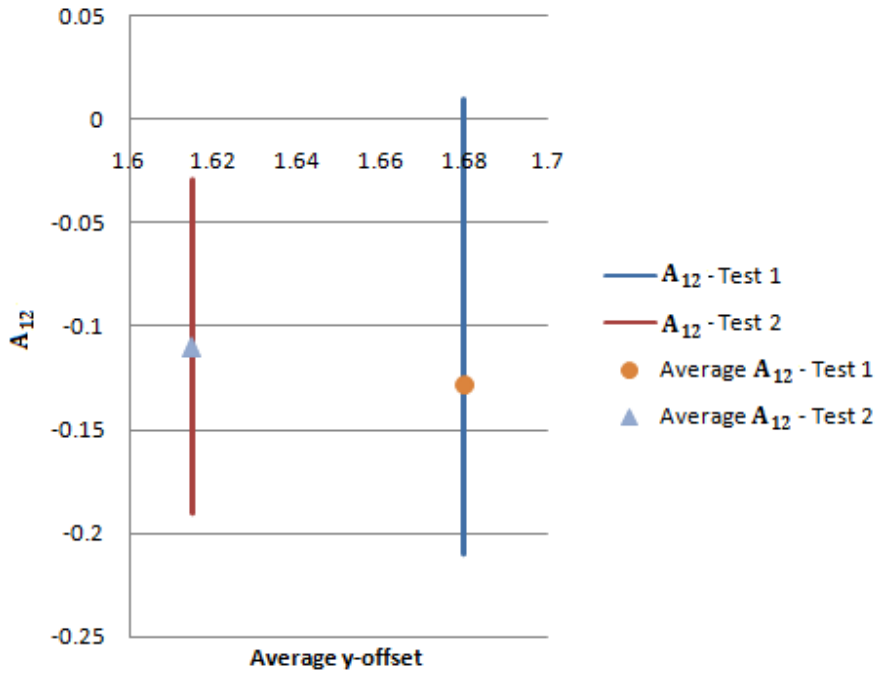

Fig 4.37 A_{12} vs. Average y-offset Graph

From the graphs above, it is clear that the gain A of g(s) varies significantly according to room temperature. Therefore, it is appropriate to conclude that the J_{ur_1} and J_{ur_2} of the simulation approximates the J_{ur_1} and J_{ur_2} of the physical system properly.

A SISO controller with both k_{11} and k_{22} elements equal to $\frac{-0.1(1+s)}{s}$, the maximum and minimum value of the gains (A_{ij}) for Test 2 were used to run simulations. A series of integrand cost function versus time graphs were obtained (The data used to plot the following graphs is given in Number 7 of Appendix A).

The Integrand cost function $J_{e_1r_1}$ and $J_{e_2r_2}$ are shown in Fig 4.38 and Fig 4.39 respectively:

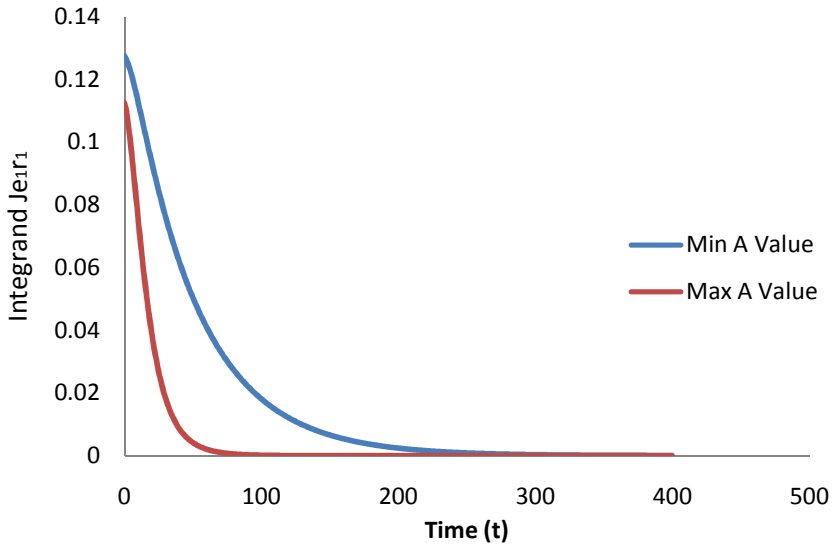

Fig 4.38 Integrand $J_{e_1r_1}$ vs. Time Graph

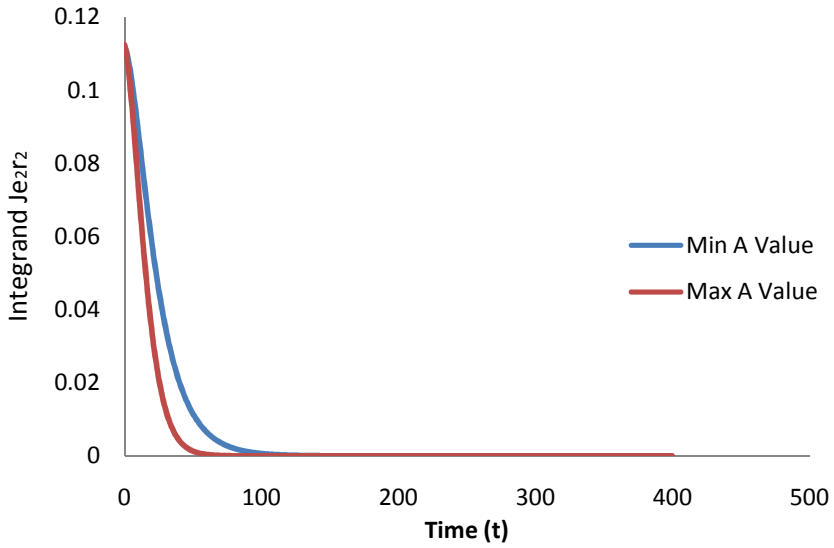

Fig 4.39 Integrand $J_{e_2r_2}$ vs. Time Graph

The Integrand cost function $J_{e_2r_1}$ and $J_{e_1r_2}$ are show below in Fig 4.40 and Fig 4.41 respectively:

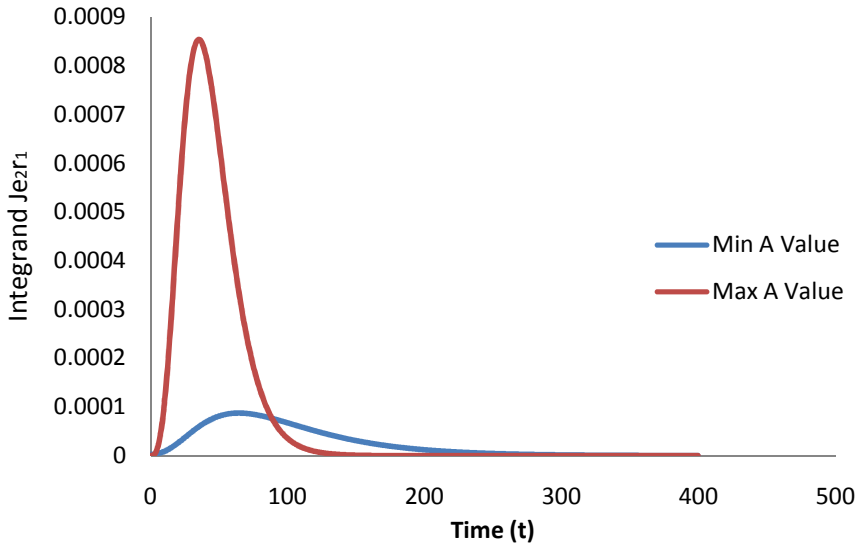

Fig 4.40 Integrand $J_{e_2r_1}$ vs. Time Graph

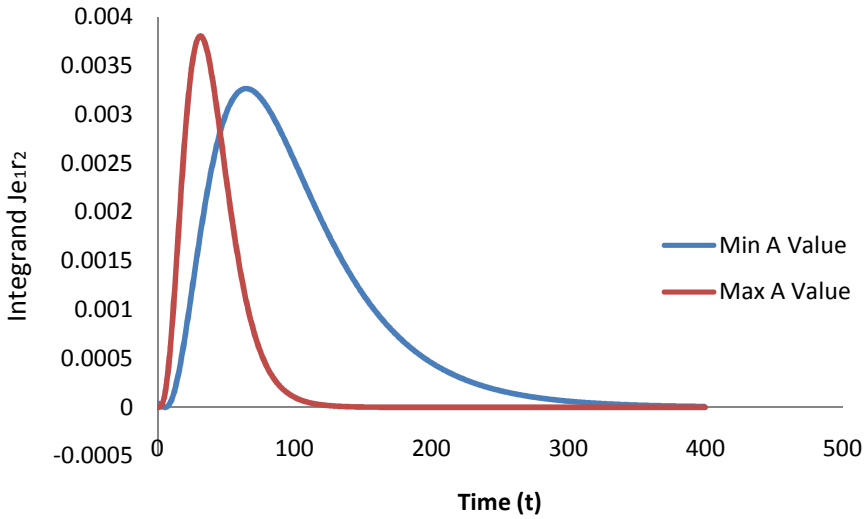

Fig 4.41 Integrand $J_{e_1r_2}$ vs. Time Graph

The Integrand cost function J_{ur_1} and J_{ur_2} are show below in Fig 4.42 and Fig 4.43 respectively:

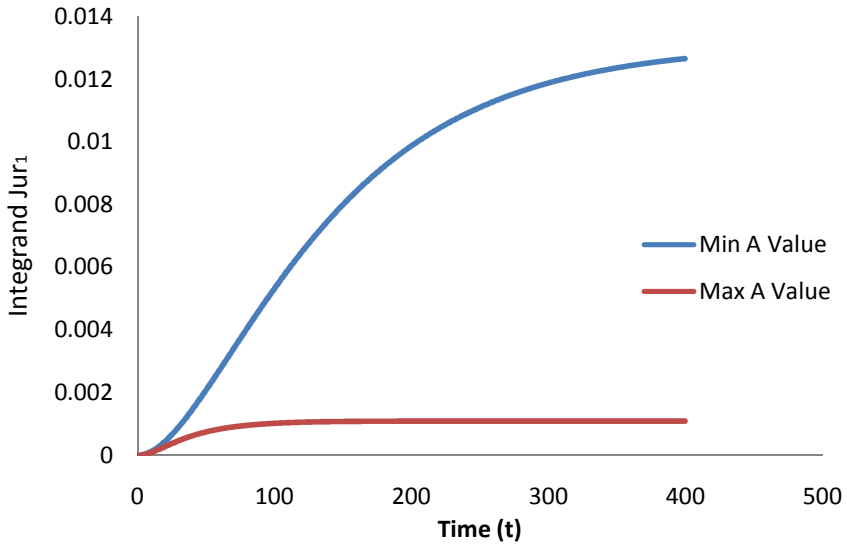

Fig 4.42 Integrand J_{ur_1} vs. Time Graph

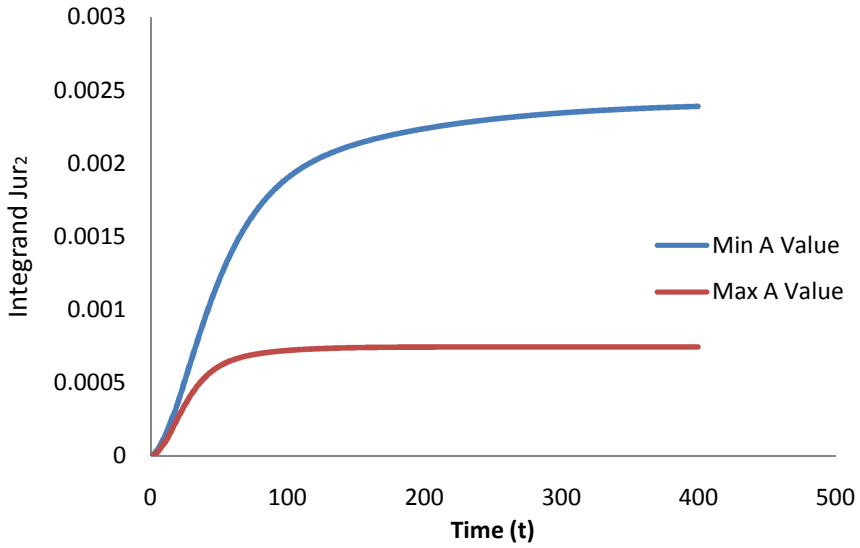

Fig 4.43 Integrand J_{ur_2} vs. Time Graph

From the above integrand cost function plots, it can be seen that as the gains (A_{ij}) changes, the integrand cost functions also change. It can therefore be concluded that the simulation does correspond to the physical system for all six different cost functions as discussed in Table 2.1.

4.3.3 DIAGONAL DOMINANCE OF SYSTEM

This study compares the SISO control scheme (which has no decoupling precompensator) and an MIMO control scheme (with decoupling precompensator) to quantify in terms of Pareto efficiency which one performs more efficiently on an MIMO system. It was therefore important to use a system which was not diagonally dominant, in order to compare the two controllers since a system that is already diagonally dominant would not benefit much from the decoupling precompensator of the MIMO controller.

In order to test for diagonal dominance, the Direct Nyquist Array (DNA) is applied to the transfer function G(s) given in Eq.(4.4), and the resulting DNA diagram is shown below in Fig 4.44:

University of Cape Tow

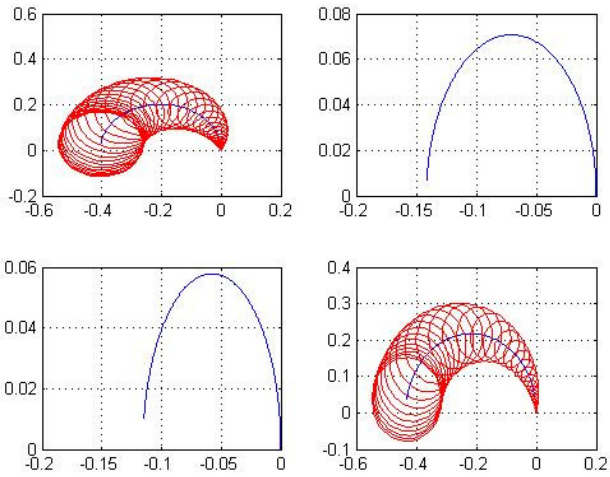

Fig 4.44 The DNA diagram of the transfer function G(s)

From the DNA diagram in Fig 4.44, it is clear that none of the Gershgorin circles encircles the origin of the diagonal $g_{11}$and g_{22} elements of the transfer function matrix G(s). This system is therefore diagonally dominant and hence not ideally suited for use in the comparison between the SISO controller and the MIMO controller.

Since the diagonal dominance of the physical thermal system cannot be altered, a decision to switch from the practical thermal system to a theoretical system based on the thermal system was made. To achieve this, the gain A_{12} was modified from -0.142 to -0.400 and the gain A_{21} from -0.116 to -0.400 to make the transfer function G(s) of the open loop system more interactive and hence not diagonally dominant. The modified transfer function G(s) is shown below in Eq. (4.12):

$$G(s)_{mod} = \begin{pmatrix} g_{11} & g_{12} \\ g_{21} & g_{22} \end{pmatrix} = \begin{pmatrix} \frac{A_{11}}{1+sT_{11}} & \frac{A_{12}}{1+sT_{12}} \\ \frac{A_{21}}{1+sT_{21}} & \frac{A_{22}}{1+sT_{22}} \end{pmatrix} = \begin{pmatrix} \frac{-0.405}{1+6.569s} & \frac{-0.400}{1+4.873s} \\ \frac{-0.400}{1+8.878s} & \frac{-0.435}{1+8.569s} \end{pmatrix} \quad (4.12)$$

The DNA diagram of the Eq. (4.14) is shown in Fig 4.45:

University of Cape Town

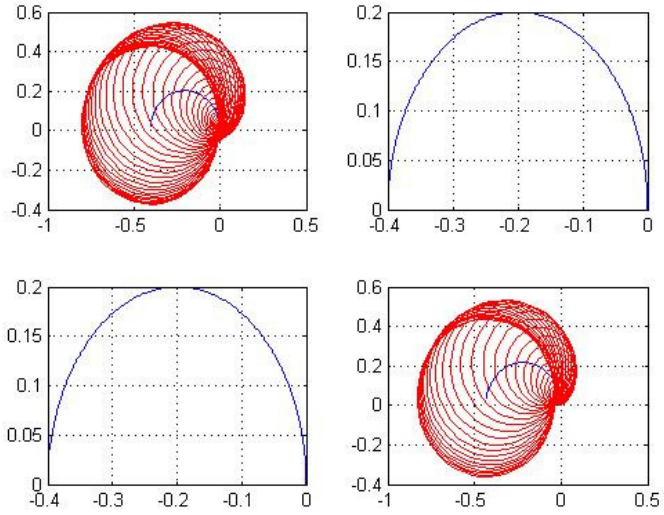

Fig 4.45 The DNA diagram of the modified transfer function G(s)

From Fig 4.45 it can be seen that some of the Gershgorin bands now enclose the origin of the diagonal $g_{11}$and g_{22} elements of the transfer function matrix. Therefore, the modified transfer function $G(s)_{mod}$ that will be used in the remainder of this investigation is not diagonally dominant.

The modified and highly interactive transfer function $G(s)_{mod}$ was used to find the six different cost functions which were defined in Table 2.1.

University of Cape Tc

Chapter 5
Method Used

This chapter explains the procedures used to obtain the results, including an explanation of the operation of the simulations.

5.1 PARETO FRONT AND LEVEL DIAGRAM

The programming language Visual Basic 6 was used to write the Pareto front simulation. This program will work out the six different cost functions for each design of the SISO controller and the MIMO controller. The results of the six different cost functions of the controller will be printed in six separate .txt files. The data from those .txt files will be pasted into Microsoft Excel, thereafter level diagrams and projected Pareto fronts will be drawn via Microsoft Excel.

This program is written based on the pseudo code in [Abbass 2001]. Once coded the operation of the program was tested by running two experimental test problems and comparing the results to those given by [Abbass 2010]. The results are given in Appendix C.

Before the Level diagram and the projected Pareto fronts could be drawn, a Region of Interest needed to be defined. (Refer to Appendix B for the significance of defining a Region of Interest.) In this study the Region of Interest is defined as shown in Table 5.1 below in order to avoid controllers that have not settled yet:

Table 5.1 Regions of Interest

Normalized value of $J_{e_1 r_1} < 0.25$
Normalized value of $J_{e_2 r_1} < 0.25$
Normalized value of $J_{e_1 r_2} < 0.25$
Normalized value of $J_{e_2 r_2} < 0.25$
Normalized value of $J_{ur_1} \in R$
Normalized value of $J_{ur_2} \in R$

University of Cape Town

5.2 HYPER VOLUME

The program to estimate the hyper volume simulation is also written in Visual Basic 6. Once the Region of Interest has been defined, one million 6-dimensional random points within the Region of Interest will be generated. The random points will be categorized into three different types, where A is the SISO controller and B is the MIMO controller as shown in Table 5.2 below:

Table 5.2 Three Different Category of Random Points

Category 1	Points dominated by Pareto front A only
Category 2	Points dominated by Pareto front B only
Category 3	Points dominated by both Pareto front A and Pareto front B

Then the program will count and keep a record of the number of points in each category. The hyper volume will be calculated as shown in Table 5.3:

Table 5.3 Hyper Volume

$I_H(A)=\frac{(\text{Category 1})+(\text{Category 3})}{1000000}$
$I_H(B)=\frac{(\text{Category 2})+(\text{Category 3})}{1000000}$
$I_H(A \cup B)=\frac{\text{Category 3}}{1000000}$

The simulation will also record the random points being generated, so it can be used to calculate the Centroid. The next step includes storing the random points in three different independent .txt files according to their category.

5.3 CENTROID

Each category's random points' data were copied and pasted into Microsoft Excel. Since the random points were in 6-dimensions, the recursive mean of each dimension could be found. The

University of Cape Town

6-dimensional mean point will be the Centroid of that specific set of data. All the necessary calculations were done in Microsoft Excel.

The recursive mean of each dimension is calculated by using the formula [Africa 2006] as shown in Eq. (5.1) below:

$$\overline{X}_{N+1} = \frac{N}{N+1}\overline{X}_N + \frac{1}{N+1}X_{N+1} \tag{5.1}$$

University of Cape Town

Chapter 6
Results and Discussion

The aim of this Chapter is to show and analyze the results obtained from the simulations.

6.1 LEVEL DIAGRAM AND PARETO FRONT

The six cost functions defined in Table 2.1 were considered when running the simulation to obtain the Pareto front. Hence, Pareto fronts with 6-dimensions were obtained from the simulation and it is probably worth recalling that each point on the Pareto front represents an optimal performance in the sense that it dominates all other points in the cost function space. Level diagrams were used to analyze these multi-dimensional Pareto fronts. When required, the concept of geometric projections was applied to obtain 2-dimensional Pareto fronts in the space defined by the two chosen cost functions. The 6-dimensional Pareto front will be discussed in Section 6.1.1, whereas the Pareto front which is 2-dimensional will be discussed in Section 6.1.2.

6.1.1 LEVEL DIAGRAM NORMALIZATION

The original level diagrams and the normalized level diagrams are shown in Fig 6.1 and Fig 6.2 respectively. In Fig 6.2 the performance and the interaction cost functions ($J_{e_1r_1}$, $J_{e_2r_1}$, $J_{e_1r_2}$ and $J_{e_2r_2}$) are normalized together and the two input cost functions (J_{ur_1} and J_{ur_2}) are normalized together.

In Fig 6.1 the cost functions J_{ur_1} and J_{ur_2} are larger in size compared to the other four cost functions. This shows that Norm-2 is biased towards indicating primarily the large cost function values (J_{ur_1} and J_{ur_2}). Comparing the smallest and the largest $J_{e_2r_2}$ cost function values of the MIMO controller in Fig 6.1; although the largest value is about 28 times bigger than the smallest value, in actual fact both values are very small, therefore there should not be a big difference on the plot of $e_1$vs. Time generated from the digital simulation. On the other hand from the level diagram of Fig 6.2, the largest normalized $J_{e_1r_1}$ cost function is about 26 times bigger than the smallest normalized $J_{e_1r_1}$ cost function. Normally one would expect that the largest $J_{e_1r_1}$ would have a significantly bigger error due to loop 1 (e_1) compared to the smallest $J_{e_1r_1}$, but in fact the difference cannot really been seen on the $e_1$vs. Time plot from the digital simulation.

Thus it was decided that using the normalized level diagrams (Fig 6.2) was more suitable in order to analyze the two controllers, therefore all the level diagrams that appear later in this project will be normalized the same way as shown in Fig 6.2.

University of Cape Town

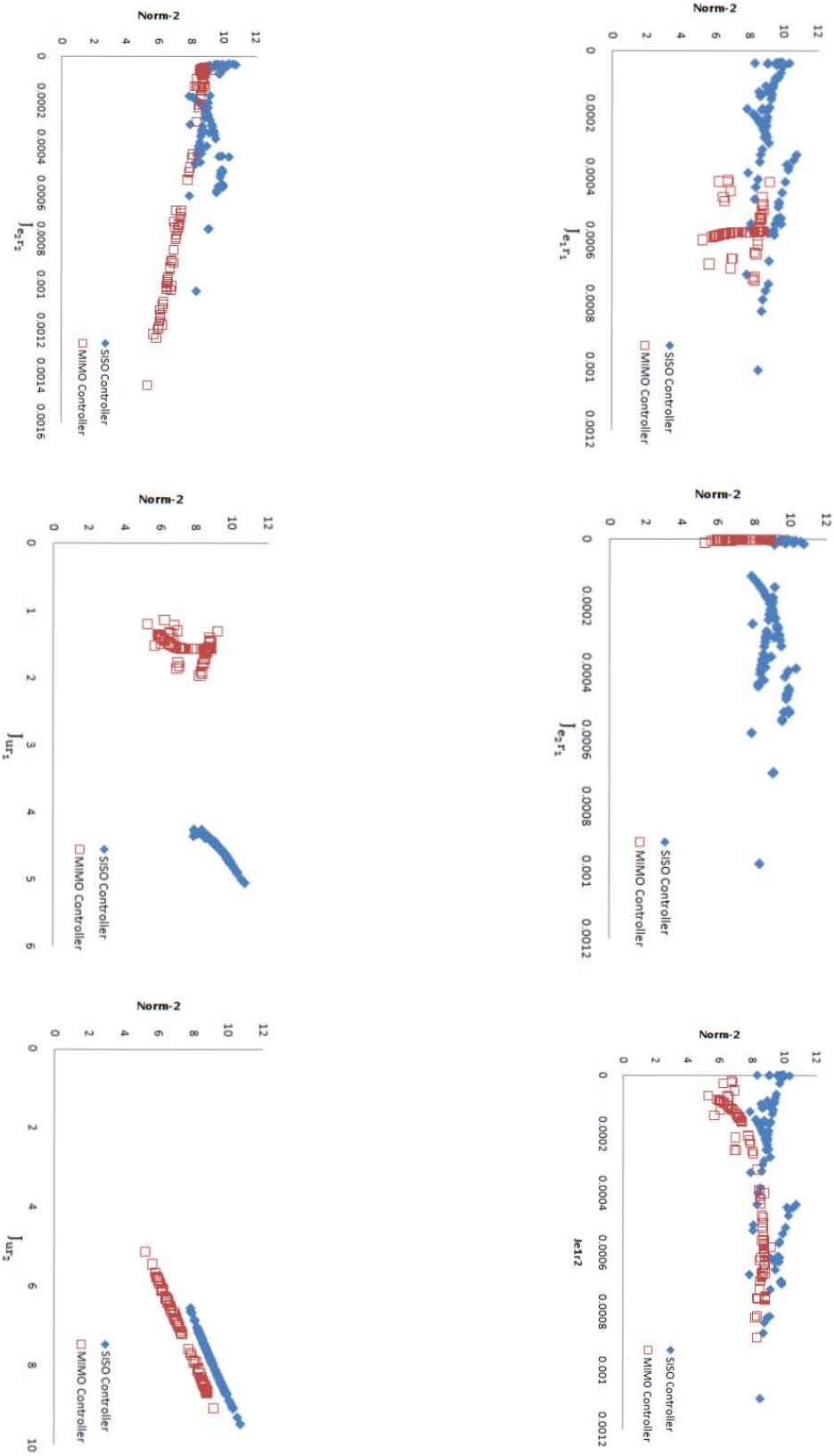

Fig 6.1 Original Level Diagrams

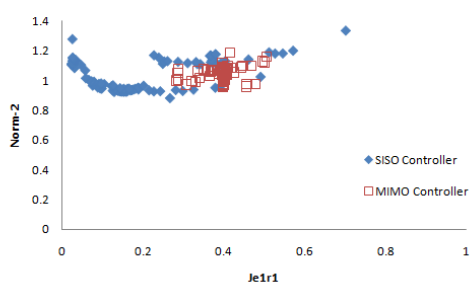

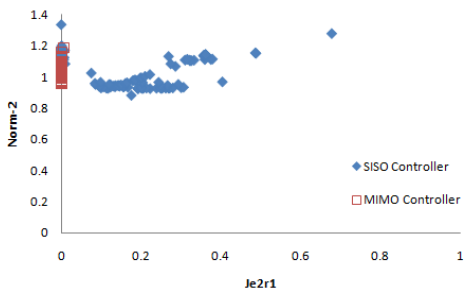

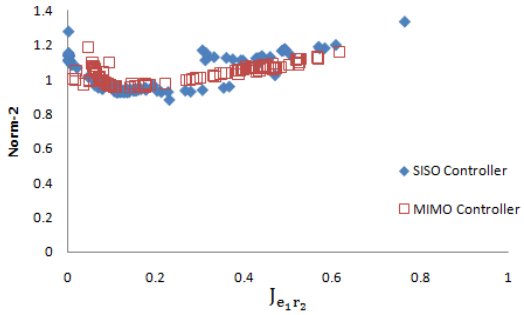

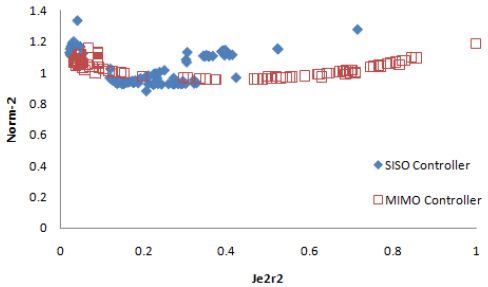

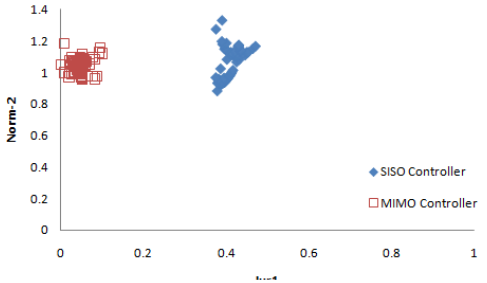

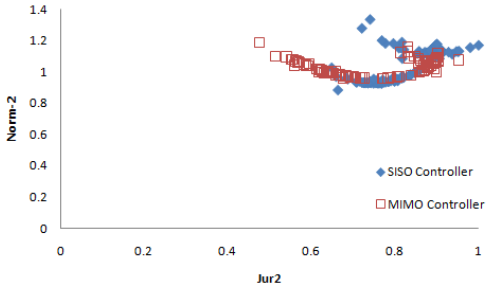

Fig 6.2 Normalized Level Diagrams

The data used to plot Fig 6.1 is given in file Number 8 listed in Appendix A, and the data used to plot Fig 6.2 is given in file Number 9.

6.1.2 LEVEL DIAGRAM AND PARETO FRONT IN 6-DIMENSIONS

The detailed results of the Pareto front that were derived from the simulation are given below, the Pareto front is in 6-dimensions and each cost function is plotted against the Norm-2, to provide simultaneous visualization of all the six different cost functions. The data used to plot the graphs is in a Microsoft Excel file, given in file Number 9 of Appendix A.

The first plot is shown in Fig 6.3. By inspecting this individual cost functions $J_{e_1r_1}$ on the level diagram it can readily be seen (1) from the y-axis values of the Pareto front points that all the points lie roughly in the same cost function space in which the overall cost function is a minimum, (2) from the x-axis values that the setpoint tracking performances of the optimal controllers of both the SISO and the MIMO configuration vary considerably within the region of interest and (3) also from the x-axis values that the performance of the SISO controller is better than the MIMO controller for tracking the setpoint in the first loop.

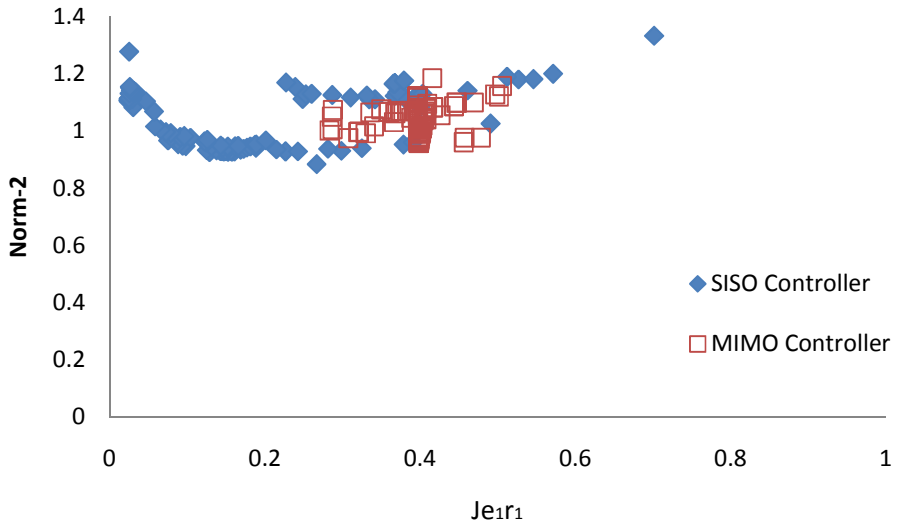

Fig 6.3 Level Diagram of $J_{e_1r_1}$ vs. Norm-2

In general the SISO controller has less or the same value of cost function $J_{e_1r_1}$ compared to the MIMO controller. The Pareto front points overlap in the level diagram indicating that some parameter values will produce SISO and MIMO controllers that track setpoints in the first loop with equal optimality. However it is also apparent that the SISO controllers outperform the MIMO controllers under other conditions, but not all. Clearly the cluster of points at very good tracking (for loop 1) are produced by the SISO controller making it the best choice for such tasks. The plot also shows that the MIMO controller can produce some optimal control systems that would not track the setpoint r_1 optimally.

Fig 6.4 is the second plot in the level diagram and shows the interaction from the setpoint in the first loop to the output in the second loop. It is very clear that in most cases the cost function $J_{e_2r_1}$ of the MIMO controller is nearly zero. This is expected since the precompensator was designed to remove this interaction exactly. Thus when looking at the cost function $J_{e_2r_1}$ of the SISO controller, its values are mostly larger than the MIMO controller's values. However with the visualization provided by the level diagram it is also clear that some optimal SISO controllers have interactions that are highly competitive with that obtained by the MIMO controller with its decoupling precompensator. Therefore, it can be concluded that the cost function $J_{e_2r_1}$ of the MIMO controller generally performs better than the same cost function of the SISO controller.

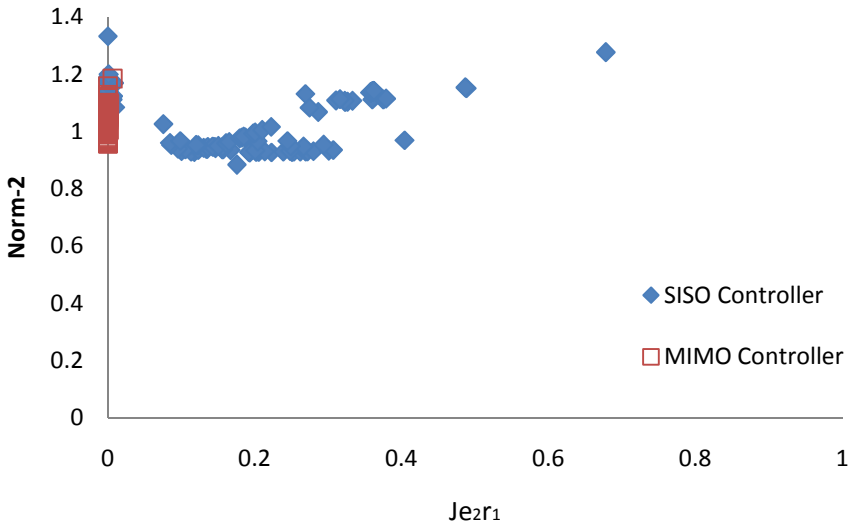

Fig 6.4 Level Diagram of $J_{e_2r_1}$ vs. Norm-2

Combining the above two plots in a level diagram illustrates the ease with which the performance of the two loops can be compared in terms of these two cost functions ($\mathbf{J_{e_1r_1}}$ and $\mathbf{J_{e_2r_1}}$). Obviously the Pareto front data could have been plotted in two-dimensions to show the trade-off between setpoint tracking in the first loop and coupling into the second loop. However this would not allow simultaneous visualization of the 6-dimensional cost function space that is allowed by the level diagrams as shown in Fig.6.2.

The next cost function considered is the disturbance to loop 1 that is caused by a change in the setpoint in loop 2. Its level diagram plot is given in Fig 6.5. From the spread of points on the Pareto front it is reasonable to say that in many cases the cost function $J_{e_1r_2}$ performs nearly the same on both the SISO controller and the MIMO controller, but that in the worse cases the SISO controller will have more interaction error compared to the MIMO controller.

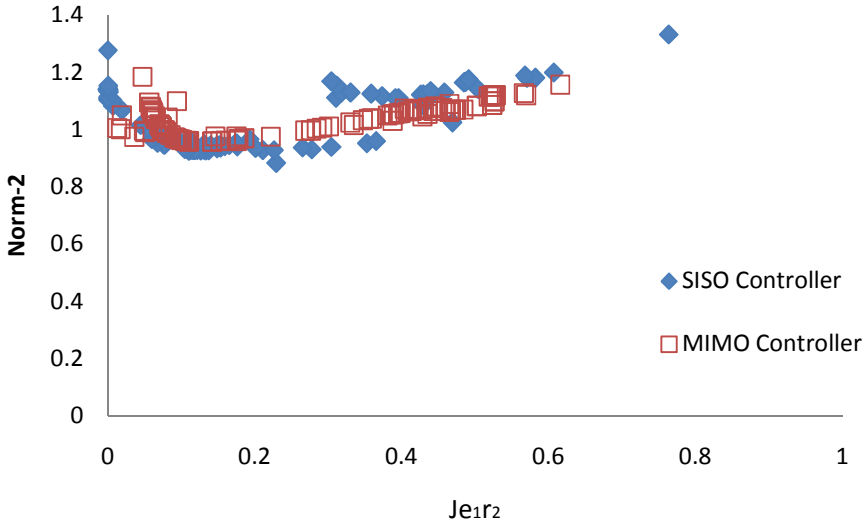

Fig 6.5 Level Diagram of $J_{e_1r_2}$ vs. Norm-2

Fig 6.6 is the next plot in the level diagram that is considered. In general both controllers perform nearly the same and in the worse case the SISO controller also performs better than the MIMO controller. But by looking at the most optimal design in terms of the overall cost function, the SISO controllers have a slightly smaller cost function $J_{e_2r_2}$ compared to the MIMO controller. Thus the plot indicates that both controllers will have a similar amount of error due to loop 2 (e_2) when the setpoint of loop 2 (r_2) is stepped. However in the worst-case scenario MIMO controllers will have more error compared to the SISO controllers.

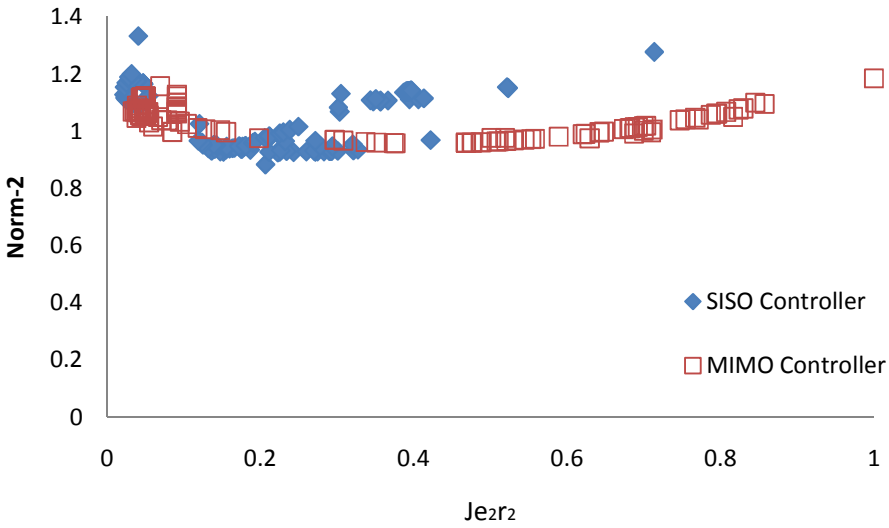

Fig 6.6 Level Diagram of $J_{e_2r_2}$ vs. Norm-2

The above four plots in the level diagram provide the design engineer with effective visualizations showing how the two control schemes, SISO and MIMO, will perform in terms of setpoint tracking and interaction between the two loops.

The next two plots deal with the cost of achieving the performance. The first plot would be the fifth plot in the level diagram for the designs. It is shown in Fig 6.7 and clearly indicates that in general the cost of input for loop 1 (J_{ur_1}) of the MIMO controller is much smaller than the cost of input for loop 1 (J_{ur_1}) of the SISO controller.

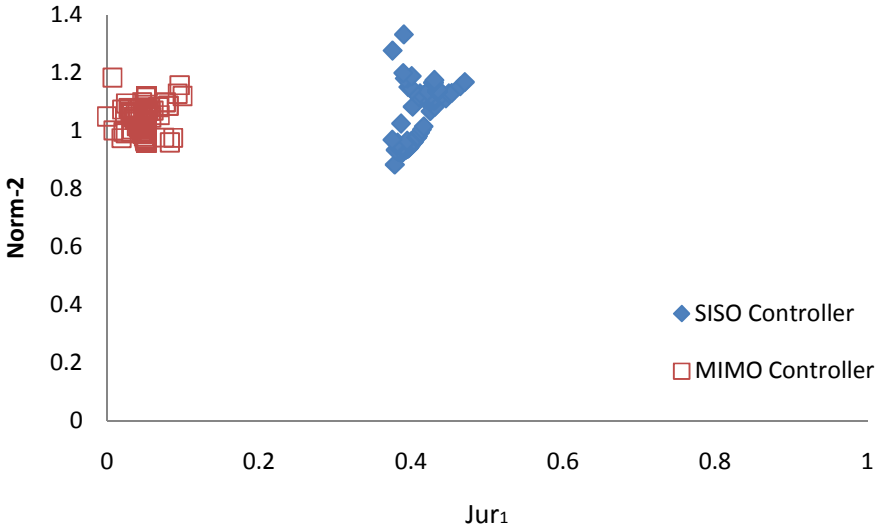

Fig 6.7 Level Diagram of J_{ur_1} vs. Norm-2

The last of the plots in the level diagram is shown in Fig 6.8. Clearly there is virtually no difference in the cost of input for loop 2 (J_{ur_2}) in most cases between the SISO controller and the MIMO controller though in the optimal cases, the MIMO controller uses less, but the overall performance gets worse. It is noted that in some cases, the MIMO controller uses more input to reduce the overall Norm-2 cost.

University

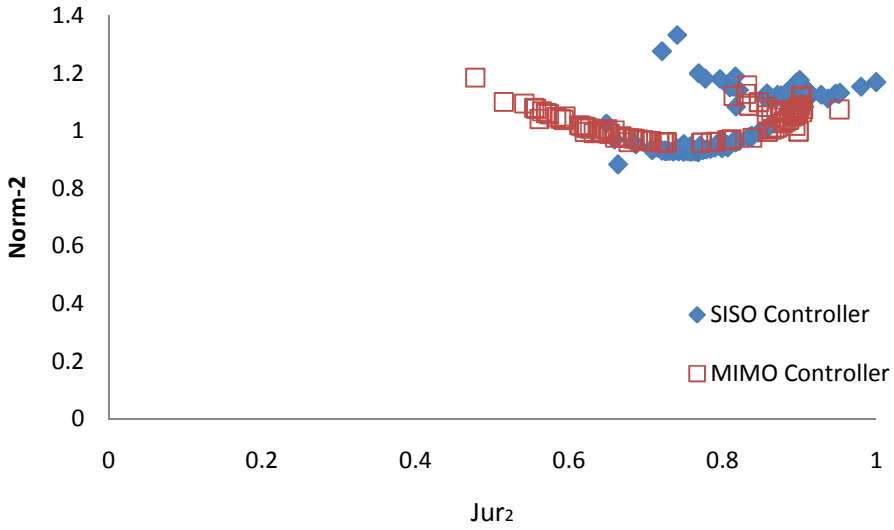

Fig 6.8 Level Diagram of J_{ur_2} vs. Norm-2

6.1.2.1 DIGITAL SIMULATIONS OF THE SISO CONTROLLER

The observations made from the Level Diagram will be verified by digital simulation for three cases that are representative of two extremes and a mid point deduced from the level diagram. These three cases will be referred to as "min" for the best controller, "max" for the worst controller and "mid" for the controller with a performance somewhere between "min" and "max". These points will be used to plot the digital simulation of the input u(t), output y(t) and error e(t) graphs of the system. The three points picked from the level diagrams of the SISO controller are shown in Table 6.1 below:

University of Cape Tow

Table 6.1 The Three Points Picked from the Level Diagrams of the SISO controller

Point	Norm-2	Parameters	Cost Functions
max of SISO	1.333	k_{11}= -0.100 ; k_{22}= -2.375 I_{11}= 0.244 ; I_{22}= 0.100	$J_{e_1r_1}$= 0.702 ; $J_{e_2r_1}$= 1.864E-04 $J_{e_1r_2}$= 0.764 ; $J_{e_2r_2}$= 0.041 J_{ur_1}= 0.391 ; J_{ur_2}= 0.740
mid of SISO	1.103	k_{11}= -3.018 ; k_{22}= -2.808 I_{11}= 0.100 ; I_{22}= 2.907	$J_{e_1r_1}$= 0.024 ; $J_{e_2r_1}$= 0.323 $J_{e_1r_2}$= 0.001 ; $J_{e_2r_2}$= 0.357 J_{ur_1}= 0.427 ; J_{ur_2}= 0.896
min of SISO	0.884	k_{11}= -2.019; k_{22}= -1.634 I_{11}= 3.424; I_{22}= 2.493	$J_{e_1r_1}$= 0.267 ; $J_{e_2r_1}$= 0.176 $J_{e_1r_2}$= 0.229 ; $J_{e_2r_2}$= 0.207 J_{ur_1}= 0.379 ; J_{ur_2}= 0.663

Figure 6.9 show where those three points are sitting on the level diagrams:

University of Cape Town

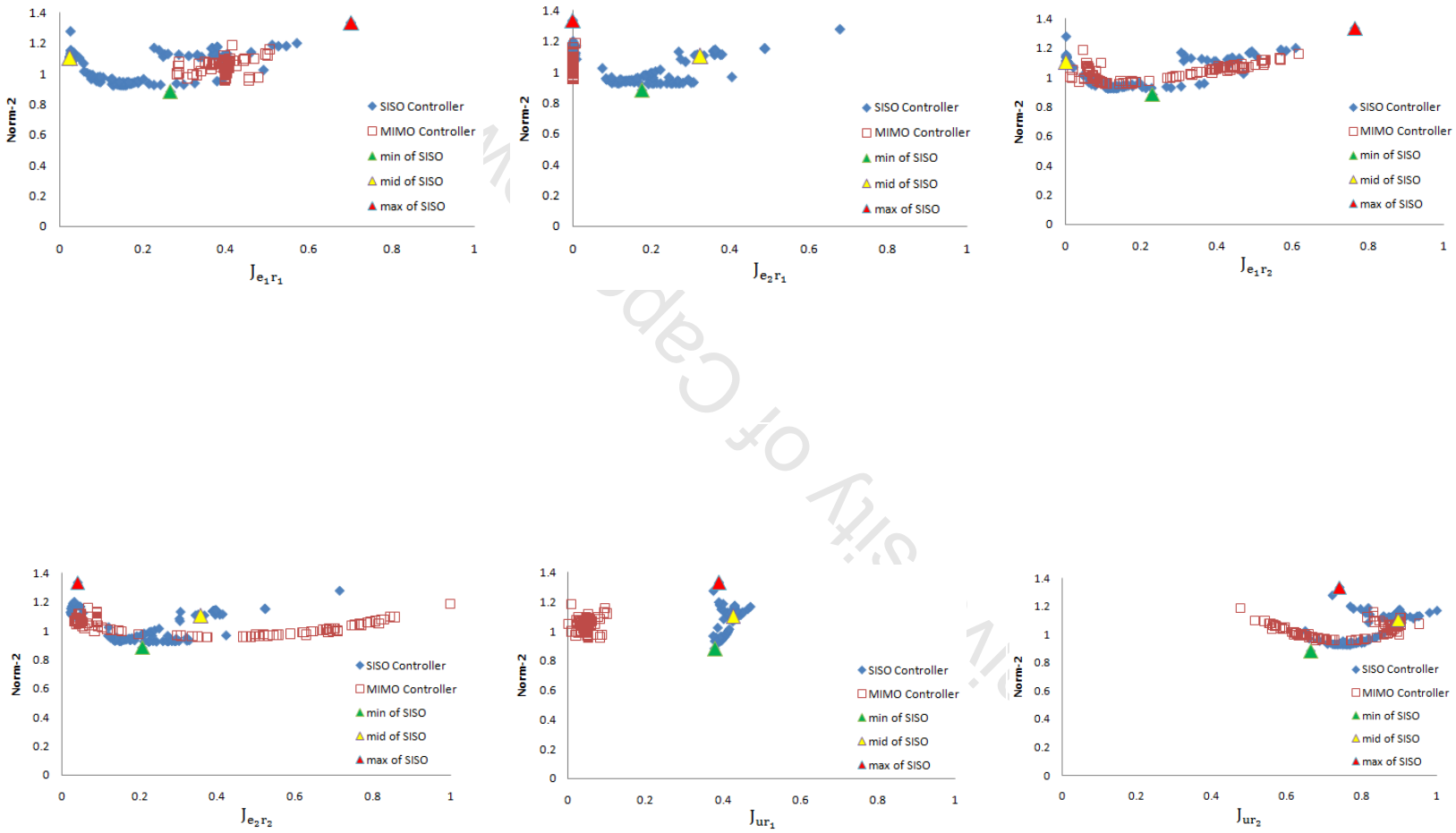

Fig 6.9 The Three Chosen Points and the Level Diagrams

ersity of Cap

The digital simulations of the input u(t), output y(t) and error e(t) graphs of the system are plotted below. The data used for these plots is given in file Number 10 listed in Appendix A. The time plots show the responses of the system to start-up at t = -50 [s], a step in r_1 at the t = 0 and a step in r_2 at t = 400. The three cases in each plot are for the min, mid and max optimal designs as indicated on the graph (Fig 6.9).

From Fig 6.9 and Fig 6.10, the max point is the one with the most error due to loop 1 (e_1). The mid point has the smallest error due to loop 1 (e_1) when either the setpoint of loop 1 (r_1) or loop 2 (r_2) is stepped. It is noted that it is not the point with the smallest Norm-2 value (min) got the smallest error due to loop 1 (e_1), it is actually the mid point that shows the smallest errors due to loop 1 (e_1).

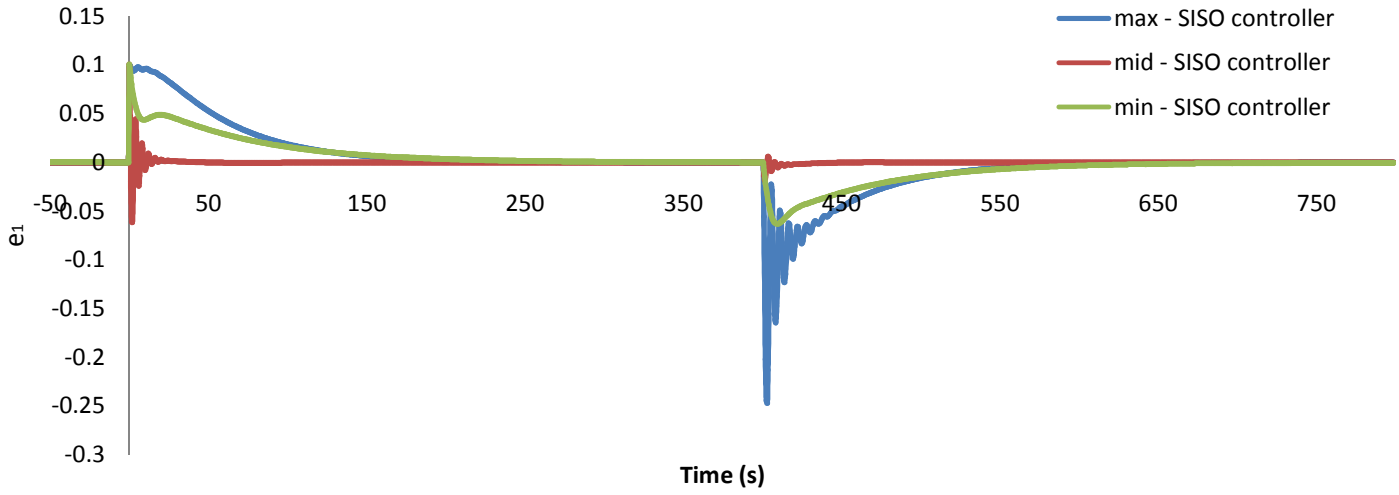

Fig 6.10 Error e_1 vs. Time plot of the SISO controller

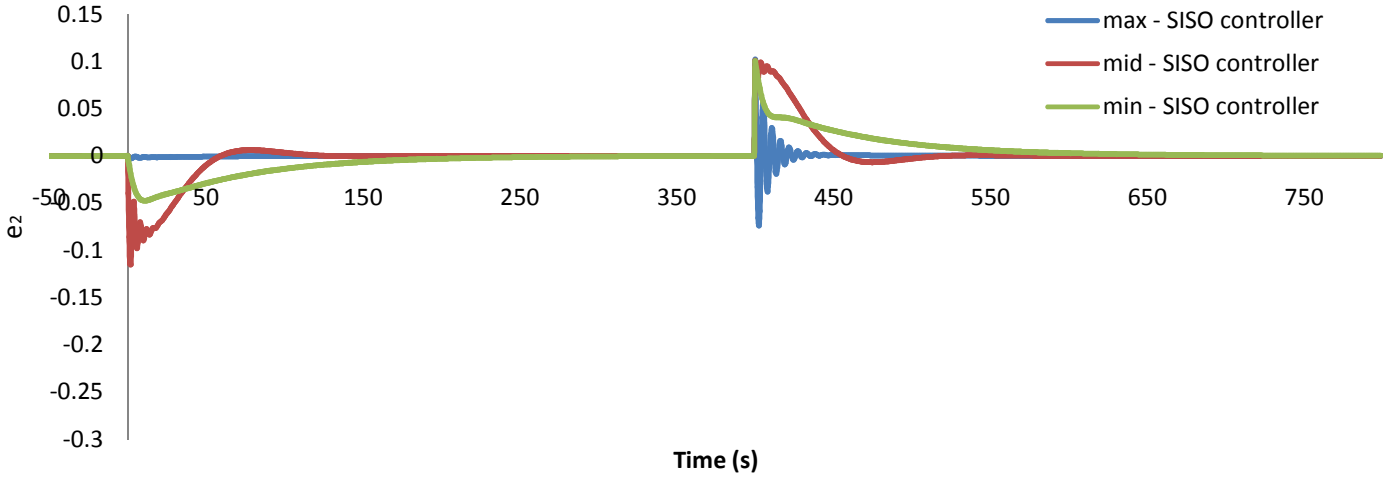

Fig 6.11 Error e_2 vs. Time plot of the SISO controller

From Fig 6.11 and Fig 6.9, it is noted that the max point is the one with the largest value of Norm-2 but it has the smallest value of error due to loop 2 (e_2). And the mid point got the largest amount of error due to loop 2 (e_2), but not the min point got the smallest error due to loop 2 (e_2).

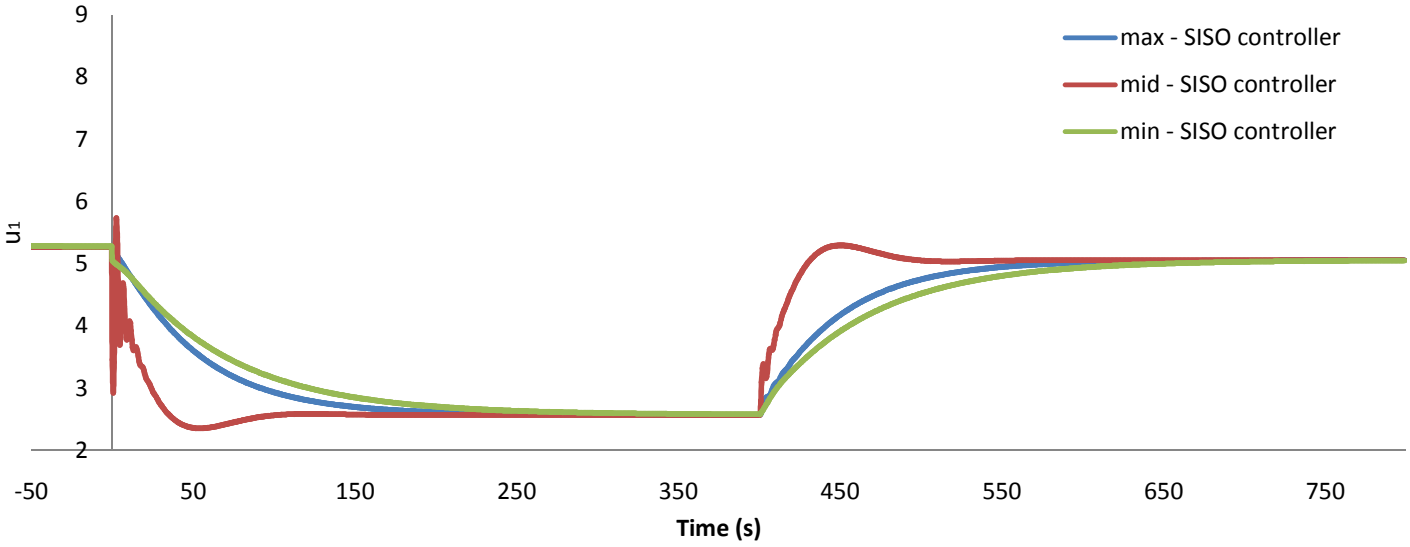

Fig 6.12 Input u_1 vs. Time plot of the SISO controller

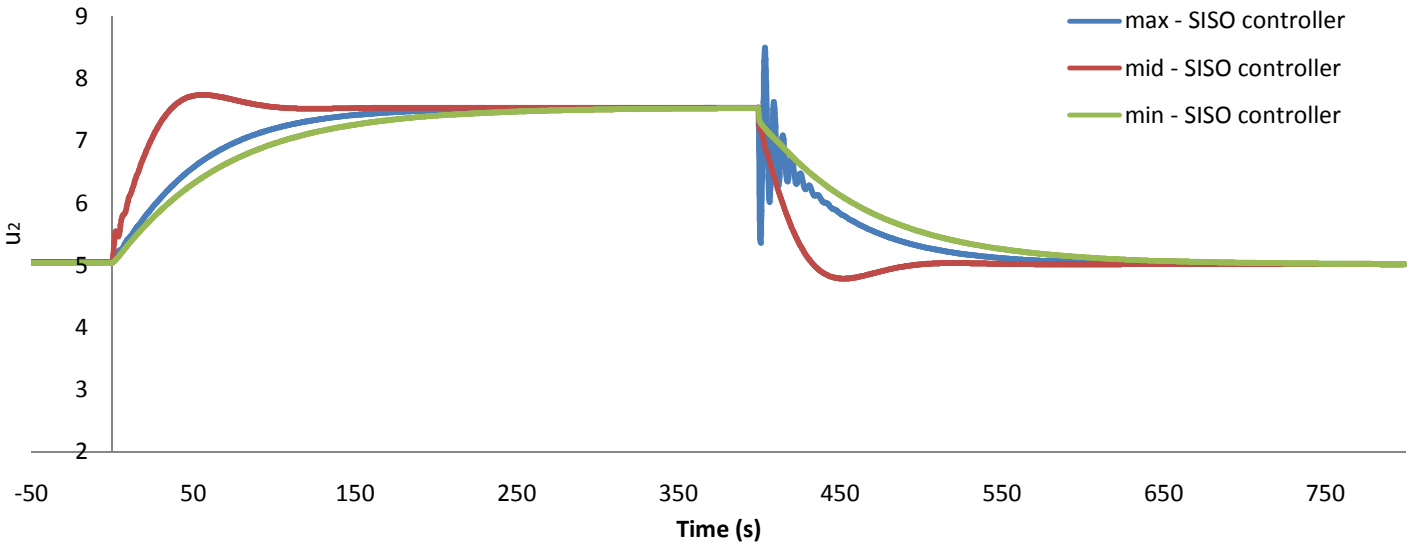

Fig 6.13 Input u_2 vs. Time plot of the SISO controller

From Fig 6.9, Fig 6.12 and Fig 6.13, it shows that SISO controller design with the larger value of Norm-2 does not mean it would require more inputs due to loop 1 (u_1) and loop 2 (u_2). The max point is one with the largest value for Norm-2, but it doesn't use the most inputs on the two loops. Whereas the mid point don't have the largest value of Norm-2, but it uses the most inputs on both loops.

From Fig 6.9, Fig 6.14 and Fig 6.15, it shows that the SISO controller design with a smallest value of Norm-2 (min) has the least oscillation, whereas the max point case has lots of oscillation at high frequency.

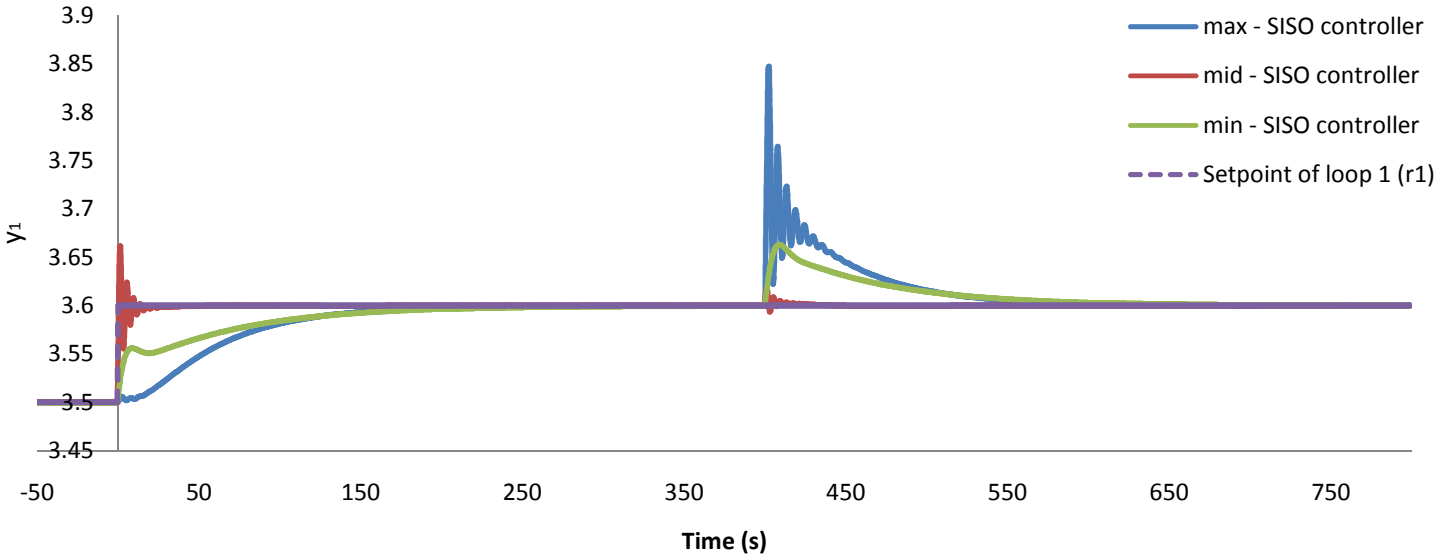

Fig 6.14 Output y_1 vs. Time plot of the SISO controller

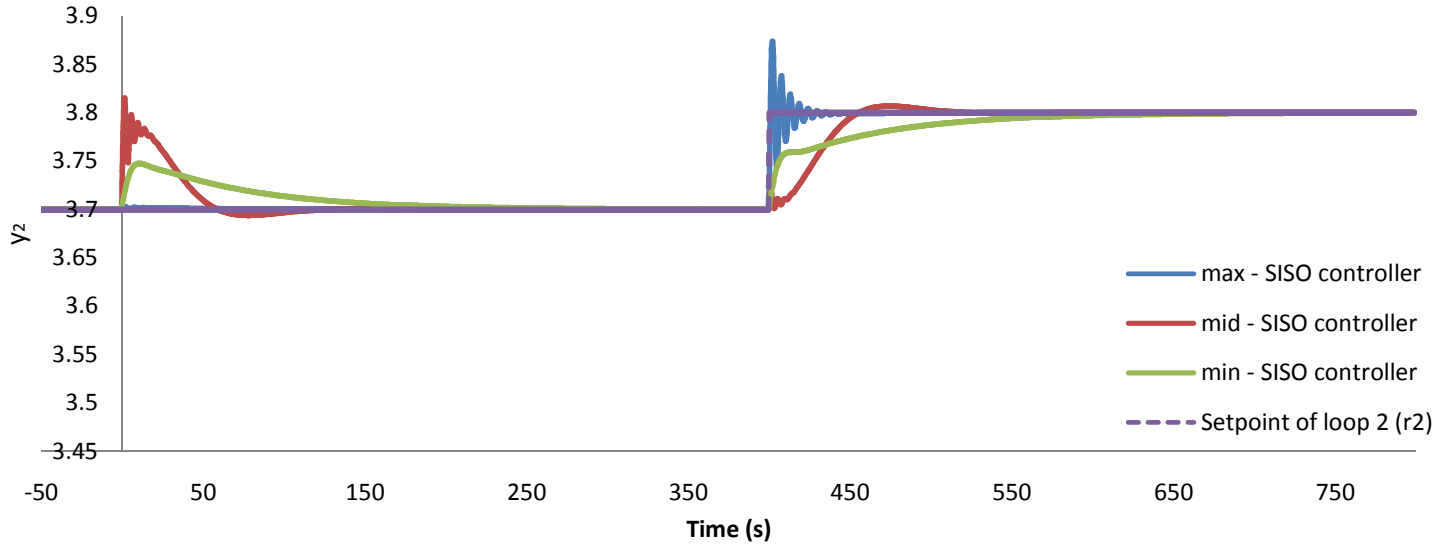

Fig 6.15 Output y_2 vs. Time plot of the SISO controller

The above digital simulations shows that, the level diagrams do predict the behavior of the SISO controller correctly.

6.1.2.2 DIGITAL SIMULATIONS OF THE MIMO CONTROLLER

The three points picked from the level diagrams of the MIMO controller are shown in Table 6.2 below:

Table 6.2 The Three Points Picked from the Level Diagrams of the MIMO controller

Point	Norm-2	Parameters	Cost Functions
max of MIMO	1.185	k_{11}= -0.100 ; k_{22}= -0.100 I_{11}= 0.100 ; I_{22}= 4.103	$J_{e_1r_1}$= 0.416 ; $J_{e_2r_1}$= 0.006 $J_{e_1r_2}$= 0.047 ; $J_{e_2r_2}$= 1.000 J_{ur_1}= 0.007 ; J_{ur_2}= 0.478
mid of MIMO	1.055	k_{11}= -0.100 ; k_{22}= -1.653 I_{11}= 0.100 ; I_{22}= 0.100	$J_{e_1r_1}$= 0.397 ; $J_{e_2r_1}$= 1.311E-07 $J_{e_1r_2}$= 0.390 ; $J_{e_2r_2}$= 0.055 J_{ur_1}= 0.052 ; J_{ur_2}= 0.893
min of MIMO	0.959	k_{11}= -3.276 ; k_{22}= -0.100 I_{11}= 3.676 ; I_{22}= 0.100	$J_{e_1r_1}$= 0.398 ; $J_{e_2r_1}$= 2.154E-04 $J_{e_1r_2}$= 0.142 ; $J_{e_2r_2}$= 0.377 J_{ur_1}= 0.052 ; J_{ur_2}= 0.772

Fig 6.16 shows where those three points are sitting on the level diagrams:

University of Cape Town

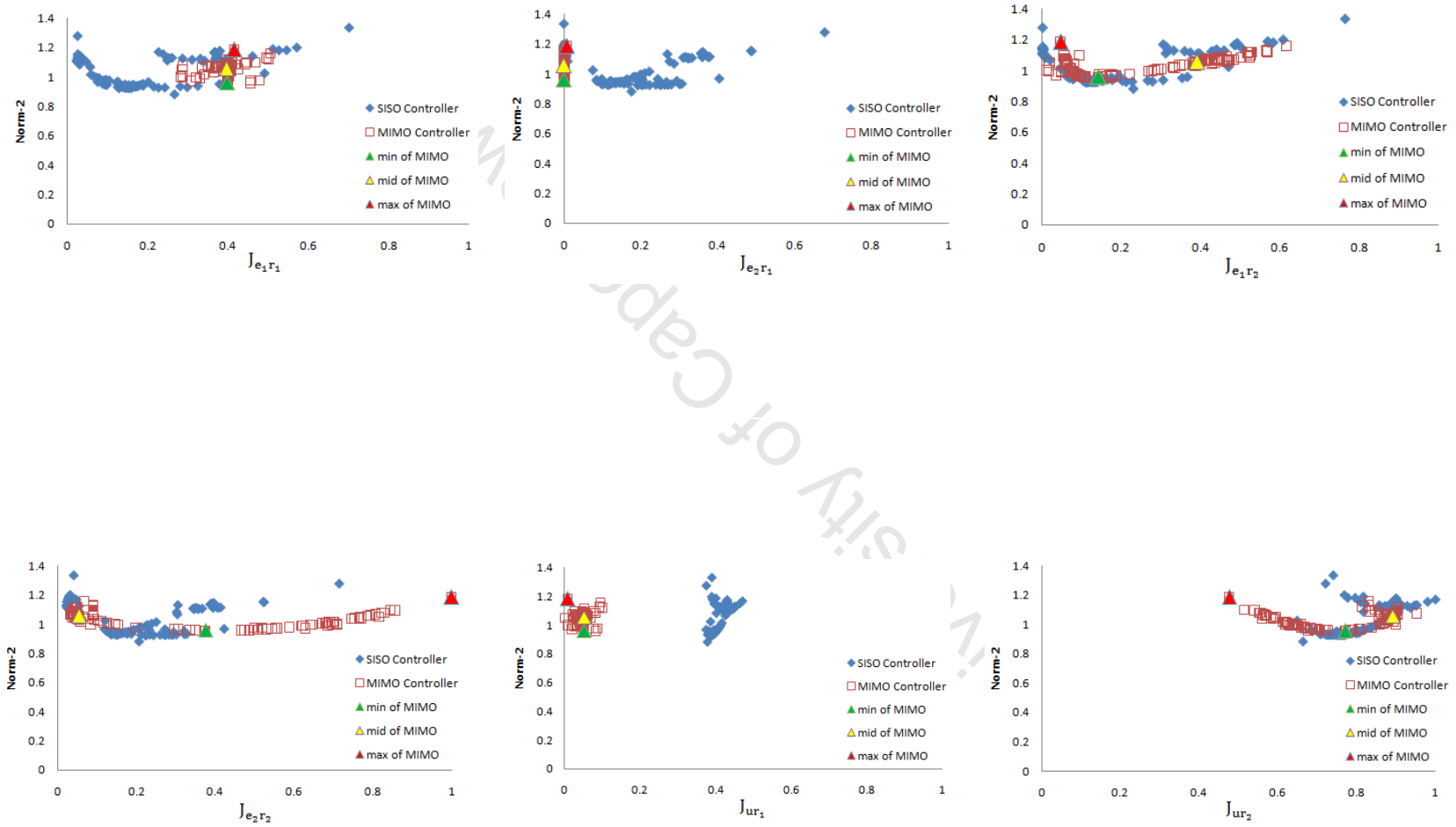

Fig 6.16 The Three Chosen Points and the Level Diagrams

...ersity of Cape...

The digital simulations of the input u(t), output y(t) and error e(t) graphs of the system are plotted below. The data used for these plots is given in file Number 10 listed in Appendix A. The time plots show the responses of the system to start-up at t = - 50 [s], a step in r_1 at the t = 0 and a step in r_2 at t = 400. The three cases in each plot are for the min, mid and max optimal designs as indicated on the graph (Fig 6.16).

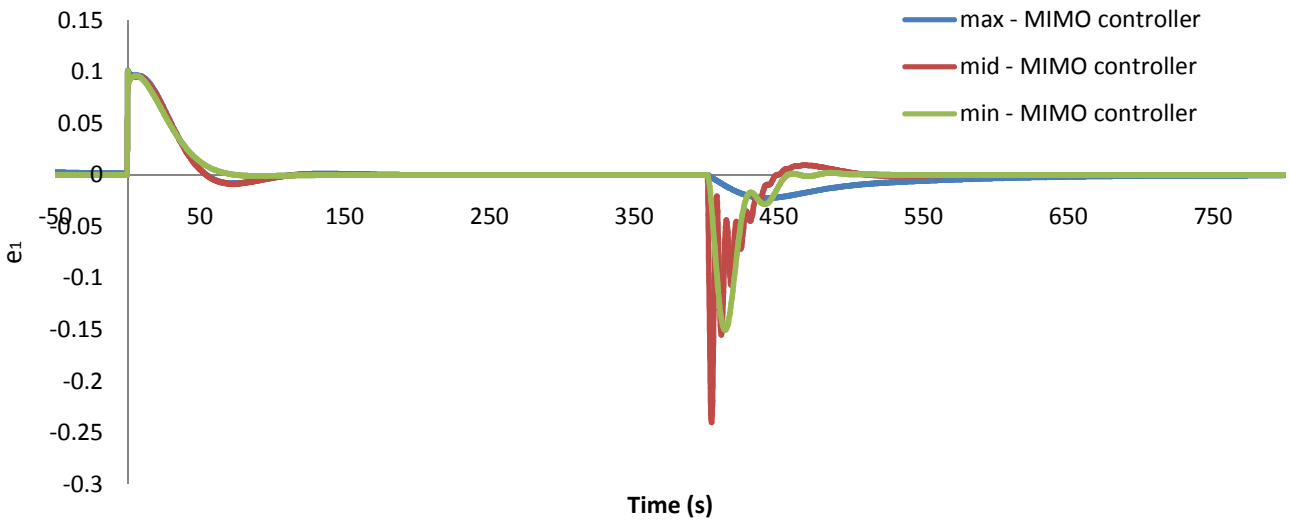

Fig 6.17 Error e_1 vs. Time plot of the MIMO controller

From Fig 6.16 and Fig 6.17, although it looks like all three points have the same amount of error due to loop 1 (e_1) when the setpoint of loop 1 (r_1) is stepped, from the level diagram it is clear that the max point is the one with the most error due to loop 1 (e_1) when the setpoint of loop 1 (r_1) is stepped. This is one drawback of the normalized level diagrams that have been mentioned in Section 6.1.1. But it is very clear that the max point is the one with the smallest error due to loop 1 (e_1) when the setpoint of loop 2 (r_2) is stepped.

Fig 6.16 and Fig 6.18 shows that the MIMO controller did ensure that no interactions due to loop 2 (e_2) occurred when the setpoint of loop 1 (r_1) was stepped. This showed that the information from the $J_{e_2 r_1}$ level diagram is correct, namely that all three points have virtually zero $J_{e_2 r_1}$. The max point is the one with the most error due to loop 2 (e_2) when the setpoint of loop 2 (r_2) is stepped. It also seems that the min point and the mid point showed similar amounts of error due to loop 2 (e_2) when the setpoint of loop 2 (r_2) was stepped. But from the normalized level diagram it shows that the min point has bigger values of $J_{e_2 r_2}$ compared to the mid point. The drawback of the normalized level diagrams that been mentioned in Section 6.1.1 is illustrated here.

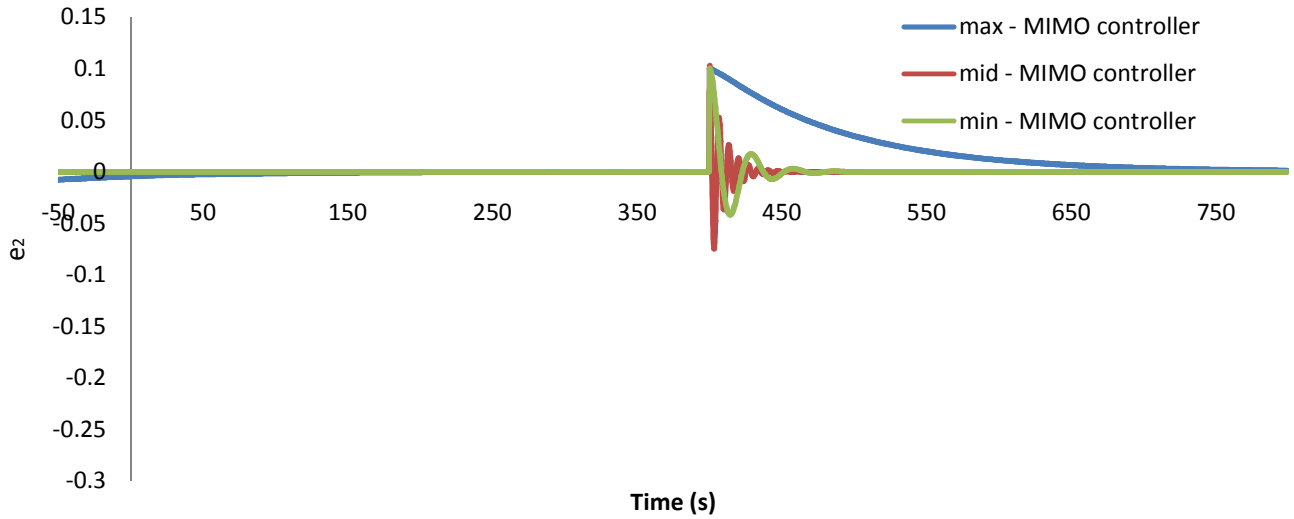

Fig 6.18 Error e_2 vs. Time plot of the MIMO controller

From Fig 6.16, Fig 6.19 and Fig 6.20, the mid point is the one using the most inputs on both loops, but it does not have the highest value of Norm-2. Whereas the max point is the one that requires the least inputs on the two loops.

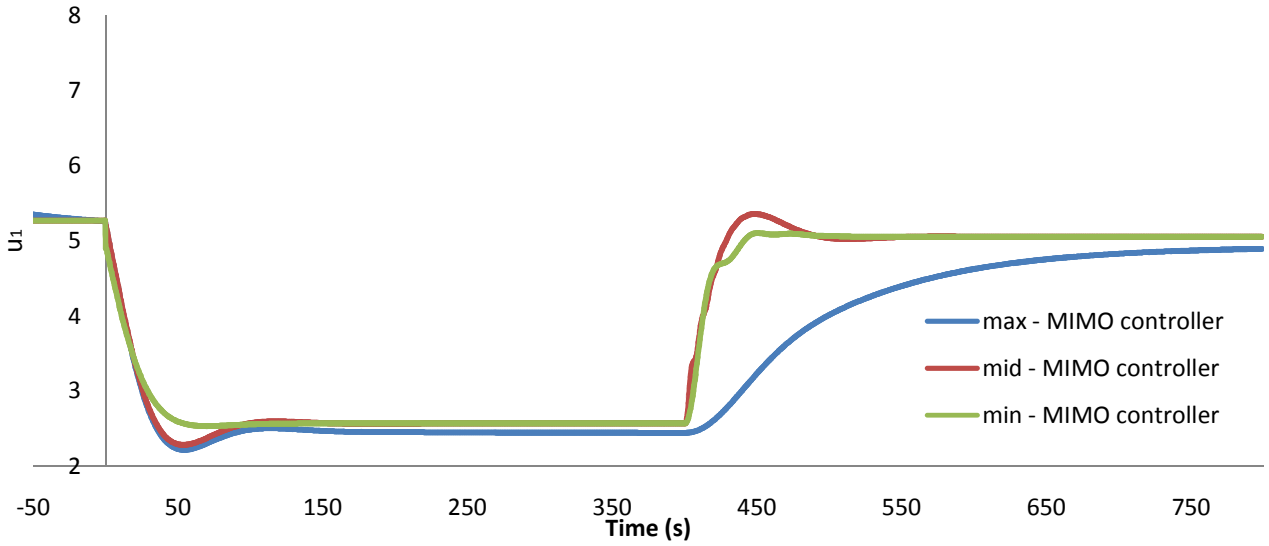

Fig 6.19 Input u_1 vs. Time plot of the MIMO controller

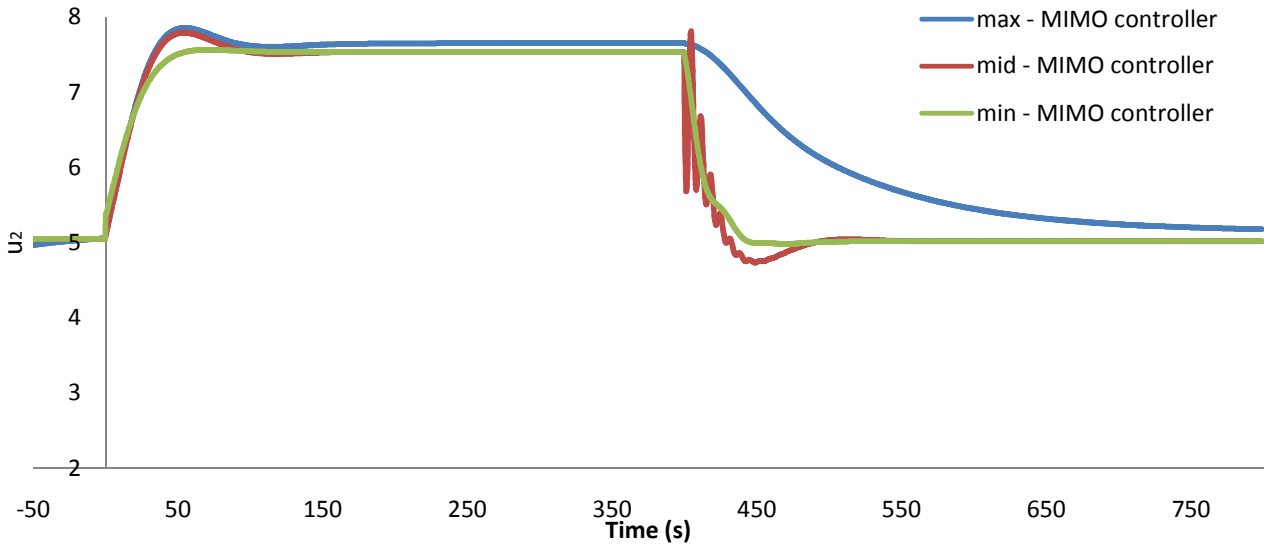

Fig 6.20 Input u_2 vs. Time plot of the MIMO controller

In Fig 6.16, Fig 6.21 and 6.22, the mid is the point with the highest frequency of oscillation and the max point shows the lowest frequency of oscillation. The mid point tracks the setpoint faster and better than the max point, which results in the mid point having smaller values for the two performance cost functions ($J_{e_1r_1}$ and $J_{e_2r_2}$) and the two interaction cost functions ($J_{e_1r_2}$ and $J_{e_2r_1}$).

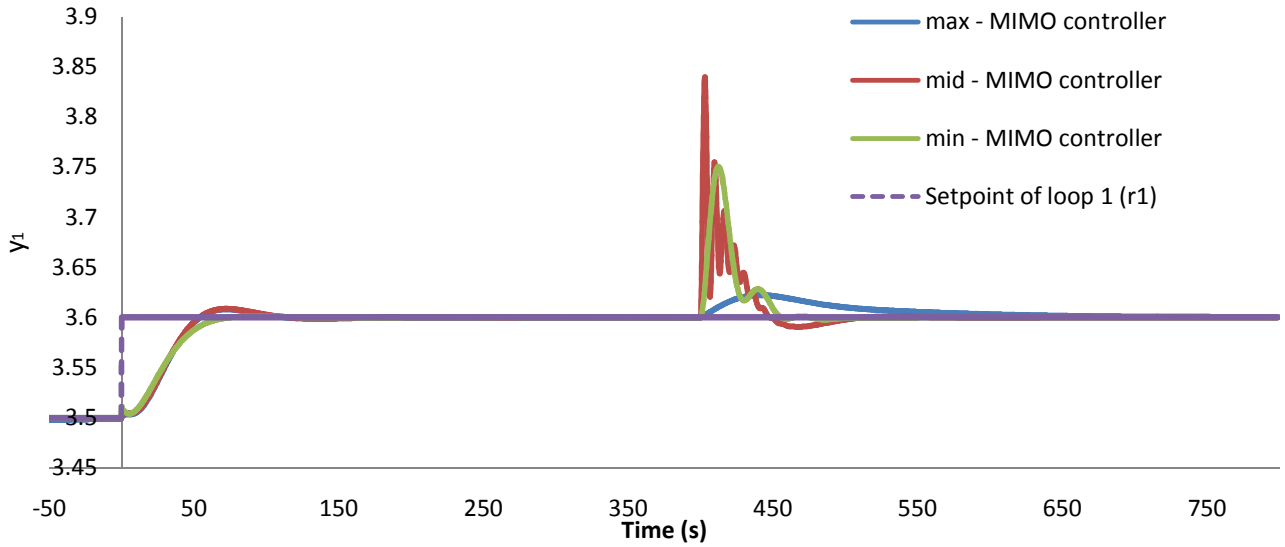

Fig 6.21 Output y_1 vs. Time plot of the MIMO controller

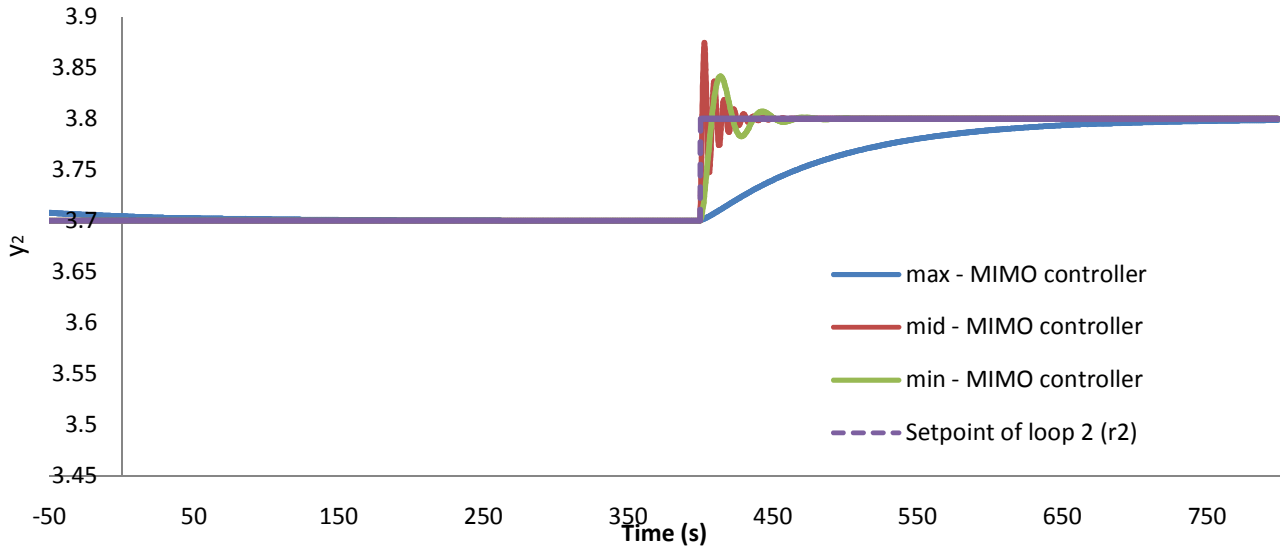

Fig 6.22 Output y_2 vs. Time plot of the MIMO controller

The above digital simulations of the input u(t), the output y(t) and the error e(t) produced time graphs for the two controllers that show that the level diagrams do predict the behavior of the two controllers correctly.

6.1.3 COMPARE THE COST OF INPUT OF THE TWO CONTROLLERS

The two controllers' cost of inputs on the two loops will be analyzed here with the aid of the two cost of input level diagrams (J_{ur_1} and J_{ur_2}). This will provide an idea of which controller requires a lesser amount of input to loop 1 or loop 2. The data used to plot the following level diagrams are given in file Number 9 listed in Appendix A.

Fig 6.23 shows that at the optimal design the MIMO controller requires smaller amounts of input on both loops compared to the SISO controller, and in the worst case the MIMO controller also requires smaller amounts of inputs on the two loops compared to the SISO controller. In some cases the MIMO controller will need a smaller amount of input for loop 1 (u_1) compared to the SISO controller, and both controllers would require a similar amount of inputs on loop 2 (u_2). Regarding both controllers, if they require less input on loop 2 (u_2), their overall performance also becomes worse. The two level diagrams of J_{ur_1} and J_{ur_2} also show that in most cases as the amount of inputs of loop 1 (u_1) increase the required amount of inputs for loop 2 (u_2) will also increase.

University of Cape Tow

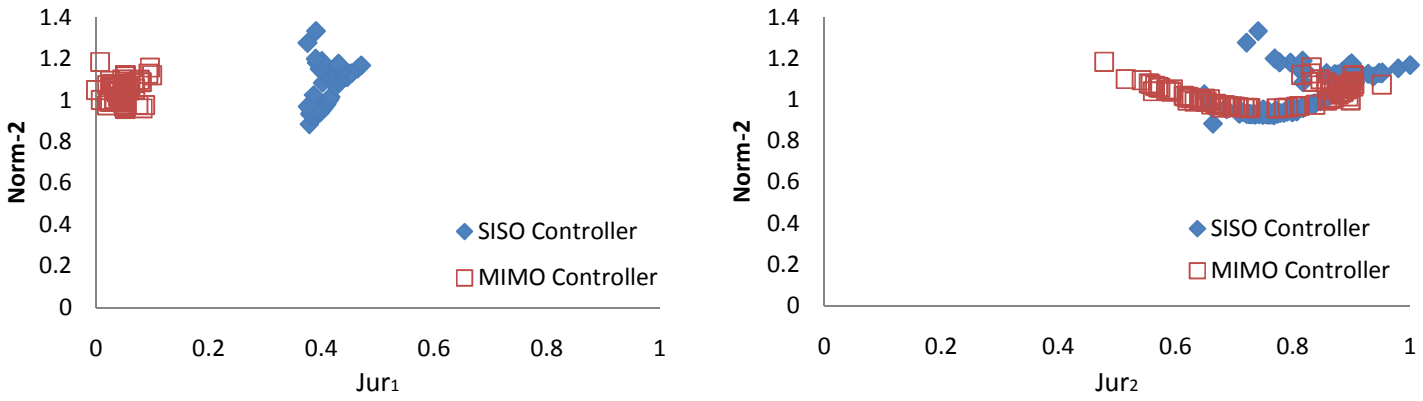

Fig 6.23 Level Diagrams of J_{ur_1} and J_{ur_2}

6.1.3.1 DIGITAL SIMULATIONS OF THE SISO CONTROLLER

In order to verify if the prediction about the two controllers from the level diagrams (J_{ur_1} and J_{ur_2}) is correct or not the behavior of the physical system is investigated, by picking points on the level diagrams diagram of J_{ur_1} and J_{ur_2} of each controller and plotting the digital simulations of the input u(t), the output y(t) and the error e(t) graphs of the system. In Table 6.3, point 1 is the one with the minimum value of J_{ur_2}, point 2 is the one with the median value of J_{ur_2} and point 3 is the one with the maximum value of J_{ur_2}:

Table 6.3 The Point Picked from the SISO Controller of the Level Diagrams of J_{ur_1} and J_{ur_2}

Point	Parameters	Cost Functions
1 of SISO	k_{11}= -0.100 ; k_{22}= -1.269 I_{11}= 0.100 ; I_{22}= 2.931	J_{ur_1}= 0.375 ; J_{ur_2}= 0.659
2 of SISO	k_{11}= -4.976 ; k_{22}= -0.100 I_{11}= 3.167 ; I_{22}= 0.100	J_{ur_1}= 0.408 ; J_{ur_2}= 0.836
3 of SISO	k_{11}= -4.109 ; k_{22}= -1.708 I_{11}= 1.481 ; I_{22}= 0.100	J_{ur_1}= 0.471 ; J_{ur_2}= 1.000

Fig 6.24 shows where those three points are sitting on the level diagrams of J_{ur_1} and J_{ur_2}:

University of Cape Town

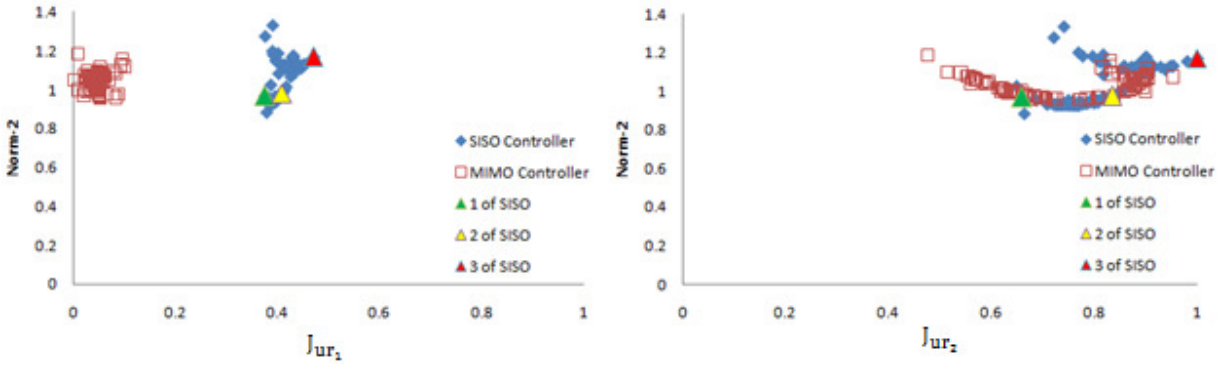

Fig 6.24 The Three Chosen Points and the Level Diagrams of J_{ur_1} and J_{ur_2}

The digital simulation of the input u(t), the output y(t) and the error e(t) graphs of the system are plotted below. The data used to plot the above mentioned graphs is given in Number 11 of Appendix A. The time plots show the responses of the system to start-up at t = - 50 [s], a step in r_1 at the t = 0 and a step in r_2 at t = 400. The three cases in each plot include Point 1, Point 2 and Point 3 optimal designs as indicated on the graph in Fig 6.24.

The error due to loop 1 (e_1) and the error due to loop 2 (e_2) are shown in Fig 6.25 and Fig 6.26 respectively. Point 3 has the largest error due to both loops and also requires the most input on both loops. Point 2 is the one with the smallest amount of error due to both loops, but does not require the largest amount of input on the two loops.

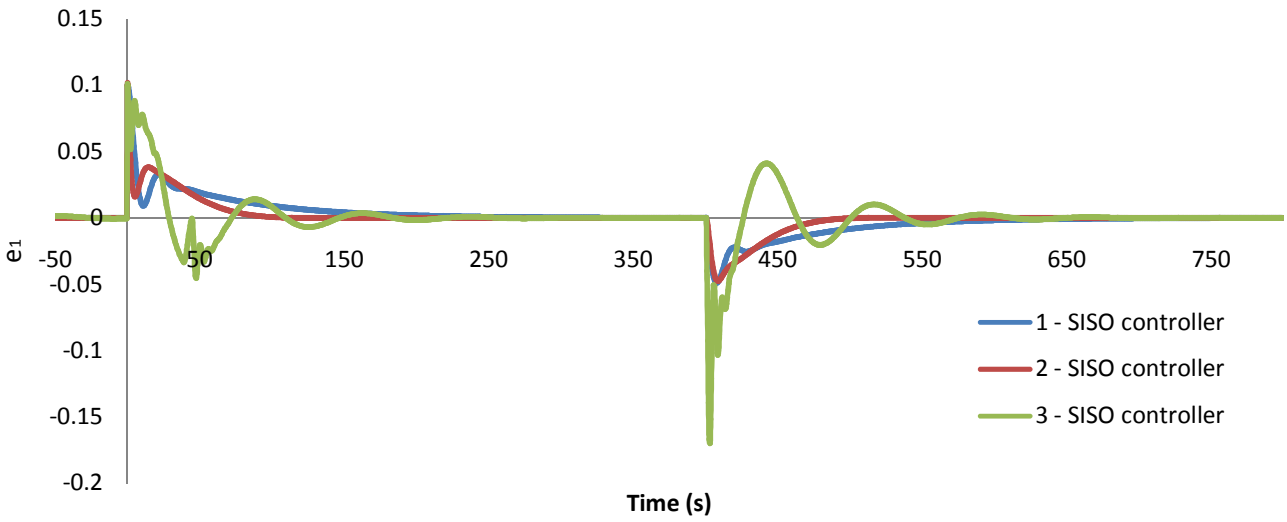

Fig 6.25 Error e_1 vs. Time plot of the SISO controller

University of Cape Town

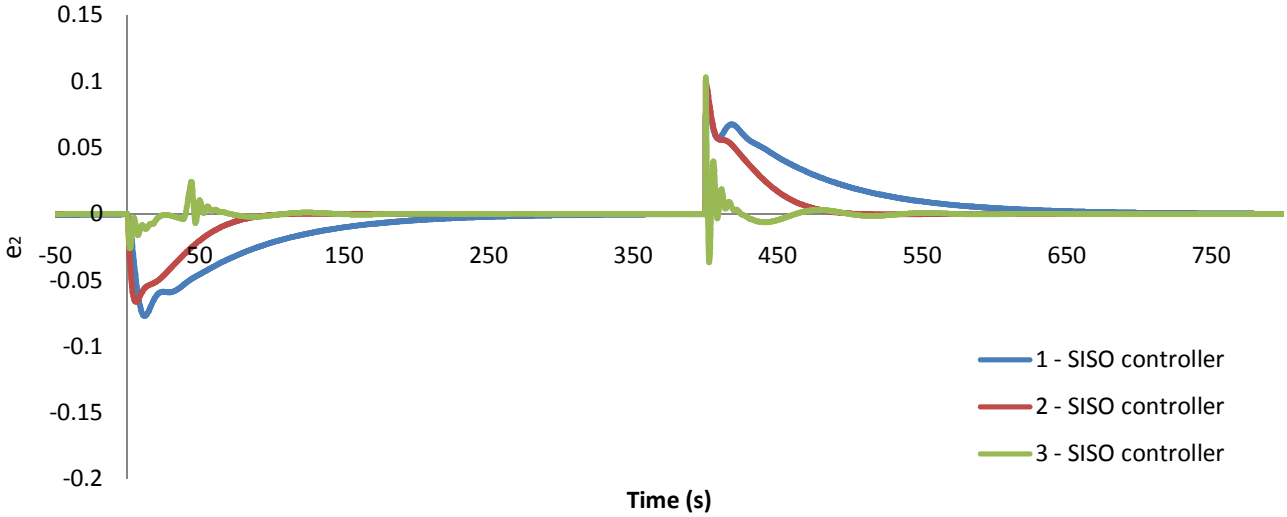

Fig 6.26 Error e_2 vs. Time plot of the SISO controller

In Fig 6.27 and Fig 6.28, it clearly shows that as the amount of input of loop 1 (u_1) increases, the required amount of input for loop 2 (u_2) will also increase. This shows that the level diagrams (J_{ur_1} and J_{ur_2}) do predict the behavior of the SISO controller correctly.

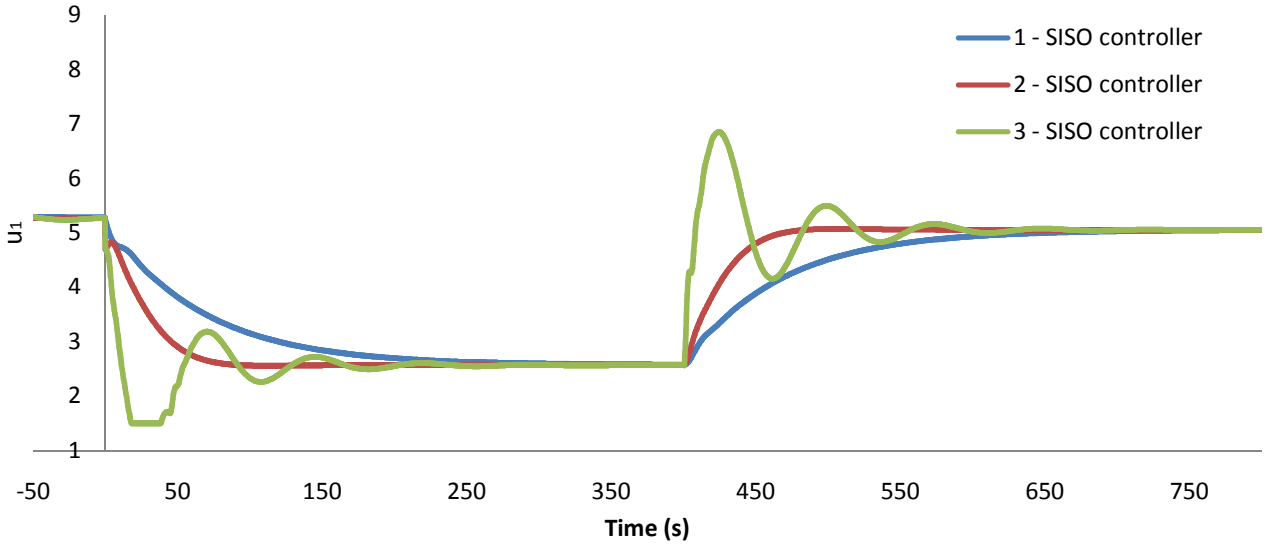

Fig 6.27 Input u_1 vs. Time plot of the SISO controller

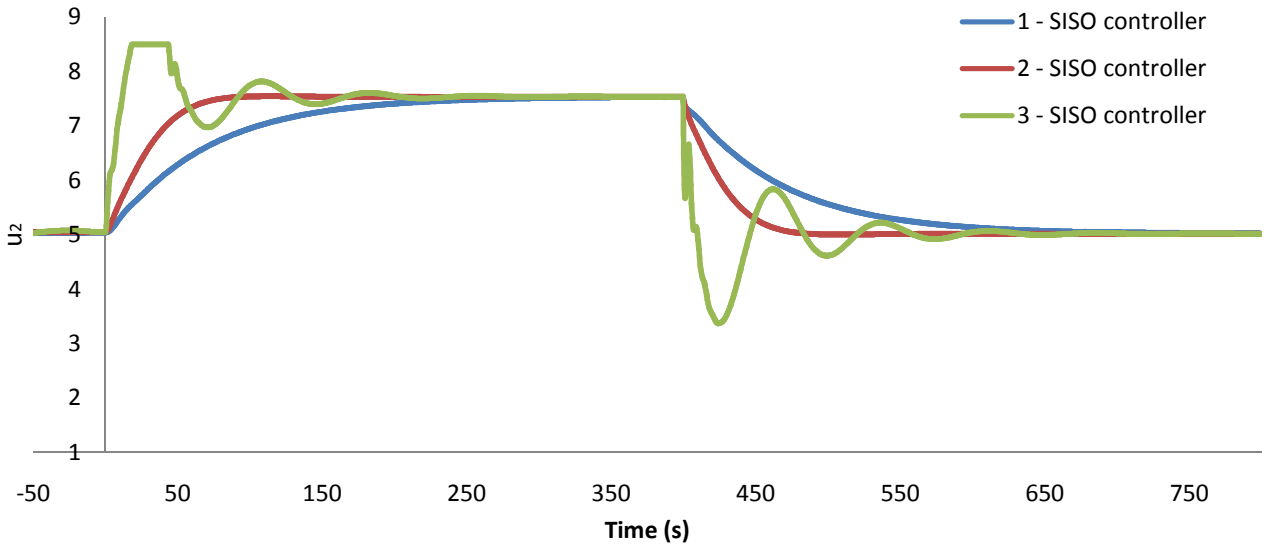

Fig 6.28 Input u_2 vs. Time plot of the SISO controller

The digital simulations of the outputs of loop 1 (y_1) and loop 2 (y_2) are shown below, where the point that requires the most inputs (point 3) has the highest frequency of oscillation and the highest overshoot on setpoint tracking on both loops:

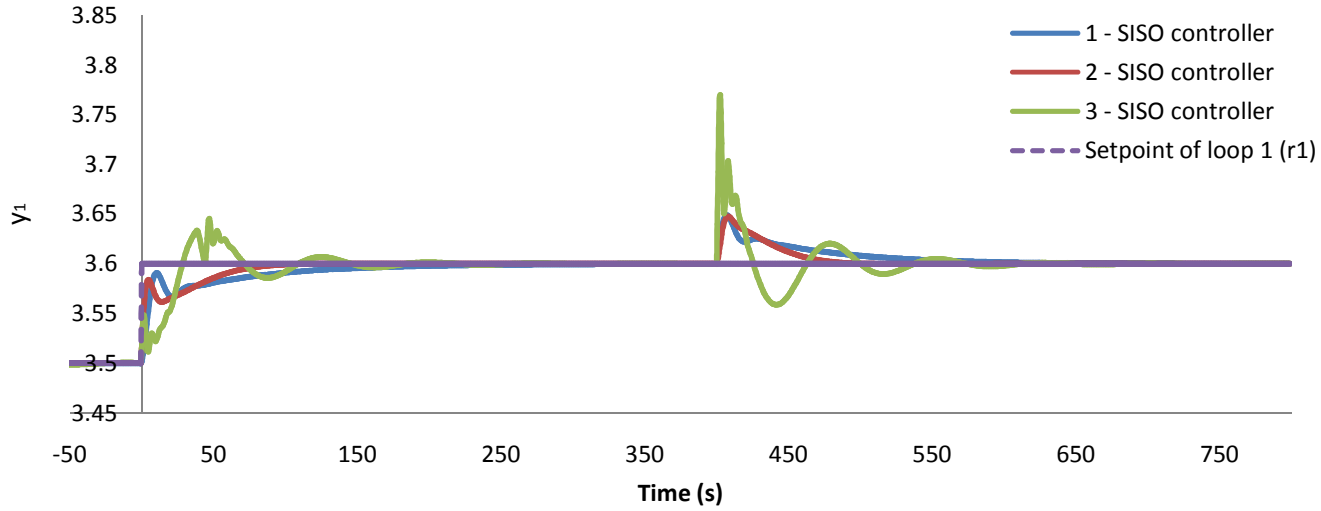

Fig 6.29 Output y_1 vs. Time plot of the SISO controller

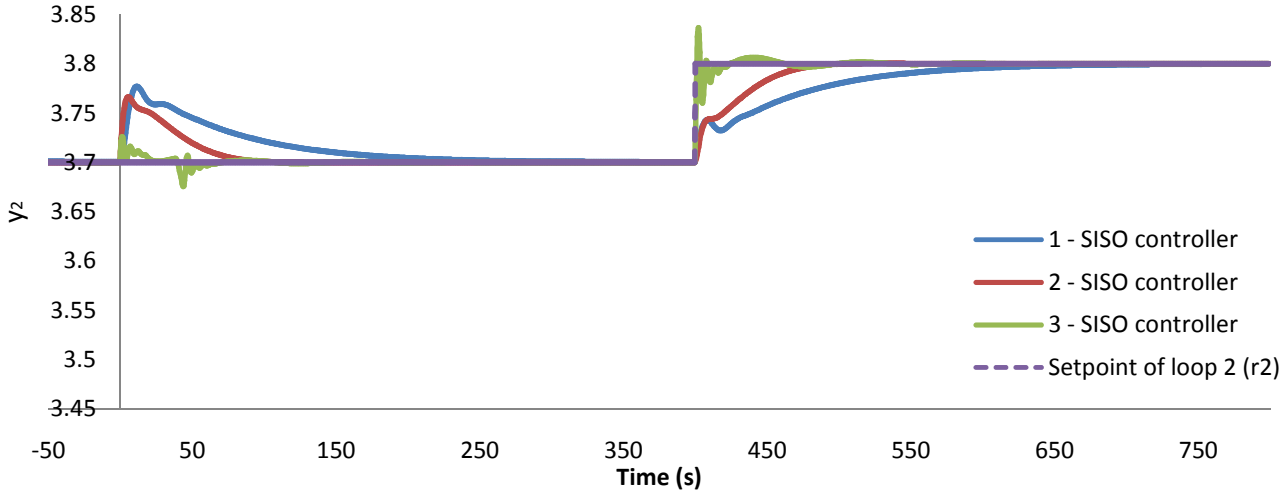

Fig 6.30 Output y_2 vs. Time plot of the SISO controller

6.1.3.2 DIGITAL SIMULATIONS OF THE MIMO CONTROLLER

The points picked from the level diagrams (J_{ur_1} and J_{ur_2}) of the MIMO controller are shown in Table 6.4:

Table 6.4 The Three Points Picked from the MIMO Controller of the Level Diagrams of J_{ur_1} and J_{ur_2}

Point	Parameters	Cost Functions
1 of MIMO	k_{11}= -0.100 ; k_{22}= -0.100 I_{11}= 0.100 ; I_{22}= 4.103	J_{ur_1}= 0.007 ; J_{ur_2}= 0.478
2 of MIMO	k_{11}= -4.976 ; k_{22}= -0.100 I_{11}= 3.167 ; I_{22}= 0.100	J_{ur_1}= 0.408 ; J_{ur_2}= 0.836
3 of MIMO	k_{11}= -3.900 ; k_{22}= -2.462 I_{11}= 2.319 ; I_{22}= 0.100	J_{ur_1}= 0.020 ; J_{ur_2}= 0.952

Fig 6.31 shows where those three points are located on the level diagrams of J_{ur_1} and J_{ur_2}:

University of Cape Town

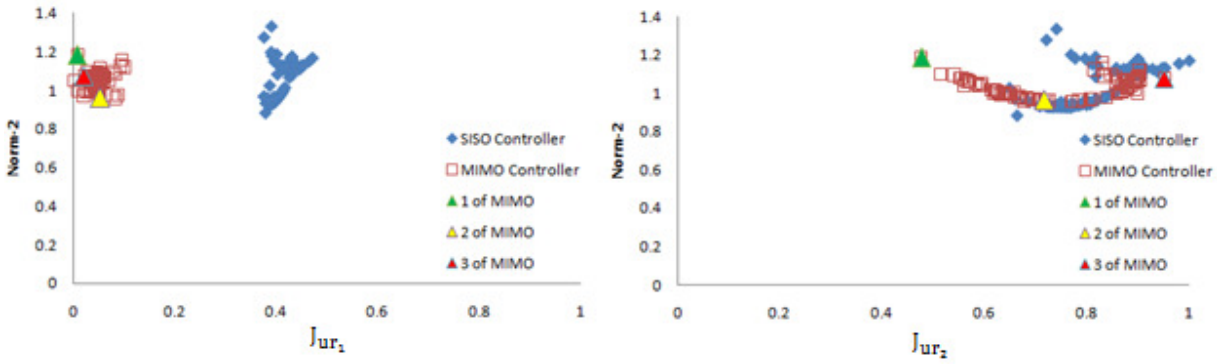

Fig 6.31 The Three Chosen Points and the Level Diagrams of J_{ur_1} and J_{ur_2}

The digital simulations of the error e(t), the input u(t), and the output y(t) graphs of the system are plotted below. The data used to plot the above mentioned graphs is given in Number 11 of Appendix A. The time plots show the response of the system to start-up at t = - 50 [s], a step in r_1 at the t = 0 and a step in r_2 at t = 400. The three cases in each plot are for the Point 1, Point 2 and Point 3 optimal designs as indicated on the graph in Fig 6.31.

From Fig 6.31 and Fig 6.32, the MIMO controller design with the smallest value of the cost function J_{ur_1} (Point 1) is the one with the largest error due to loop 1 (e_1) when the setpoint of loop 1 (r_1) is stepped, but with the lowest error due to loop 1 (e_1) when the setpoint of loop 2 (r_2) is stepped. Point 3 is the one with largest value of the cost function J_{ur_1} which is also the one with the smallest error due to loop 1 (e_1) when the setpoint of loop 1 (r_1) is stepped, but with the largest error due to loop 1 (e_1) when the setpoint of loop 2 (r_2) is stepped:

University of Cape Town

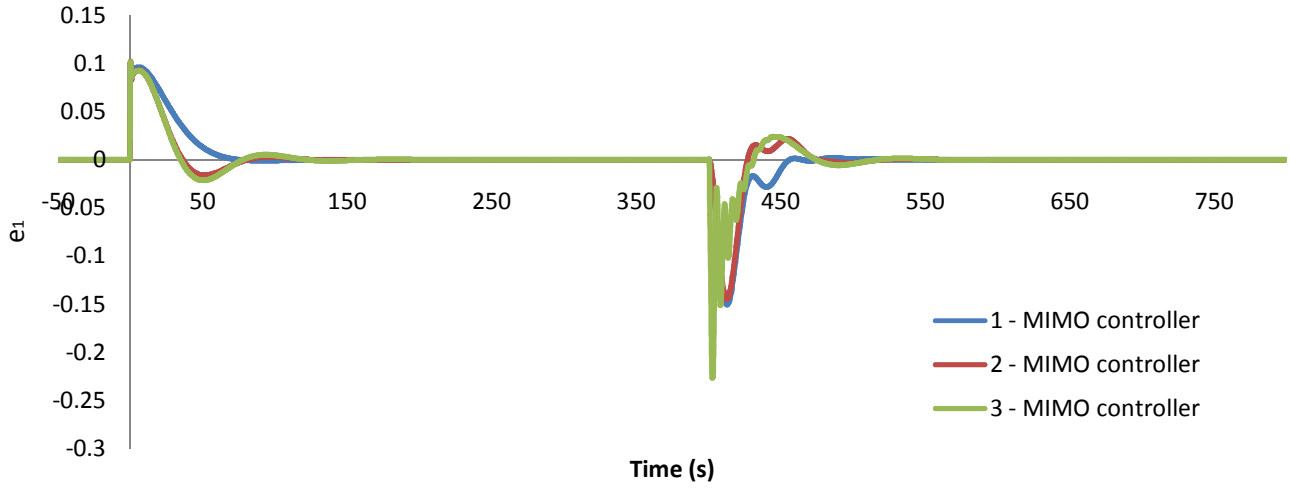

Fig 6.32 Error e_1 vs. Time plot of the MIMO controller

In Fig 6.31 and Fig 6.33, point 1 is the one with the most error due to loop 2 (e_2) and it is also the one with the smallest cost function J_{ur_2}. As expected the MIMO controller eliminated all the interactions to this loop:

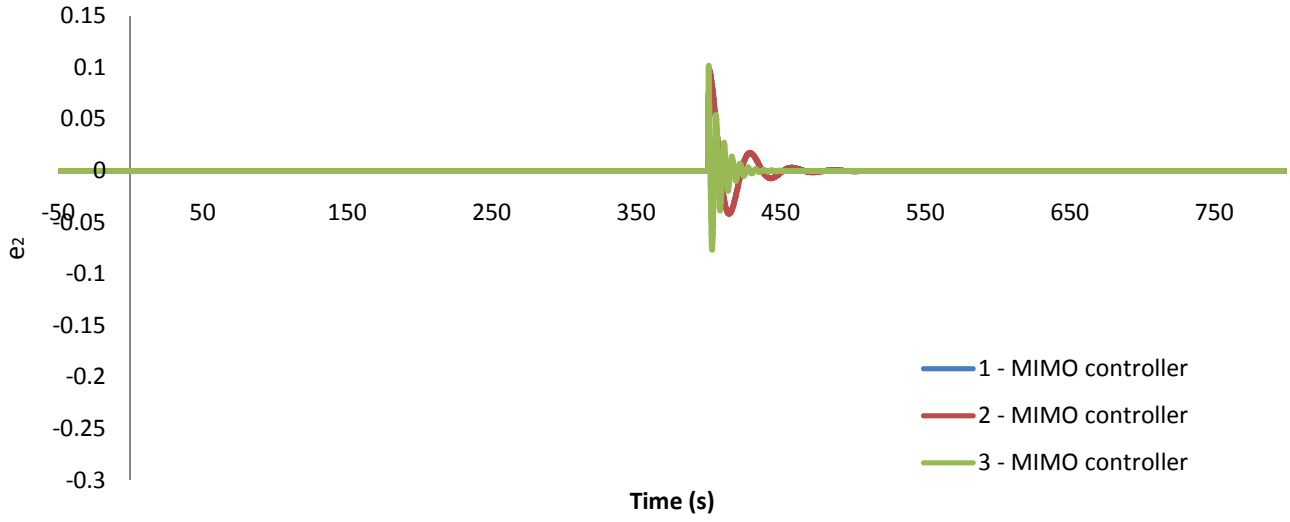

Fig 6.33 Error e_2 vs. Time plot of the MIMO controller

In Fig 6.31, Fig 6.34 and Fig 6.35, it clearly shows that in most cases, as the amount of input of loop 1 increases, the required amount of inputs for loop 2 (u_2) will also increase, though point 3 is an exceptional case. This shows that the level diagrams (J_{ur_1} and J_{ur_2}) do predict the behavior of the MIMO controller correctly.

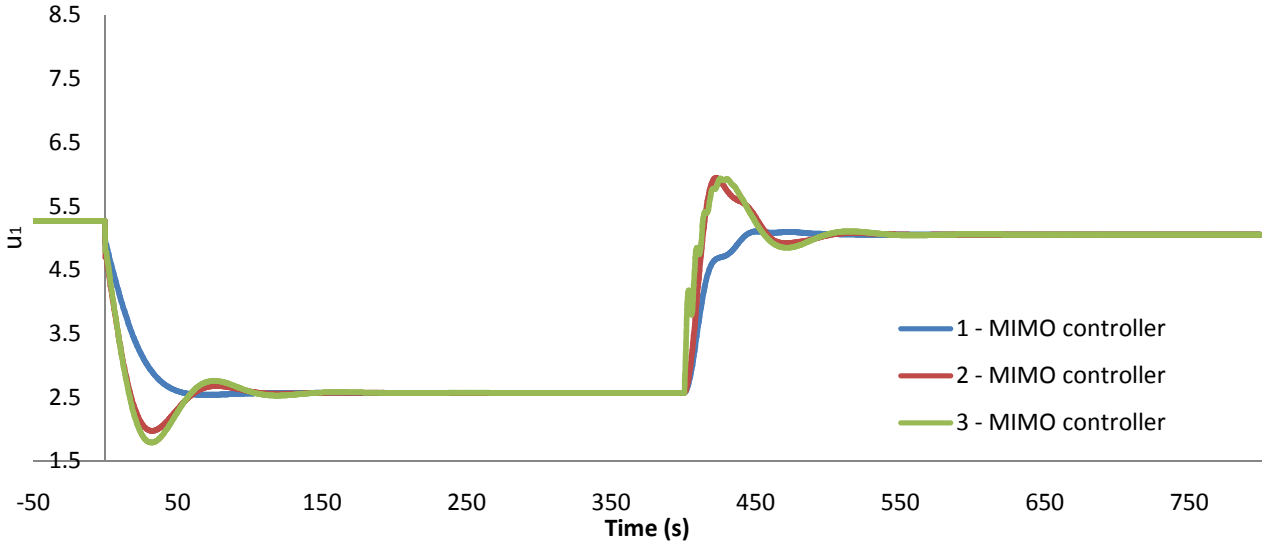

Fig 6.34 Input u_1 vs. Time plot of the MIMO controller

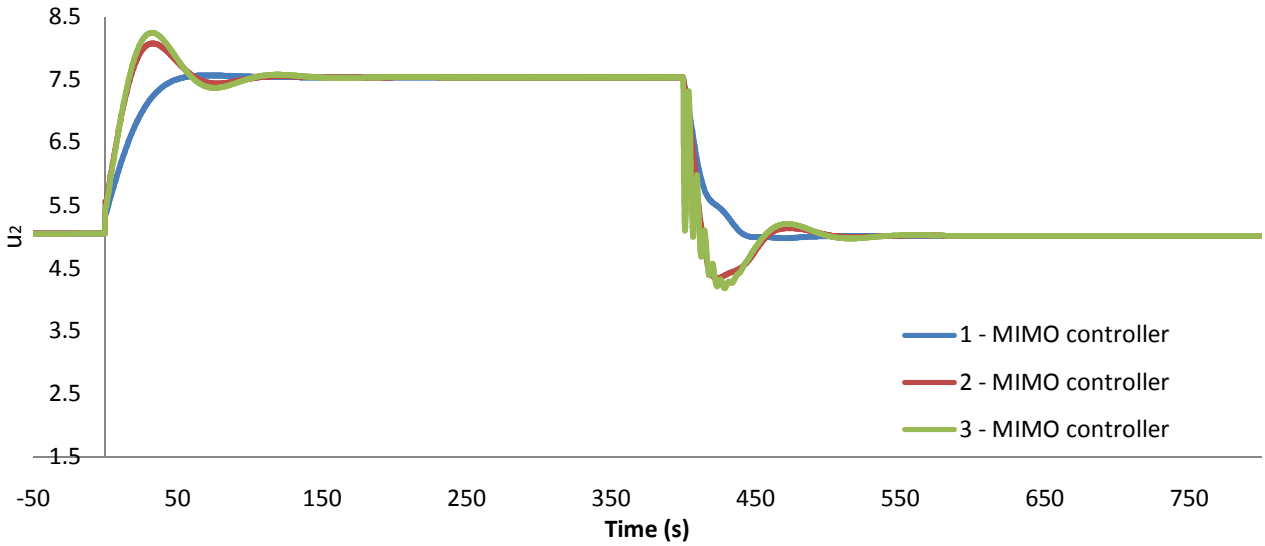

Fig 6.35 Input u_2 vs. Time plot of the MIMO controller

In Fig 6.31, Fig 6.36 and Fig 6.37, point 3 has the highest cost functions (J_{ur_1} and J_{ur_2}) and its also the one with the largest overshoot and the highest frequency of oscillation.

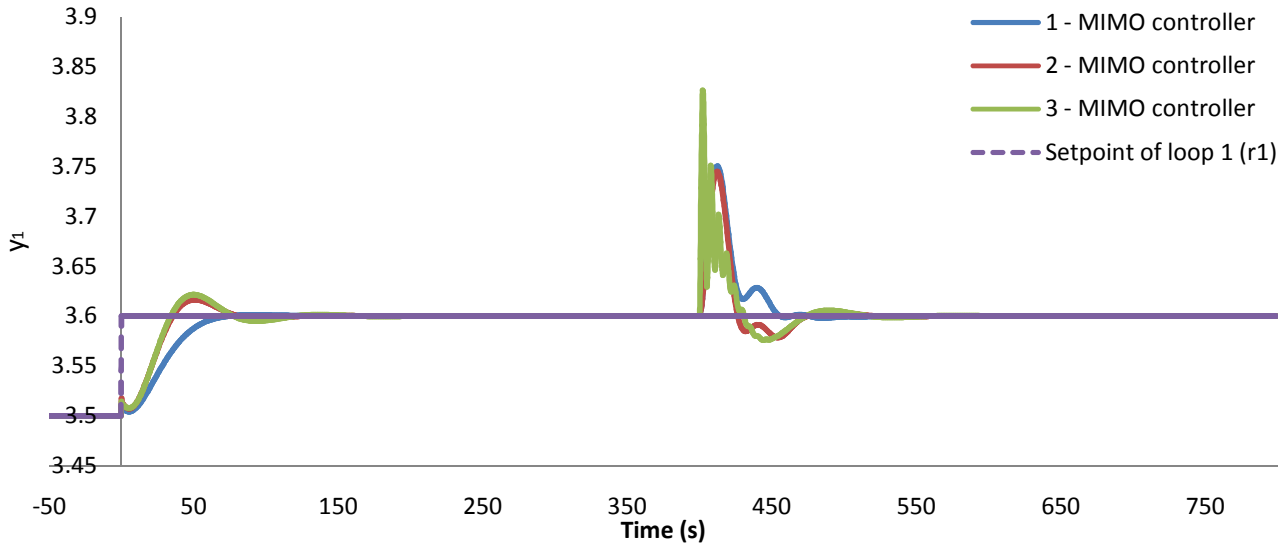

Fig 6.36 Output y_1 vs. Time plot of the MIMO controller

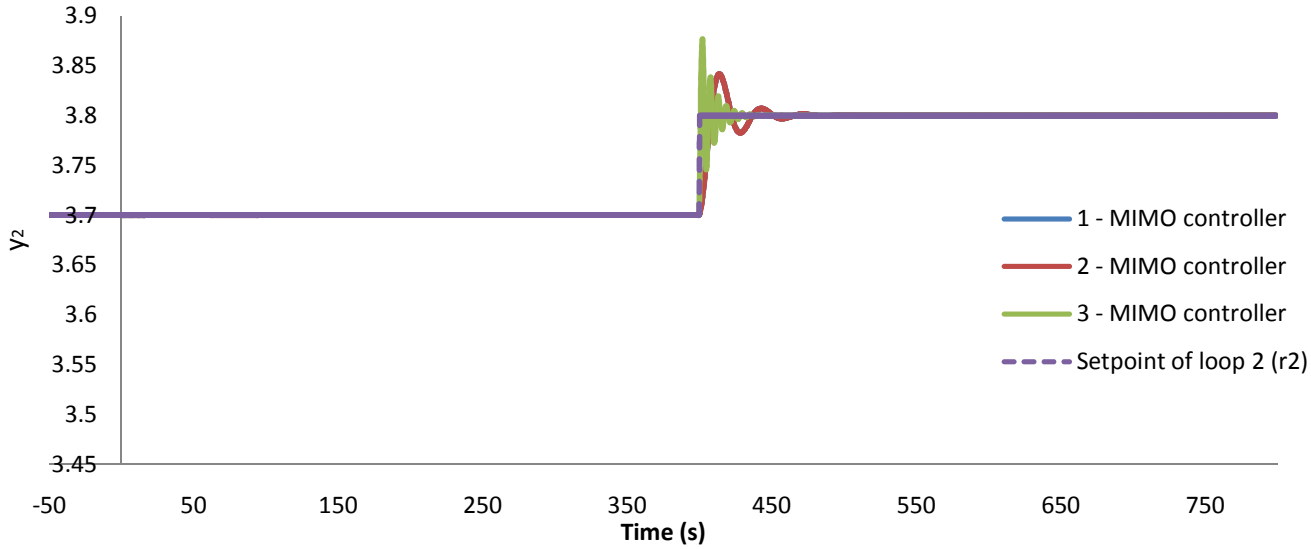

Fig 6.37 Output y_2 vs. Time plot of the MIMO controller

The prediction from the level diagrams (J_{ur_1} and J_{ur_2}) of the two controllers, do correspond with the digital simulations of the input u(t), the output y(t) and the error e(t) graphs of the two controllers. This shows that the level diagrams (J_{ur_1} and J_{ur_2}) do predict correctly the behavior with respect to the amount of inputs needed by the two controllers.

6.1.4 THE RELATIONSHIP BETWEEN THE ERROR AND THE INTERACTION

In the process of designing a controller for a MIMO system, it is essential to know the tradeoffs between performance and interaction in order to design a controller which will be able to satisfy the criteria set for the MIMO system.

6.1.4.1 THE RELATIONSHIP BETWEEN THE ERROR AND THE INTERACTION OF LOOP 1

Figure 6.38, shows that when the setpoint of loop 1 (r_1) is stepped, the SISO controller will have less performance error (e_1) compared to the MIMO controller in most cases. However the MIMO controller will have virtually no interaction error (e_2) in all cases which is what is expected from this MIMO controller design. By observing the two points which have a Norm-2 value of 1.3 and 1.4 respectively; the former one has the smallest Je1r1 value but the largest Je2r1 value and the later one has the largest Je1r1 values but the smallest Je2r1 value. Therefore, it shows that as the error due to loop 1 (e_1) of the SISO controller increases, the interaction error (e_2) decreases:

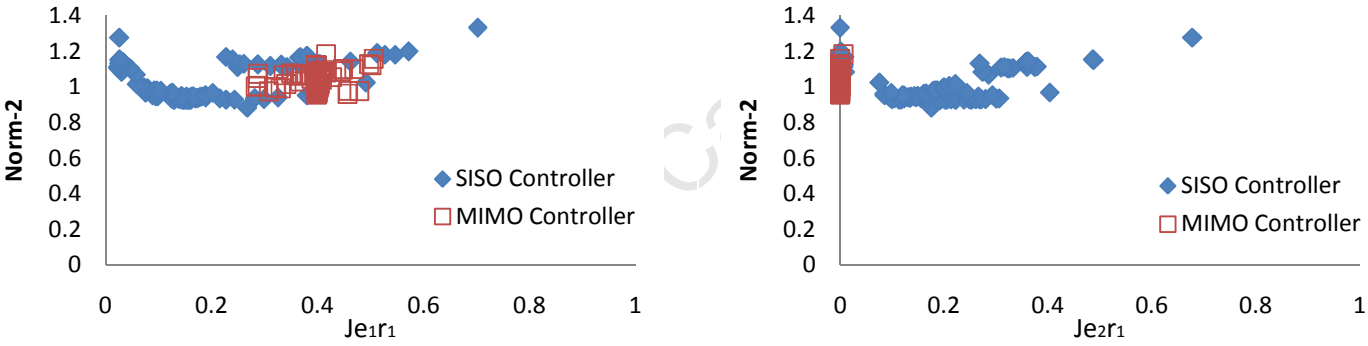

Fig 6.38 Level Diagrams of $J_{e_1r_1}$ and $J_{e_2r_1}$

6.1.4.1.1 DIGITAL SIMULATIONS OF THE SISO CONTROLLER

A series of points from the level diagrams of $J_{e_1r_1}$ and $J_{e_2r_1}$ (Fig 6.38) were picked to plot the digital simulations of the input u(t), the output y(t) and the error e(t) graphs of the system, in order to verify that the prediction of the performance of the two controllers from the level diagram of $J_{e_1r_1}$ vs. $J_{e_2r_1}$ (Fig 6.44) is correct.

The points picked from the level diagram of $J_{e_1r_1}$ and $J_{e_2r_1}$ (Fig 6.38) of the SISO controller are shown below, where point 1 is the one with the maximum value of the cost function $J_{e_1r_1}$, point 2 is the one with the maximum value of the cost function $J_{e_2r_1}$ and point 3 is a random point picked form the level diagrams:

Table 6.5 The Three Points Picked from the SISO Controller of the Level Diagrams of $J_{e_1r_1}$ and $J_{e_2r_1}$

Point	Parameters	Cost Functions
1 of SISO	k_{11}= -0.100 ; k_{22}= -2.666 I_{11}= 0.100 ; I_{22}= 0.100	$J_{e_1r_1}$= 0.702 ; $J_{e_2r_1}$= 1.864E-04
2 of SISO	k_{11}= -0.499 ; k_{22}= -3.529 I_{11}= 0.290 ; I_{22}= 1.771	$J_{e_1r_1}$= 0.025 ; $J_{e_2r_1}$= 0.678
3 of SISO	k_{11}= -4.379 ; k_{22}= -3.214 I_{11}= 0.323 ; I_{22}= 1.845	$J_{e_1r_1}$= 0.366 ; $J_{e_2r_1}$= 0.002

Fig 6.39 shows where those three points are sitting on the level diagrams of $J_{e_1r_1}$ and $J_{e_2r_1}$:

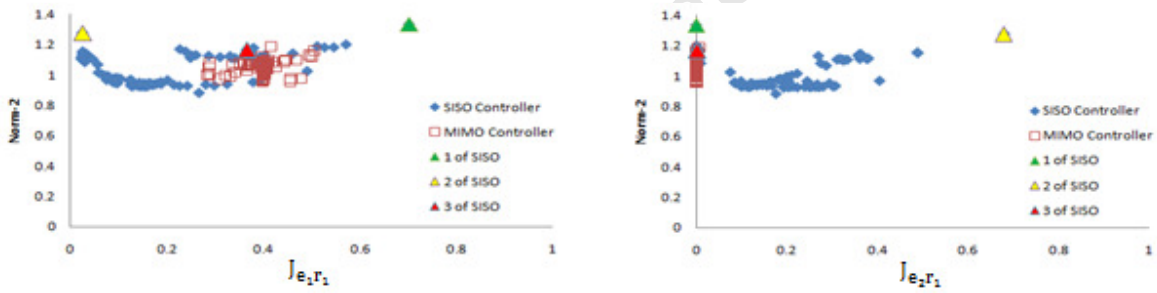

Fig 6.39 The Three Chosen Points and the Level Diagrams of $J_{e_1r_1}$ and $J_{e_2r_1}$

The digital simulations of the error e(t), the input u(t) and the output y(t) graphs of the system are plotted below, the data used to plot the above mentioned graphs is given in file Number 12 of Appendix A. The time plots show the responses of the system to start-up at t = - 50 [s], a step in r_1 at the t = 0 and a step in r_2 at t = 400. The three cases in each plot are for Point 1, Point 2 and Point 3 optimal designs as indicated on the graph in Fig 6.39.

In Fig 6.39, Fig 6.40 and Fig 6.41, by looking at all three points of the SISO controller, it is clear that when the setpoint of loop 1(r_1) is stepped, the performance error (e_1) decreases as the interaction error (e_2) increases, which corresponds to what the level diagrams of $J_{e_1r_1}$ and $J_{e_2r_1}$ predict:

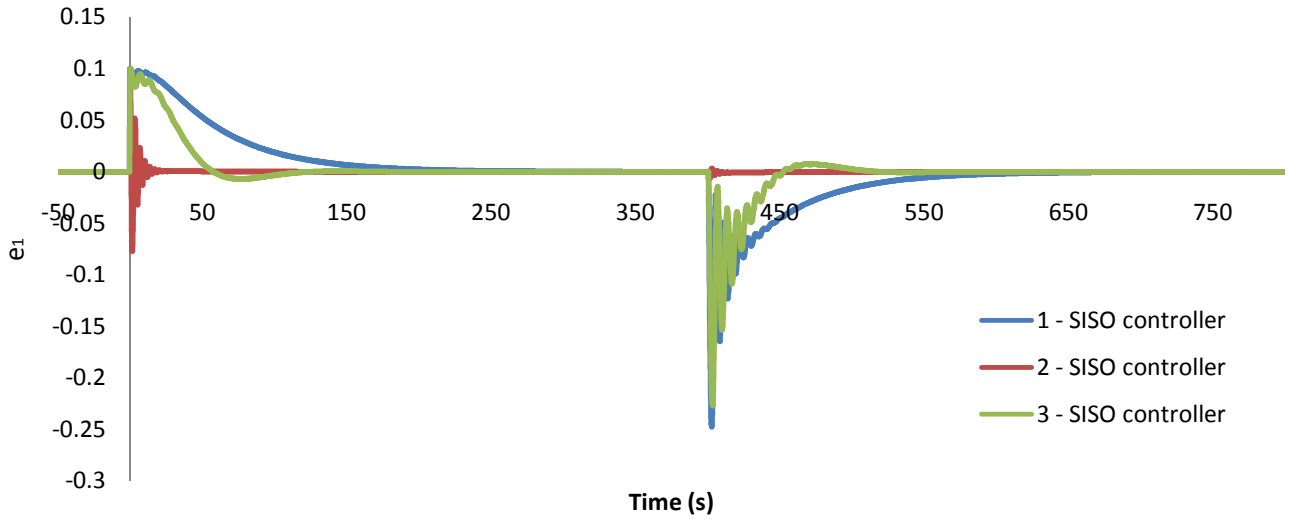

Fig 6.40 Error e_1 vs. Time plot of the SISO controller

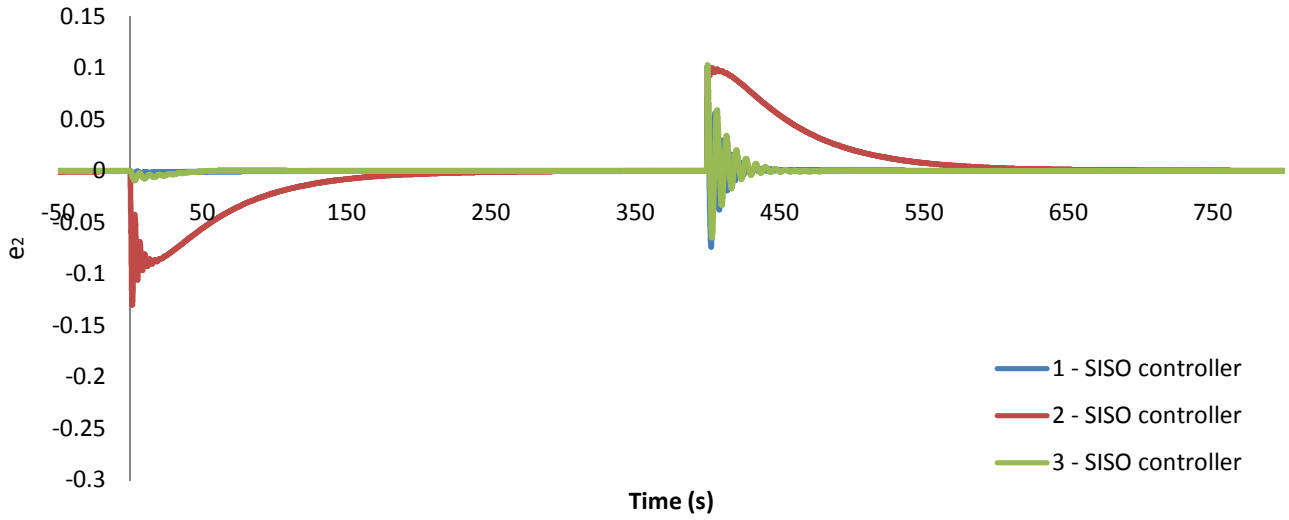

Fig 6.41 Error e_2 vs. Time plot of the SISO controller

Fig 6.39, Fig 6.42 and Fig 6.43 show that the amount of input used by point 1 and point 2 of the SISO controller are similar for both loops, there is not much difference. However, point 3 uses a much larger amount of input due to the two loops, compared to the other two points:

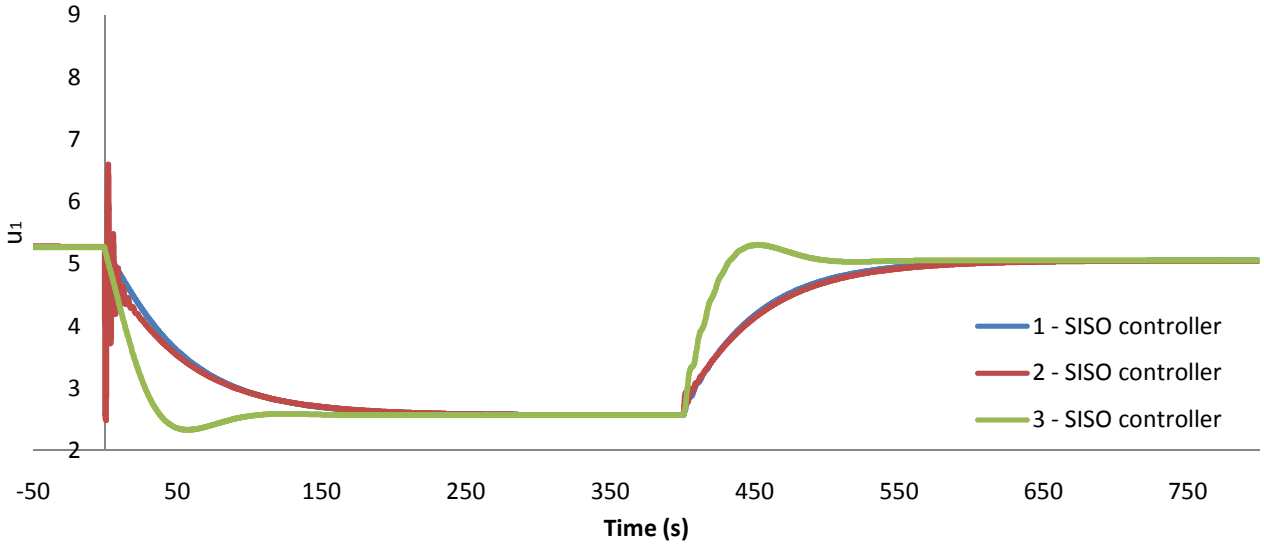

Fig 6.42 Input u_1 vs. Time plot of the SISO controller

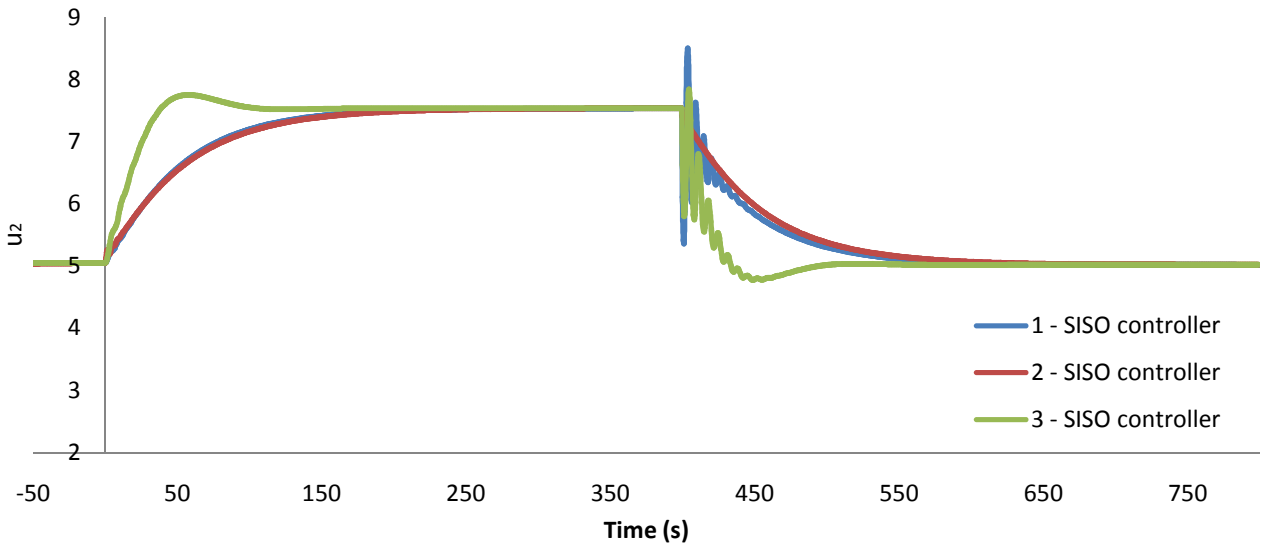

Fig 6.43 Input u_2 vs. Time plot of the SISO controller

Fig 6.39, Fig 6.44 and Fig 6.45, show that the prediction of the SISO controller from the level diagrams of $J_{e_1 r_1}$ and $J_{e_2 r_1}$ is correct once again: when the setpoint of loop 1(r_1) is stepped the performance error (e_1) decreases as the interaction error (e_2) increases:

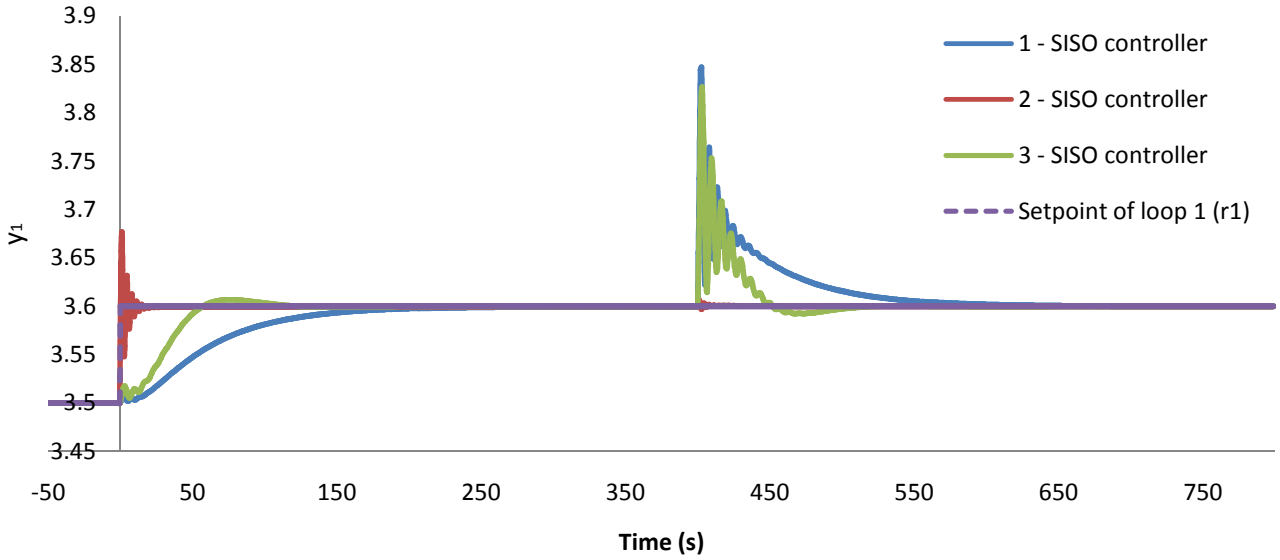

Fig 6.44 Output y_1 vs. Time plot of the SISO controller

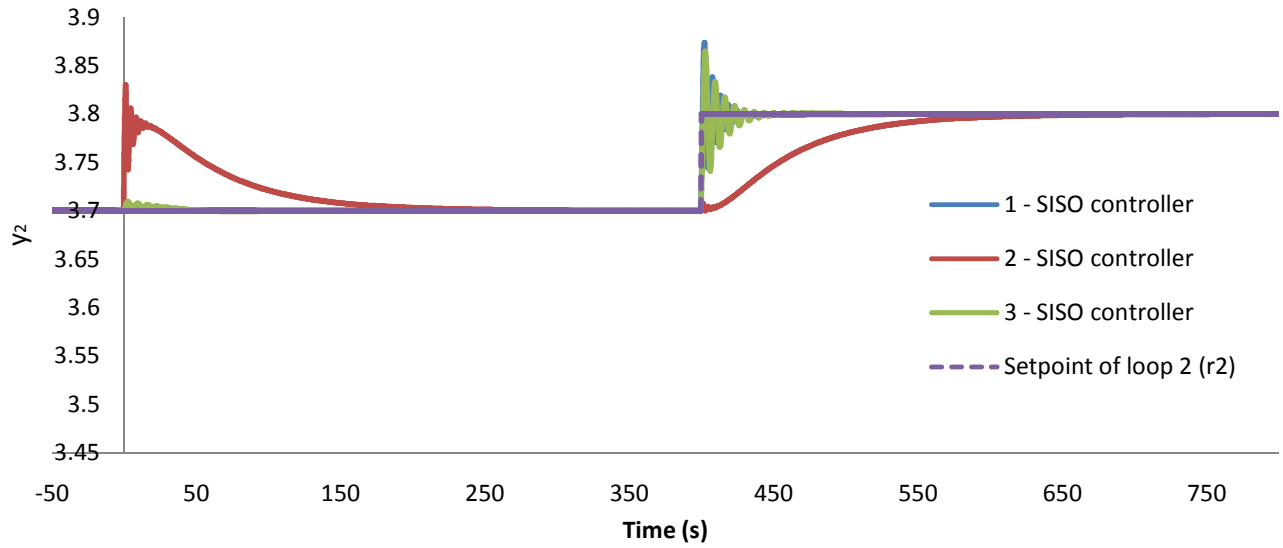

Fig 6.45 Output y_2 vs. Time plot of the SISO controller

6.1.4.1.2 DIGITAL SIMULATIONS OF THE MIMO CONTROLLER

The points picked from the level diagrams of $J_{e_1r_1}$ and $J_{e_2r_1}$ of the MIMO controller are given in Table 6.6. Point 1 is the one with the smallest value of the cost function $J_{e_1r_1}$, point two with the median value of the cost function $J_{e_1r_1}$ and point 3 will be the one with the highest value of the cost function $J_{e_1r_1}$:

Table 6.6 The Three Points Picked from the MIMO Controller of the Level Diagrams of $J_{e_1r_1}$ and $J_{e_2r_1}$

Point	Parameters	Cost Functions
1 of MIMO	k_{11}= -0.100 ; k_{22}= -0.100 I_{11}= 0.100 ; I_{22}= 2.278	$J_{e_1r_1}$= 0.283 ; $J_{e_2r_1}$= 0.001
2 of MIMO	k_{11}= -0.100 ; k_{22}= -2.817 I_{11}= 0.100 ; I_{22}= 2.376	$J_{e_1r_1}$= 0.394 ; $J_{e_2r_1}$= 8.324E-08
3 of MIMO	k_{11}= -0.100 ; k_{22}= -2.576 I_{11}= 0.100 ; I_{22}= 3.460	$J_{e_1r_1}$= 0.506 ; $J_{e_2r_1}$= 2.963E-09

Fig 6.46 shows where those three points are situated on the level diagrams of $J_{e_1r_1}$ and $J_{e_2r_1}$:

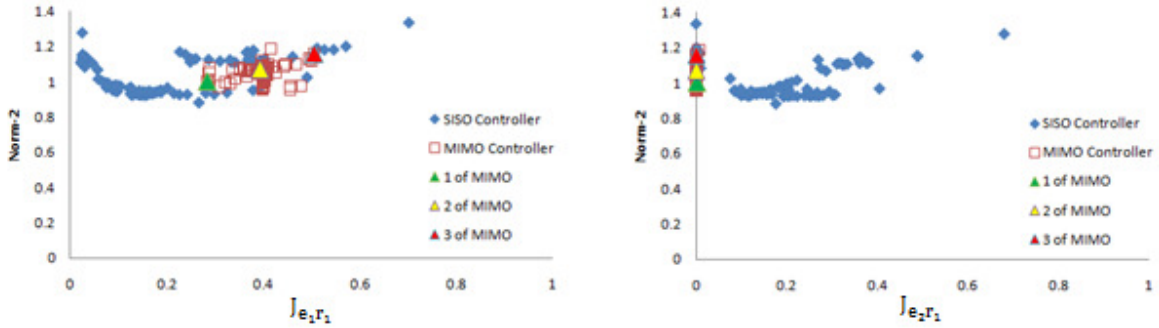

Fig 6.46 The Three Chosen Points and the Level Diagrams of $J_{e_1r_1}$ and $J_{e_2r_1}$

The digital simulations of the error e(t), the input u(t) and the output y(t) of the system are plotted below. The data used to plot the above mentioned graphs is given in Number 12 of Appendix A. The time plots show the responses of the system to start-up at t = - 50 [s], a step in r_1 at the t = 0 and a step in r_2 at t = 400. The three cases in each plot are for Point 1, Point 2 and Point 3 optimal designs as indicated on the graph in Fig 6.46.

From Fig 6.46, Fig 6.47 and Fig 6.48, it can be seen that as the setpoint of loop 1 (r_1) is stepped, the interaction error (e_2) is virtually zero for all three different MIMO controller points picked from the level diagrams of $J_{e_1r_1}$ and $J_{e_2r_1}$. This corresponds to the prediction of the MIMO controller from the level diagrams of $J_{e_1r_1}$ and $J_{e_2r_1}$:

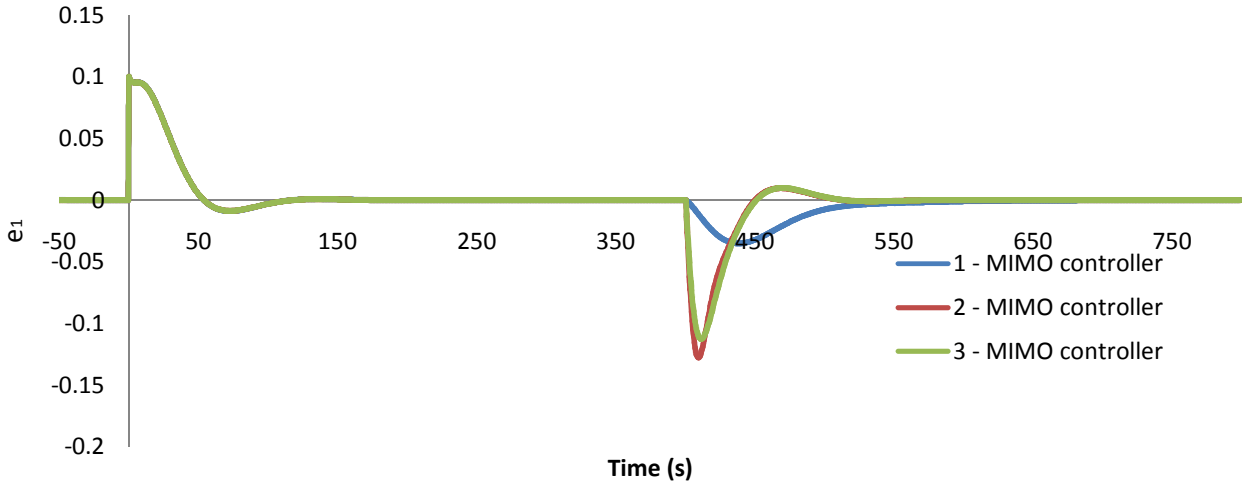

Fig 6.47 e_1 vs. Time plot of the MIMO controller

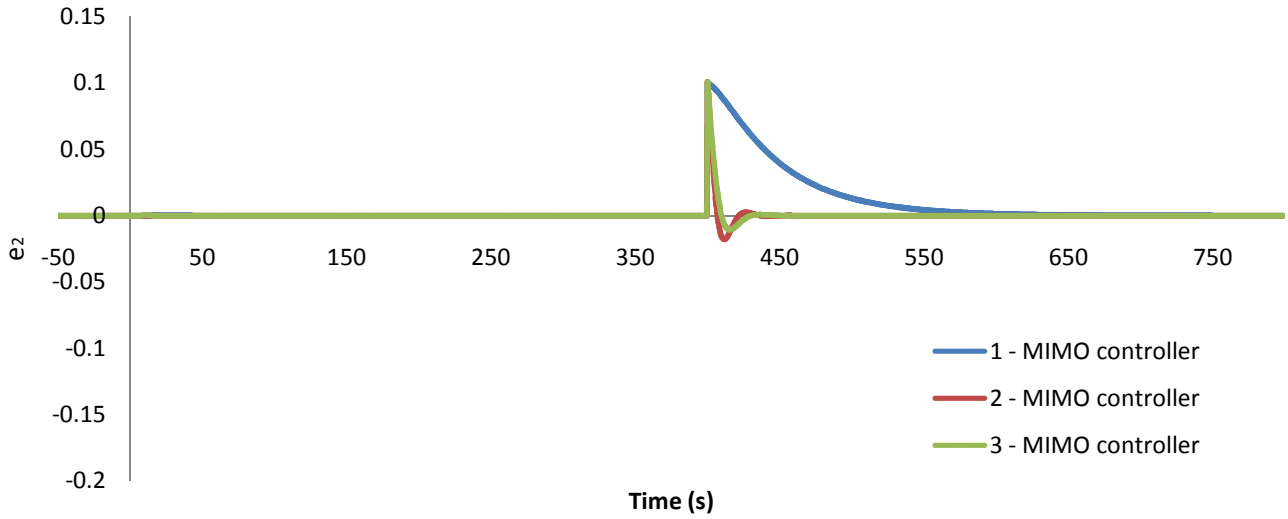

Fig 6.48 e_2 vs. Time plot of the MIMO controller

Fig 6.46, Fig 6.49 and Fig 6.50, show that similar inputs are need for both tracking the setpoint of loop 1 (r_1) and dealing with interaction of loop 2 (e_2).

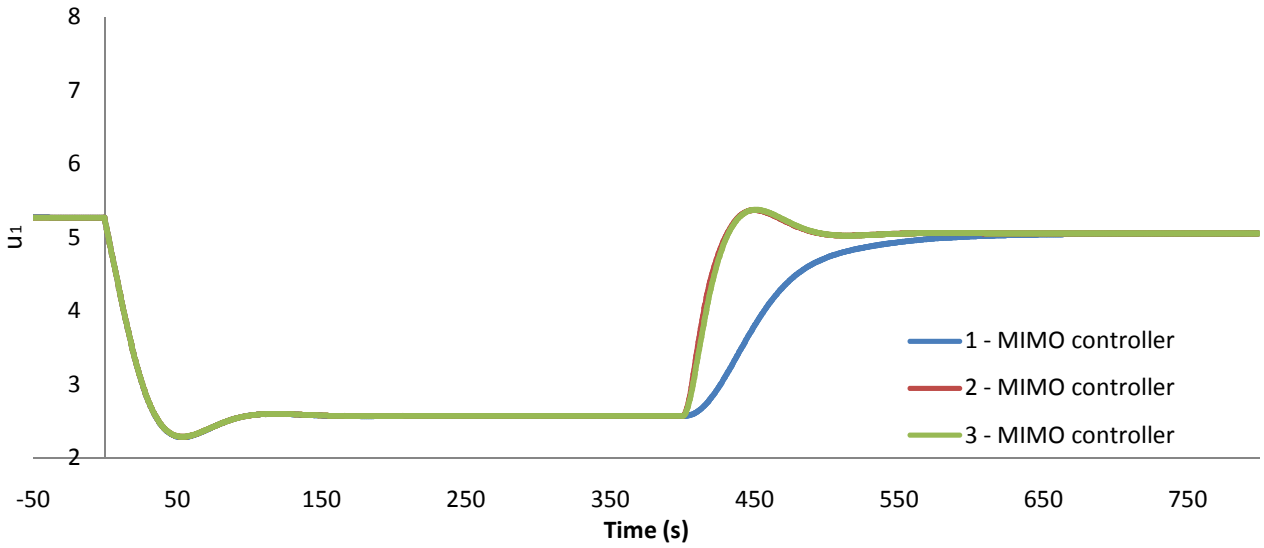

Fig 6.49 u_1 vs. Time plot of the MIMO controller

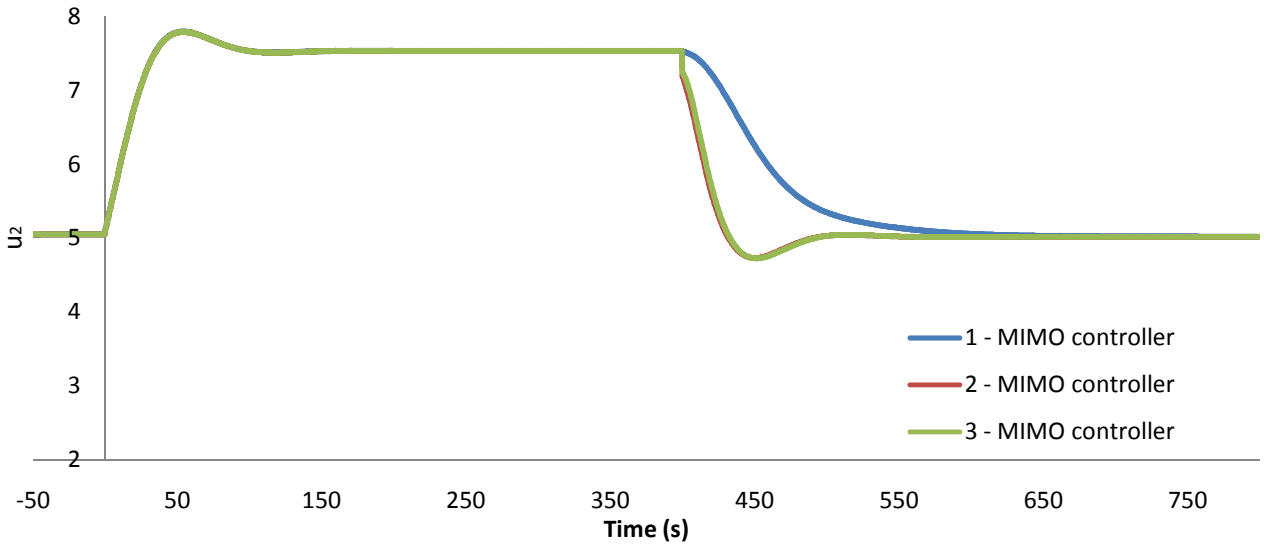

Fig 6.50 u_2 vs. Time plot of the MIMO controller

From Fig 6.46, Fig 6.51 and Fig 6.52, it can be seen that as the setpoint of loop 1 (r_1) is stepped, the interaction to the output of loop 2 (y_2) is virtually zero for all three different MIMO controller points picked from the level diagrams of $J_{e_1 r_1}$ and $J_{e_2 r_1}$. This confirms the prediction for the MIMO controller from the level diagrams of $J_{e_1 r_1}$ and $J_{e_2 r_1}$:

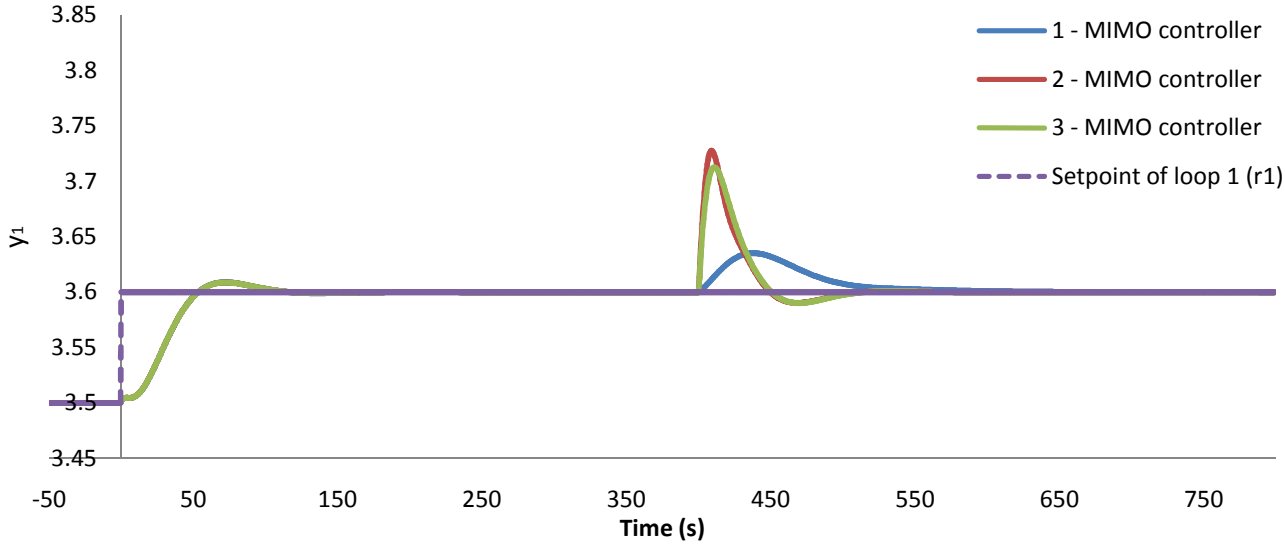

Fig 6.51 y_1 vs. Time plot of the MIMO controller

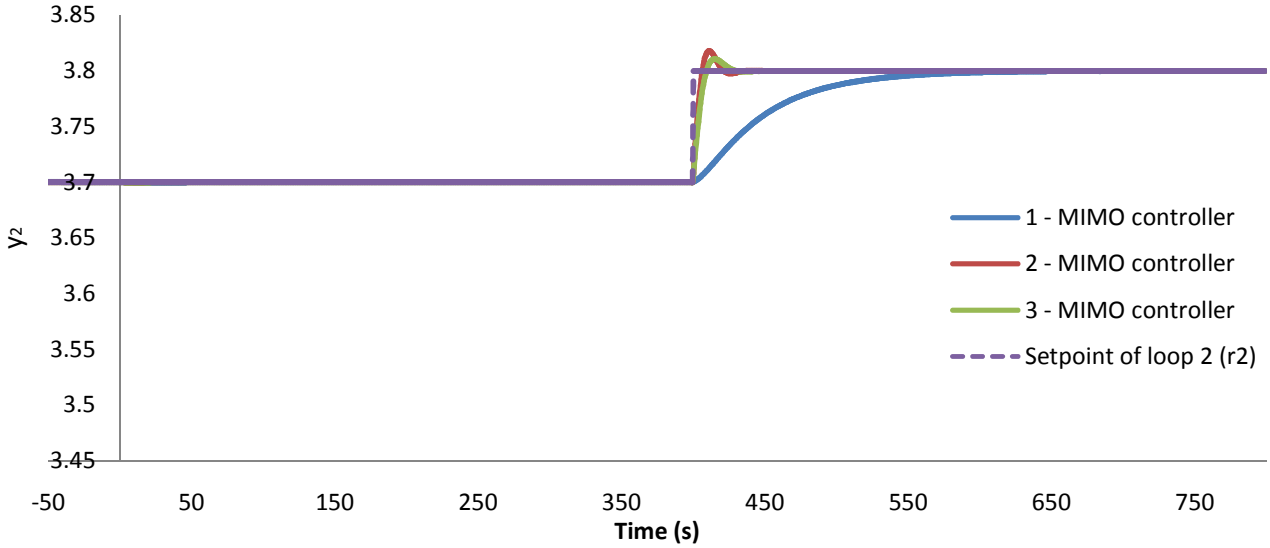

Fig 6.52 y_2 vs. Time plot of the MIMO controller

The digital simulations of the input u(t), the output y(t) and the error e(t) graphs of the two controllers shows that the prediction of the level diagrams of $J_{e_1 r_1}$ and $J_{e_2 r_1}$ in Fig 6.46 is correct.

6.1.4.2 THE RELATIONSHIP BETWEEN THE ERROR AND THE INTERACTION OF LOOP 2

The level diagrams below show that on both controllers; in most cases when the setpoint of loop 2 (r_2) is stepped, the performance error (e_2) decreases as the interaction error (e_1) increases, and vice versa. However, in some optimal designs the SISO controller and the MIMO controller can have virtually zero interaction error (e_1):

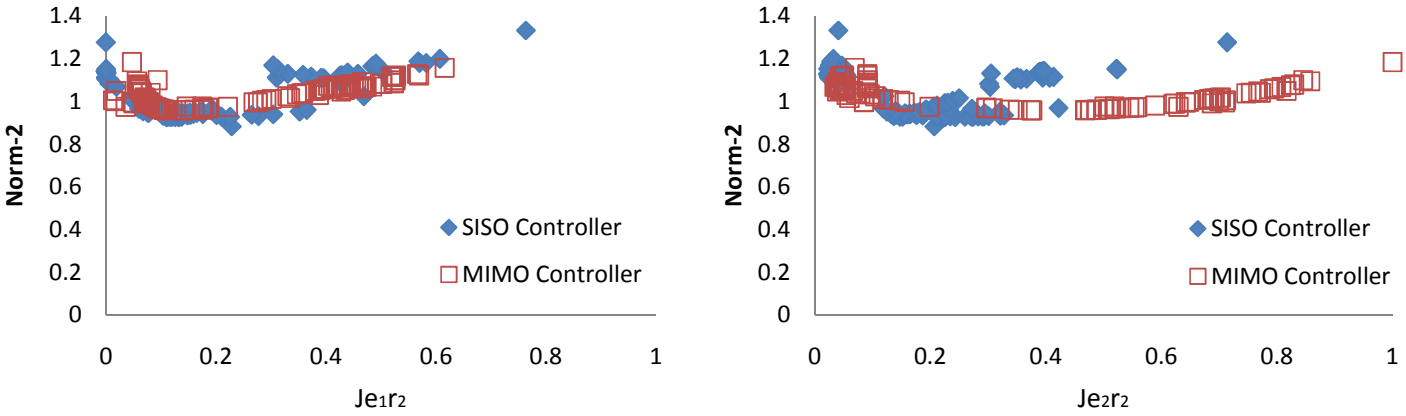

Fig 6.53 Level Diagrams of $J_{e_1r_2}$ and $J_{e_2r_2}$

University of Cape

6.1.4.2.1 DIGITAL SIMULATIONS OF THE SISO CONTROLLER

A series of points from the level diagrams of $J_{e_1r_2}$ and $J_{e_2r_2}$ are picked to plot the actual input u(t), output y(t) and error e(t) graphs of the system, in order to verify that the prediction of the two controllers from the level diagrams of $J_{e_1r_2}$ and $J_{e_2r_2}$ is correct.

The points picked from the level diagrams of $J_{e_1r_2}$ and $J_{e_2r_2}$ of the SISO controller are given in Table 6.7. Point 1 is the one with the smallest value of the cost function $J_{e_1r_2}$, point 2 is a random point sitting between Point 1 and Point 3, and point 3 is the one with the highest value of the cost function $J_{e_1r_2}$.

Table 6.7 The Three Points Picked from the SISO Controller of the Level Diagrams of $J_{e_1r_2}$ and $J_{e_2r_2}$

Point	Parameters	Cost Functions
1 of SISO	k_{11}= -4.494 ; k_{22}= -1.211 I_{11}= 0.100 ; I_{22}= 3.278	$J_{e_1r_2}$= 1.451E-04 ; $J_{e_2r_2}$= 0.714
2 of SISO	k_{11}= -0.100 ; k_{22}= -0.100 I_{11}= 0.237 ; I_{22}= 0.100	$J_{e_1r_2}$= 0.469 ; $J_{e_2r_2}$= 0.121
3 of SISO	k_{11}= -0.100 ; k_{22}= -2.375 I_{11}= 0.244 ; I_{22}= 0.100	$J_{e_1r_2}$= 0.764 ; $J_{e_2r_2}$= 0.041

Fig 6.54 show where the three points are sitting on the level diagrams of $J_{e_1r_2}$ and $J_{e_2r_2}$:

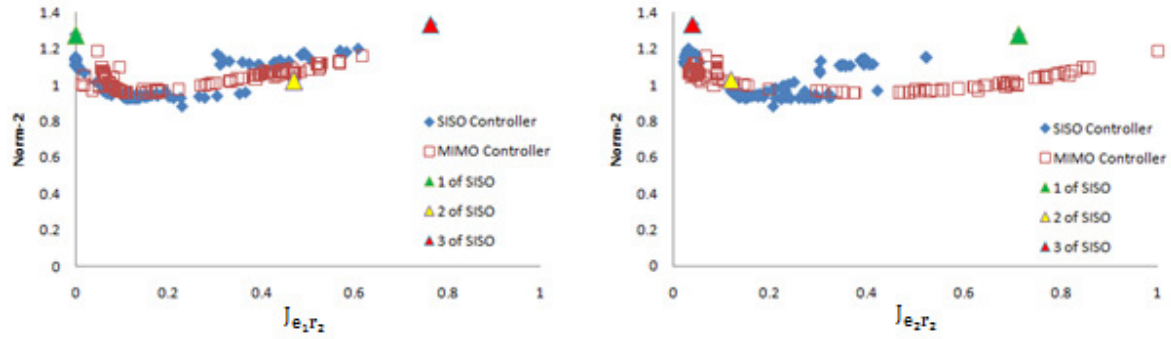

Fig 6.54 The Three Chosen Points and the Level Diagrams of $J_{e_1r_2}$ vs. $J_{e_2r_2}$

The digital simulations of the input u(t), the output y(t) and the error e(t) graphs of the system are plotted below and the data used to plot the above mentioned graphs are give in file Number 13 of Appendix A. The time plots show the response of the system to start-up at t = - 50 [s], a step in r_1 at the t = 0 and a step in r_2 at t = 400. The three cases in each plot are for the Point 1, Point 2 and Point 3 optimal designs as indicated on the graph in Fig 6.54.

In Fig 6.54, Fig 6.55 and Fig 6.56, by looking at all three points of the SISO controller it is easy to tell that when the setpoint of loop 2 (r_2) is stepped the performance error (e_2) decrease as the interaction error (e_1) increases:

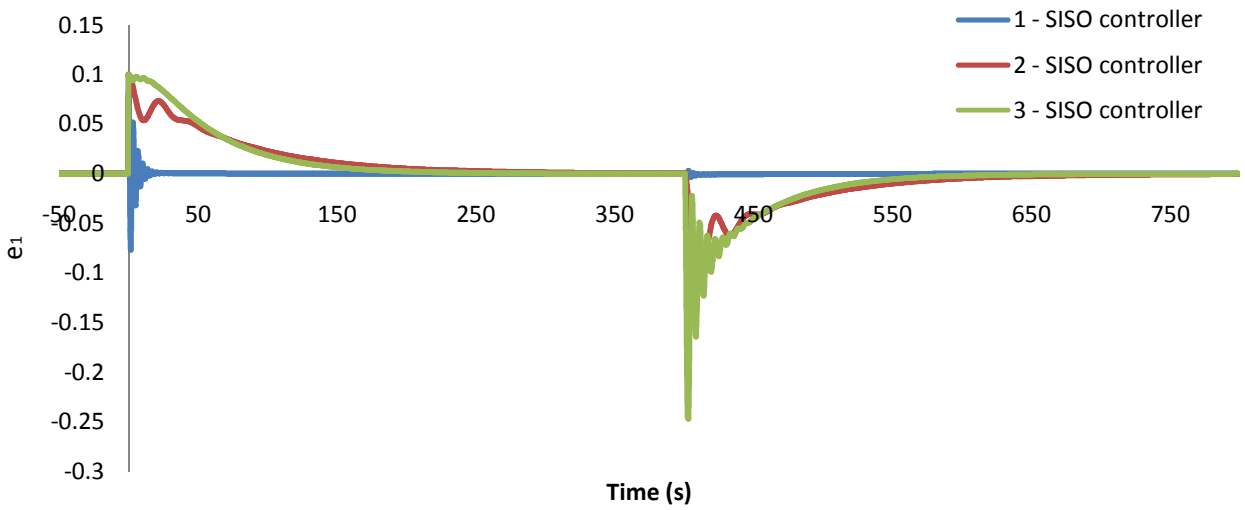

Fig 6.55 Error e_1 vs. Time plot of the SISO controller

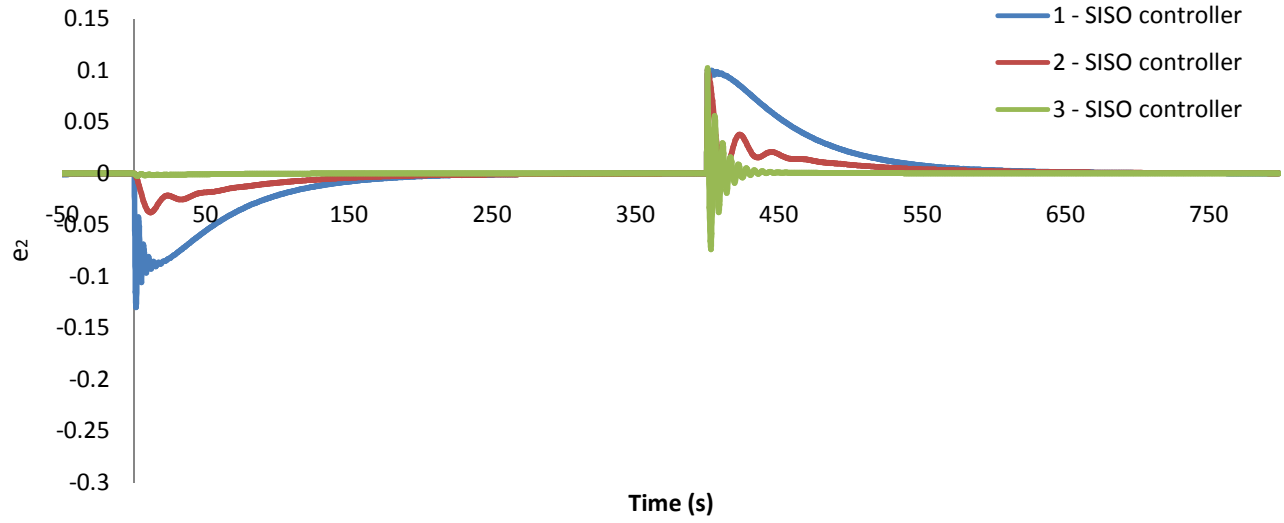

Fig 6.56 Error e_2 vs. Time plot of the SISO controller

Fig 6.54, Fig 6.57 and Fig 6.58 show that the amount of input used by all three different points of the SISO controller are similar when the setpoint of loop 2 (r_2) is stepped:

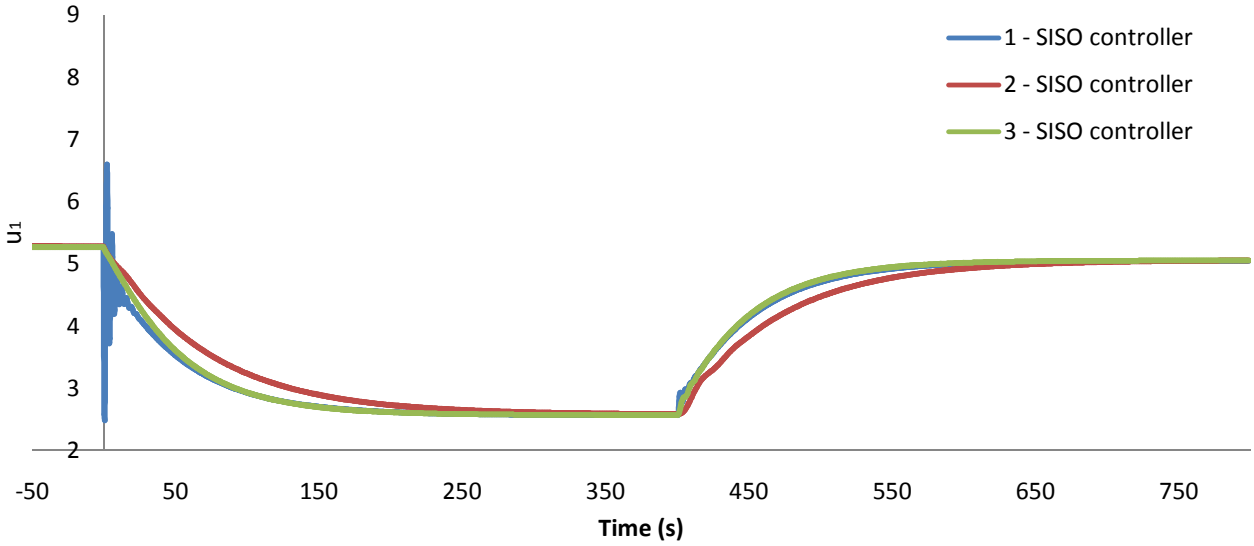

Fig 6.57 Input u_1 vs. Time plot of the SISO controller

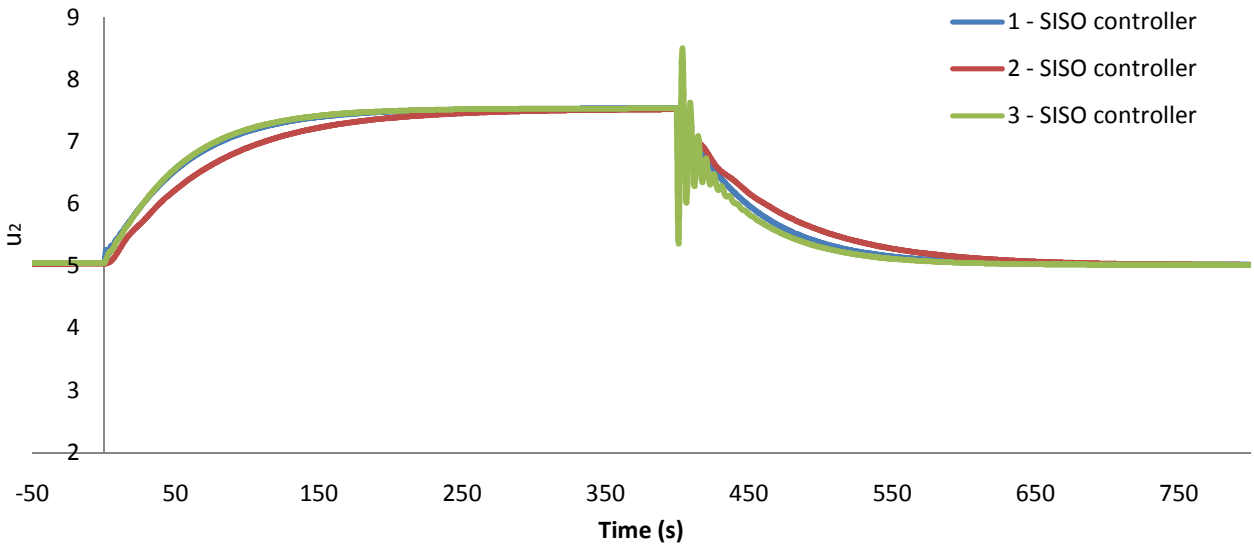

Fig 6.58 Input u_2 vs. Time plot of the SISO controller

Fig 6.54, Fig 6.59 and Fig 6.60, show that the prediction of the SISO controller from the level diagrams of $J_{e_1 r_2}$ and $J_{e_2 r_2}$ is correct once again, that when the setpoint of loop 2 (r_2) is stepped the performance error (e_2) decreases as the interaction error (e_1) increases:

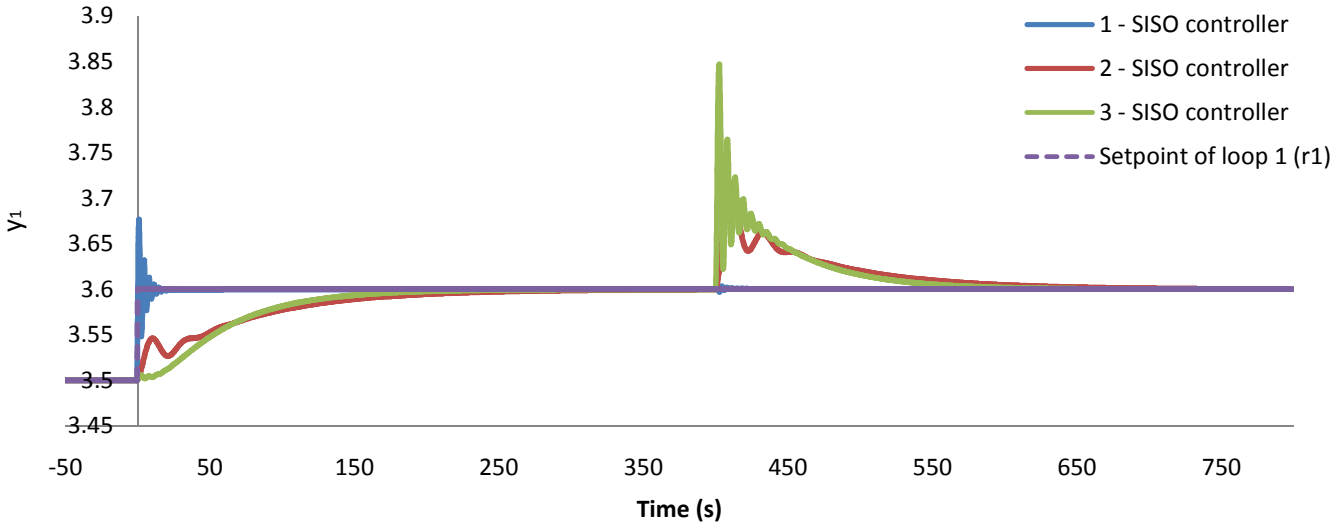

Fig 6.59 Output y_1 vs. Time plot of the SISO controller

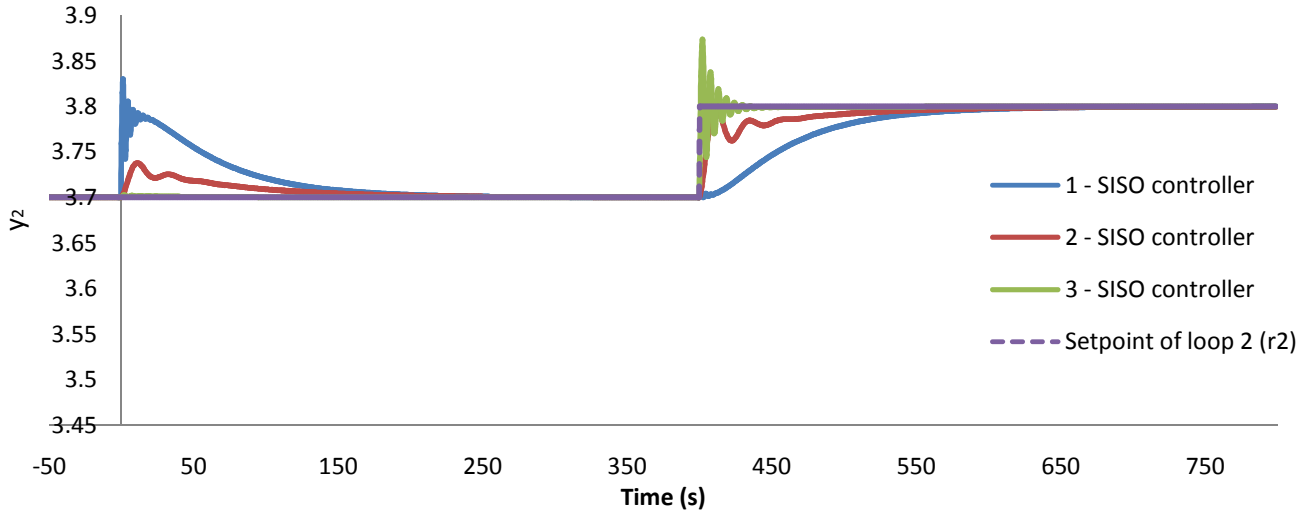

Fig 6.60 Output y_2 vs. Time plot of the SISO controller

6.1.4.2.2 DIGITAL SIMULATIONS OF THE MIMO CONTROLLER

The points picked from the level diagrams of $J_{e_1r_2}$ and $J_{e_2r_2}$ of the MIMO controller, where point 1 is the one with the smallest value of the cost function $J_{e_1r_2}$, point two is a random point sitting between Point 1 and Point 3, and point 3 is the one with the highest value of the cost function $J_{e_1r_2}$:

Table 6.8 The Three Points Picked from the MIMO Controller of the Level Diagrams of $J_{e_1r_2}$ and $J_{e_2r_2}$

Point	Parameters	Cost Functions
1 of MIMO	k_{11}= -0.100 ; k_{22}= -0.100 I_{11}= 0.100 ; I_{22}= 2.292	$J_{e_1r_2}$= 0.013 ; $J_{e_2r_2}$= 0.712
2 of MIMO	k_{11}= -3.429 ; k_{22}= -0.100 I_{11}= 3.120 ; I_{22}= 0.100	$J_{e_1r_2}$= 0.301 ; $J_{e_2r_2}$= 0.118
3 of MIMO	k_{11}= -0.100 ; k_{22}= -2.576 I_{11}= 0.100 ; I_{22}= 3.460	$J_{e_1r_2}$= 0.616 ; $J_{e_2r_2}$= 0.069

Fig 6.61 show where the three points are sitting on the level diagrams of $J_{e_1r_2}$ and $J_{e_2r_2}$:

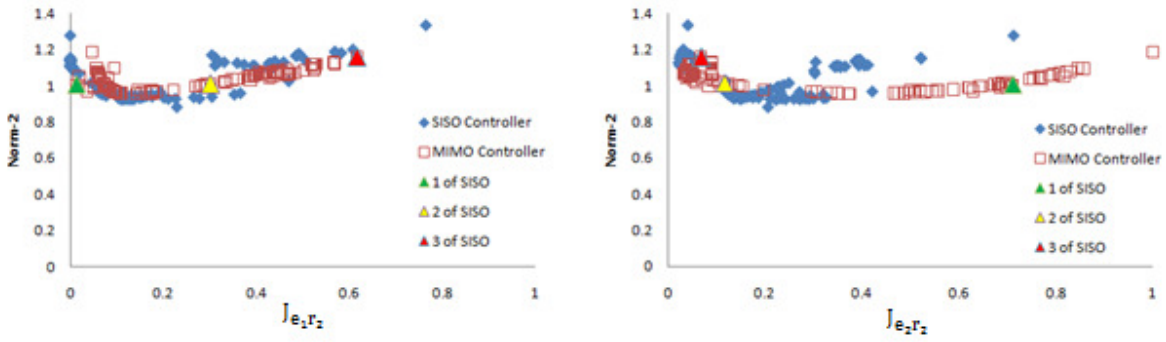

Fig 6.61 The Three Chosen Points and the Level Diagrams of $J_{e_1r_2}$ vs. $J_{e_2r_2}$

The digital simulations of the error e(t), the input u(t) and the output y(t) graphs of the system are plotted below and the data is used to plot the above mentioned graphs are given in Number 13 of Appendix A.

The time plots show the responses of the system to start-up at t = - 50 [s], a step in r_1 at the t = 0 and a step in r_2 at t = 400. The three cases in each plot are for the Point 1, Point 2 and Point 3 optimal designs as indicated on the graph in Fig 6.61.

Fig 6.62 and Fig 6.63 show that as the setpoint of loop 2 (r_1) is stepped, the interaction error (e_1) decreases as the performance error (e_2) increases. This corresponds to the prediction of the level diagrams of $J_{e_1 r_2}$ and $J_{e_2 r_2}$ in Fig 6.61:

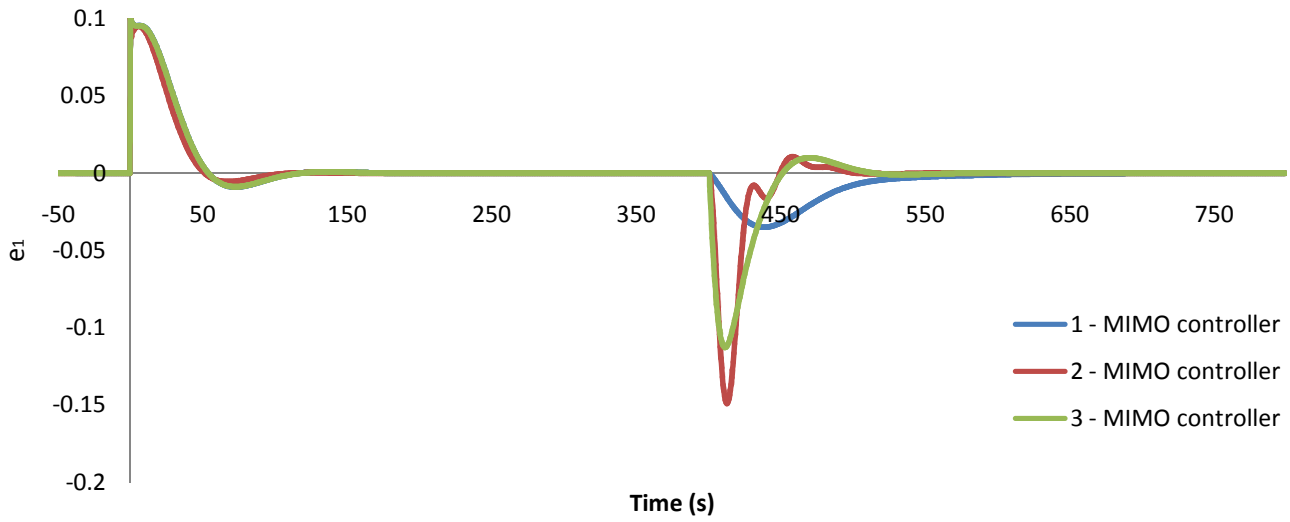

Fig 6.62 Error e_1 vs. Time plot of the MIMO controller

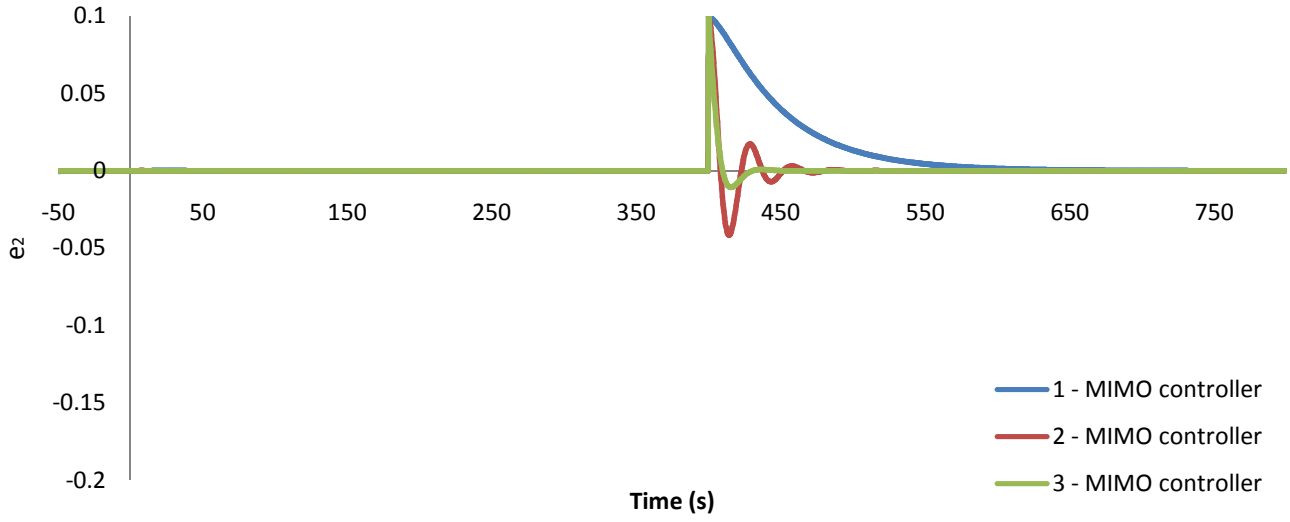

Fig 6.63 Error e_2 vs. Time plot of the MIMO controller

In Fig 6.61, Fig 6.64 and Fig 6.65, it shows that inputs are need on both tracking the setpoint of loop 2 and dealing with interaction of loop 1 (e_1):

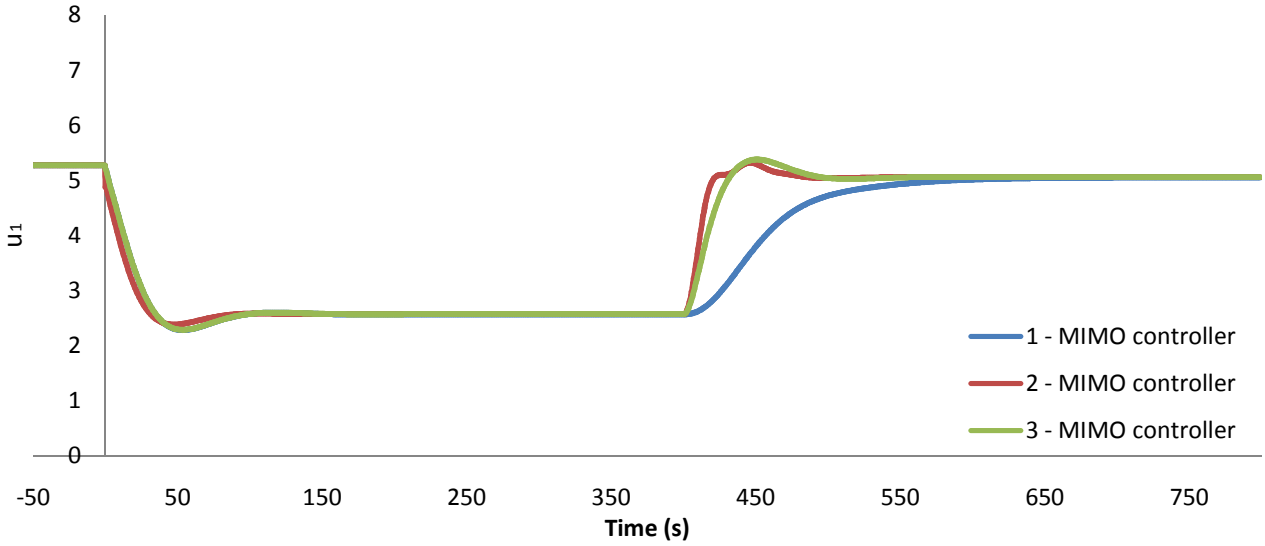

Fig 6.64 Input u_1 vs. Time plot of the MIMO controller

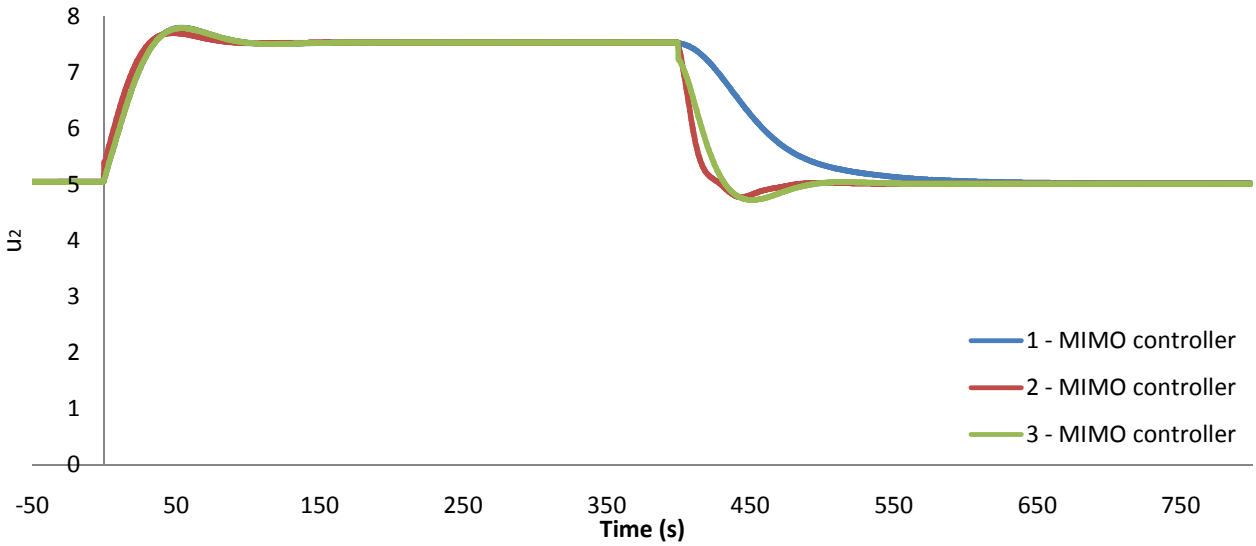

Fig 6.65 Input u_2 vs. Time plot of the MIMO controller

In Fig 6.61, Fig 6.66 and Fig 6.67 shows that as the setpoint of loop 2 (r_2) is stepped, the interaction error of loop 1 (e_1) increases as the performance error of loop 2 (e_2) decreases. This corresponds to the prediction of the level diagrams of $J_{e_1 r_2}$ and $J_{e_2 r_2}$:

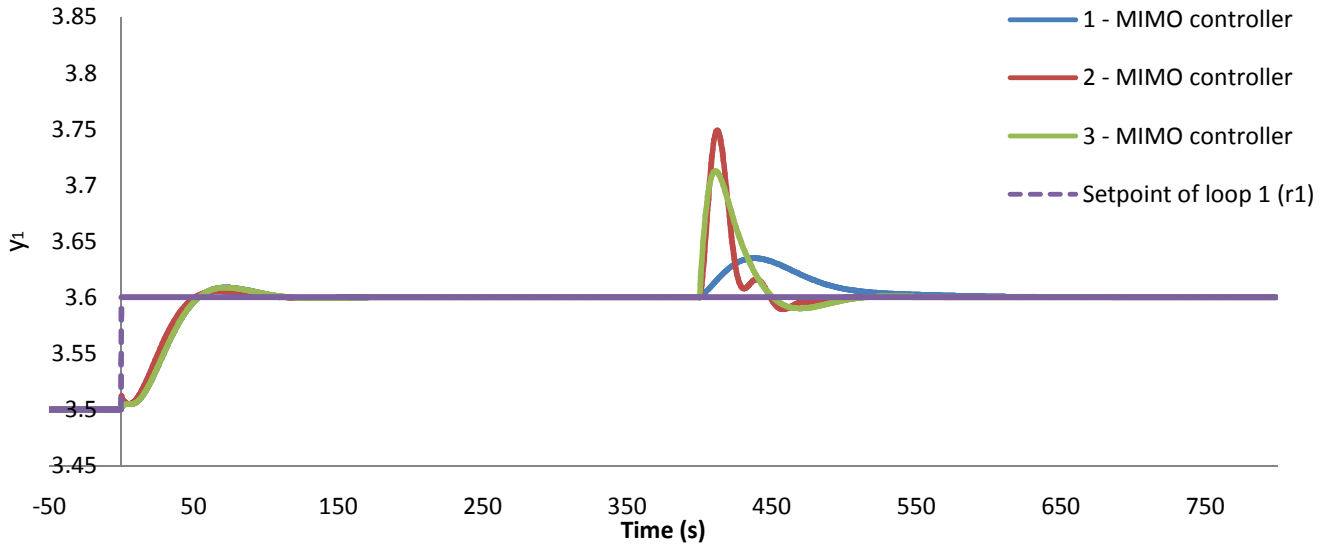

Fig 6.66 Output y_1 vs. Time plot of the MIMO controller

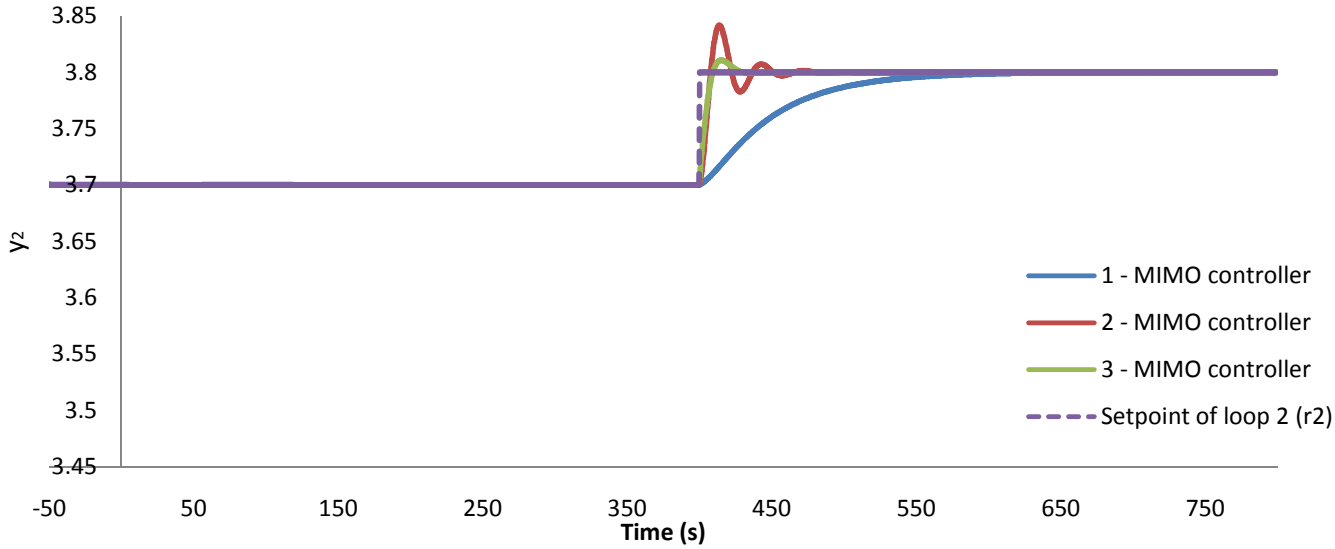

Fig 6.67 Output y_2 vs. Time plot of the MIMO controller

The digital simulations of the input u(t), the output y(t) and the error e(t) of the two controllers demonstrate that the prediction of the level diagrams of $J_{e_1 r_2}$ and $J_{e_2 r_2}$ is correct.

6.2 HYPER VOLUME

The level diagrams give the details of the behavior of each design of the two controllers, but it is time consuming to check every single design of the two controllers carefully. However, hyper volumes offer an alternative representation of the data and provide a quick indication of which controller has a better overall performance. The hyper volume results determine if the SISO system or the MIMO system performs better (in an a priori, global sense). It shows that MIMO systems dominate more space in the Region of Interest than SISO systems, where A is the SISO controller and B is the MIMO controller:

Table 6.9 Hyper Volume Results

	SISO Controller $I_H(A)$	MIMO Controller $I_H(B)$	$I_H(A \cup B)$
Hyper Volume	0.0750	0.2648	0.039

From Table 6.9, it is clear that the MIMO controller will have a better overall performance compared to the SISO controller (since it dominates a larger hyper volume). Although the hyper volume gives a quick look at which controller has a better overall performance, it doesn't give an indication of the individual features of the controller as captured in its cost functions.

University of Cape Town

6.3 CENTROID

The 6-Dimensional centroids of the coverage indices $I_{H2}(A,B)$ and $I_{H2}(B,A)$, where A is the Pareto front of the SISO system and B is that of the MIMO system. The centroid of the more interactive modified transfer function ($G_{mod}(s)$) and that of the less interactive original transfer function (G(s)) are shown in section 6.3.1 and section 6.3.2 respectively.

6.3.1 CENTROID OF THE MODIFIED TRANSFER FUNCTION ($\mathbf{G_{mod}(s)}$)

The six cost functions of the modified transfer function ($\mathbf{G_{mod}(s)}$) are computed and are shown in Table 6.10:

Table 6.10 Centroid Results of the Modified Transfer Function ($G_{mod}(s)$)

Cost Function	$I_{H2}(A,B)$	$I_{H2}(B,A)$	Cost Function (J) on Fig 6.68 and Fig 6.69
$J_{e_1r_1}$	4.101E-04	7.314E-04	1
$J_{e_2r_1}$	6.054E-04	4.753E-04	2
$J_{e_1r_2}$	5.900E-04	5.893E-04	3
$J_{e_2r_2}$	7.354E-04	1.004E-03	4
J_{ur_1}	4.696	2.920	5
J_{ur_2}	8.103	7.881	6

University of Cape Town

Since no controllers will be optimal in every situation, Fig 6.68 and Fig 6.69 quantify the strengths and weaknesses of the (Pareto) optimal SISO and MIMO control structures in terms of individual cost functions of the modified transfer function ($G_{mod}(s)$):

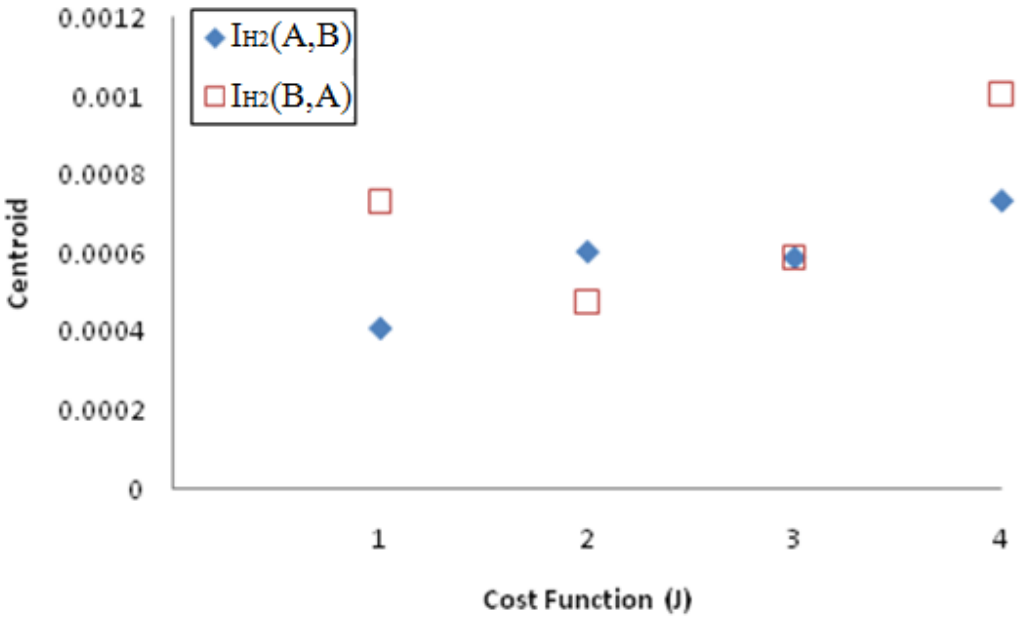

Fig 6.68 Centroid Plots for Tracking and Interaction of the Modified Transfer Function ($G_{mod}(s)$)

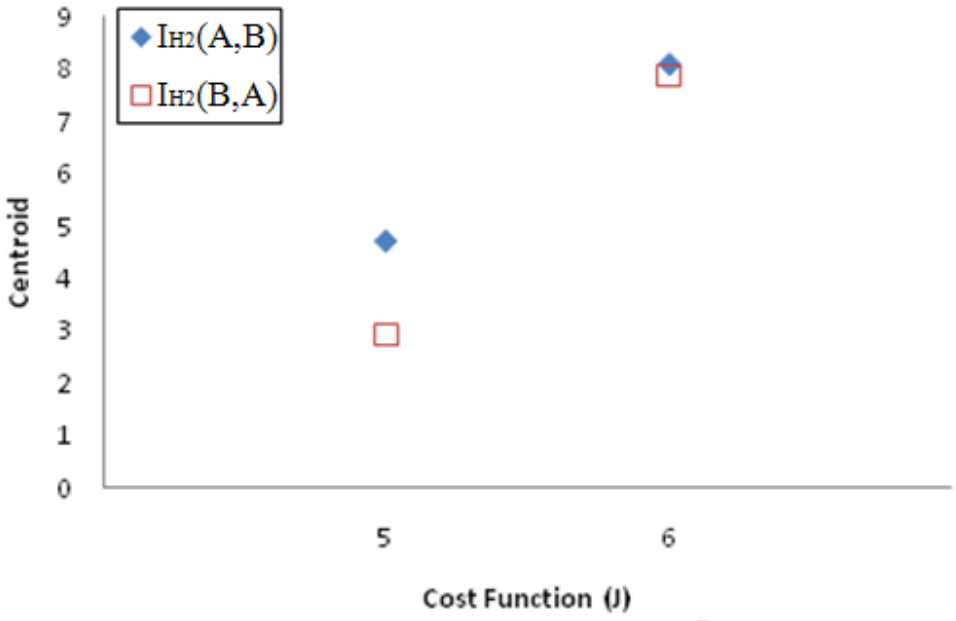

Fig 6.69 Centroid Plots for Input of the Modified Transfer Function ($G_{mod}(s)$)

From Fig 6.68 and Fig 6.69, it is clear that both controllers have similar cost functions for $J_{e_1r_2}$. The MIMO controller has better ability when dealing with the interaction error ($J_{e_2r_1}$), but the SISO controller is better at tracking the setpoint of loop 1 ($J_{e_1r_1}$) and loop 2 ($J_{e_2r_2}$). The MIMO controller requires less input on both loops (J_{ur_1} and J_{ur_2}) compared to the SISO controller.

6.3.2 CENTROID OF THE ORIGINAL TRANSFER FUNCTION (G(s))

The six cost functions of the original transfer function (G(s)) are computed and are shown in Table 6.11 below:

University of Cape

Table 6.11 Centroid Results of the Modified Transfer Function ($G_{mod}(s)$)

Cost Function	$I_{H2}(A,B)$	$I_{H2}(B,A)$	Cost Function (J) on Fig 6.68 and Fig 6.69
$J_{e_1r_1}$	7.391E-03	3.853E-03	1
$J_{e_2r_1}$	6.159E-03	5.913E-03	2
$J_{e_1r_2}$	1.004E-02	8.371E-03	3
$J_{e_2r_2}$	1.093E-02	8.628E-03	4
J_{ur_1}	6.371	1.048E+01	5
J_{ur_2}	6.359	7.210	6

Fig 6.70 and Fig 6.71 quantify the strengths and weaknesses of the (Pareto) optimal SISO and MIMO control structures in terms of individual cost functions of the Original Transfer Function (G(s)):

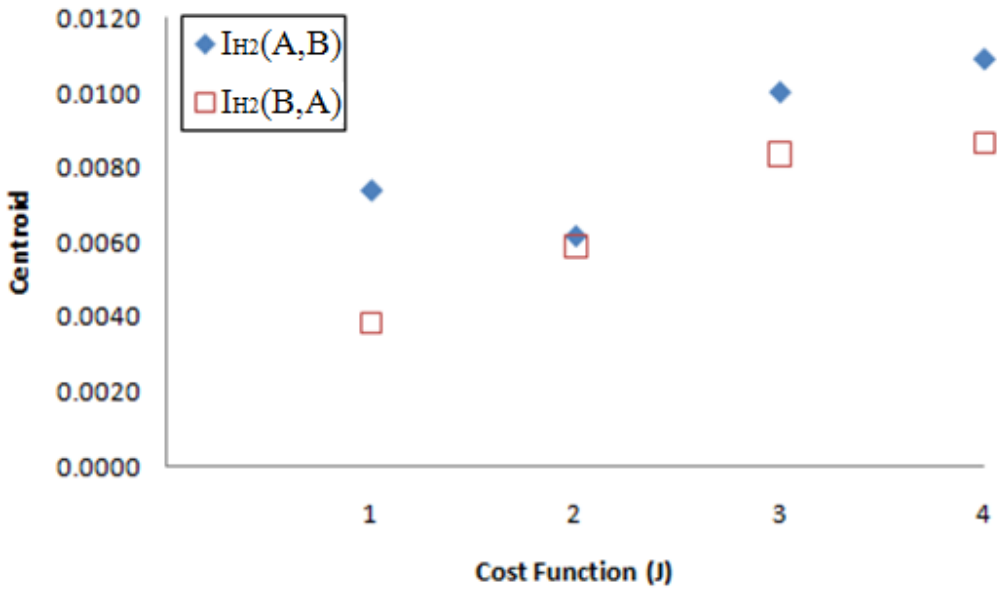

Fig 6.70 Centroid Plots for Tracking and Interaction of the Original Transfer Function (G(s))

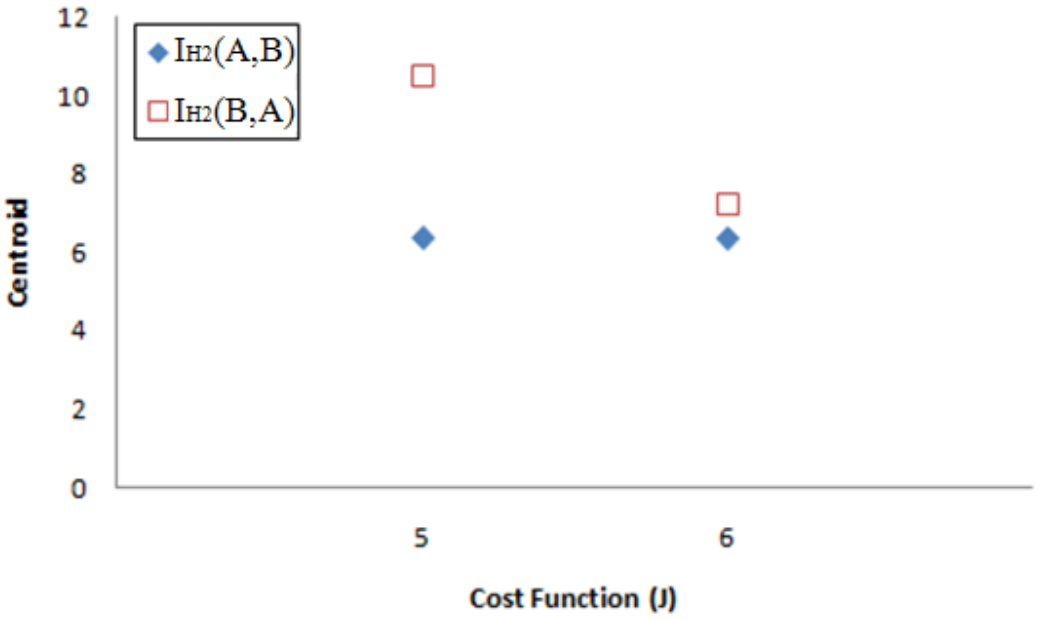

Fig 6.71 Centroid Plots for Input of the Original Transfer Function (G(s))

From Fig 6.70 and Fig 6.71, it is clear that the MIMO controller has the better ability when dealing with the interaction error and setpoint tracking, but the SISO controller requires less input on both loops (J_{ur_1} and J_{ur_2}).

From section 6.3.1 and section 6.3.2, the results of the centroid analysis show that MIMO controllers have a better ability to deal with interactions on both transfer functions (G(s) and $G_{mod}(s)$). This illustrates that Centroid has the ability to quantify the strengths and weaknesses of the (Pareto) optimal SISO and MIMO control structures in terms of individual cost functions.

University of Cape

Chapter 7
Conclusion and Recommendation for Future Works

This project explored the high-dimensional problem of determining the overall performance of one or more control systems. Techniques such as Pareto front, hyper volume, binary hyper volume and the concept of centroids of coverage indices based on binary hyper volumes with application to the SISO controller and the MIMO controller were used.

In high dimensional problems, hyper volume could be used to determine the overall performance of a controller easily, but in real engineering design there is no such thing as one design being the best in every situation. In order to have a better insight visualization of the performance of each individual feature of controller design; level diagrams, binary hyper volumes and the concept of centroids are needed..

University of Cape Town

7.1 CONCLUSION

Effective visualization for a posterior-decision-making in multi-objective optimization implies the ability to look at individual features of the design and is critical for producing effective engineering designs since it provides the engineer with invaluable insight into the problem and its proposed solutions. For high dimensional problems this becomes difficult and level diagrams are a means to visualize such spaces effectively.

Further enhancements of the Pareto efficient design methods through the concept of the centroid of coverage indices for two or more designs provide quantitative measures of the relative performance of these designs, within the region of interest and based on the chosen cost functions. This is illustrated here by their application to SISO and MIMO control structures.

From the analysis of hyper volume, it was seen that the overall performance of the MIMO controller is better than the SISO controller. However, level diagrams give a more detailed insight of the performance of each individual feature of the two controllers, and show that for certain features, the SISO controller performs better than the MIMO controller. Thus it was found that the MIMO controller is not performing better than the SISO controller in each individual feature.

Experience showed that the multiple plots of the level diagrams are difficult to read, so the concept of Centroid was proposed for use with binary hyper volumes. These centroids give similar details to those

obtained from the inspection of level diagrams, but in a way that is easier to understand. This led to an alternative graphical representation of a design that resembles parallel processing technique.

When applied to the fully interactive thermal process G mod (s), centroids showed clearly that the MIMO controller has a very good ability to minimize the interaction due to loop 2 (e_2) when the setpoint of loop 1 was stepped, which is what we would expect from a MIMO controller. Also, the MIMO controller required less input on both loops compared to the SISO controller, which not so obvious. On the other hand, the SISO controller has better setpoint tracking for both loops.

When applied to the diagonally dominant thermal process G(s), centroids shows that the MIMO controller has better setpoint tracking and can deal with interaction better compare to the SISO controller on both loops. However the MIMO controller also requires more inputs on both loops as might be expected.

Thus centroids were able to quantify the tradeoffs between the two controller structures in a way that was both simple and useful, especially when compared to the level diagrams.

7.2 RECOMMENDATION FOR FUTURE WORKS

The settling time for the closed loop system varies for different designs of controllers. Therefore, when simulating Pareto fronts in the future the fixed time simulations used in the current project should be replaced by a variable simulation time that takes settling time ($t_{\pm 2\%}$) into account. This would speed up simulations while ensuring that steady state is achieved for every simulation.

Furthermore, some designs had a very small value for their performance cost function, implying that they were optimal in terms of the chosen cost functions but on closer inspection it was found that their closed loops were very oscillatory. Therefore, a cost function which is related to a damping factor would be useful to eliminate such oscillatory designs.

The Centroid assumes that the binary hyper-volume generated by two Pareto fronts forms one cluster in the multi-dimensional space, but these binary hyper volumes may form two or more clusters in the space and require a different approach to that based on the assumption made here. Thus more investigations need to be done on the clustering of binary hyper volumes, in order to ensure that Centroid is suitable for use in such cases.

University of Cape Town

Appendix A: INDEX TO FILES ON CD

All the data for this project is contained in Microsoft Excel files on the CD. The list is:

Number	Filename	Description
1	Number 1.xlsx	Open loop step test of the thermal system.
2	Number 2.xlsx	Open loop step test of the thermal system and the simulation.
3	Number 3.xlsx	Close loop step and disturbance test of the thermal system and simulation.
4	Number 4.xlsx	Cost functions of the thermal system and the simulation.
5	Number 5.xlsx	Integrand cost functions of the thermal system and the simulation.
6	Number 6.xlsx	Change of the gains (A_{ij}) of the thermal system due to change in room temperature
7	Number 7.xlsx	Integrand cost functions of the thermal system and the simulation with different value of gains (A_{ij}).
8	Number 8.xlsx	Original level diagrams.
9	Number 9.xlsx	Normalized level diagrams.
10	Number 10.xlsx	Time plots of the max, mid and min points picked from the level diagrams.
11	Number 11.xlsx	Time plots of the three different point picked from the level diagrams of J_{ur_1} and J_{ur_2}.
12	Number 12.xlsx	Time plots of the three different point picked from the level diagrams of $J_{e_1r_1}$ and $J_{e_2r_1}$.
13	Number 13.xlsx	Time plots of the three different point picked from the level diagrams of $J_{e_1r_2}$ and $J_{e_2r_2}$.

University of Cape Town

Appendix B

It's essential to define a Region of Interest before finding the Pareto front, in this appendix an example of a six dimensional Pareto front of the SISO controller is simulated without defining the Region of Interest. Five hundred and ten designs of the SISO controller were simulated to produce the Pareto fronts used in this project.

In order to observe the behavior of the physical system, two points on the level diagrams of each controller are picked to plot the actual input u(t), output y(t) and error e(t) graphs of the system. The details of the two points picked from the level diagrams of the SISO controller are shown in Table B.1 below:

Table B.1 The Two Points Picked from the Level Diagrams of the SISO controller

Point	Norm-2	Parameters	Cost Functions
1 of SISO	13.436	k_{11}= -0.100 ; k_{22}= -0.100 I_{11}= 1.379 ; I_{22}= 1.602	$J_{e_1r_1}$= 4.642E-04 ; $J_{e_2r_1}$= 3.386E-04 $J_{e_1r_2}$= 0.002 ; $J_{e_2r_2}$= 0.003 J_{ur_1}= 13.405 ; J_{ur_2}= 0.909
2 of SISO	7.298	k_{11}= -4.259; k_{22}= -0.100 I_{11}= 0.324 ; I_{22}= 1.145	$J_{e_1r_1}$= 3.455E-05 ; $J_{e_2r_1}$= 0.004 $J_{e_1r_2}$= 2.536E-07 ; $J_{e_2r_2}$= 0.006 J_{ur_1}= 6.254 ; J_{ur_2}= 3.761

The actual input u(t), output y(t) and error e(t) graphs of the system are plotted below, it's clear that the error due to loop 1 (e_1) of point 2 haven't settled yet as shown in Fig B.1 below:

University of Cape Town

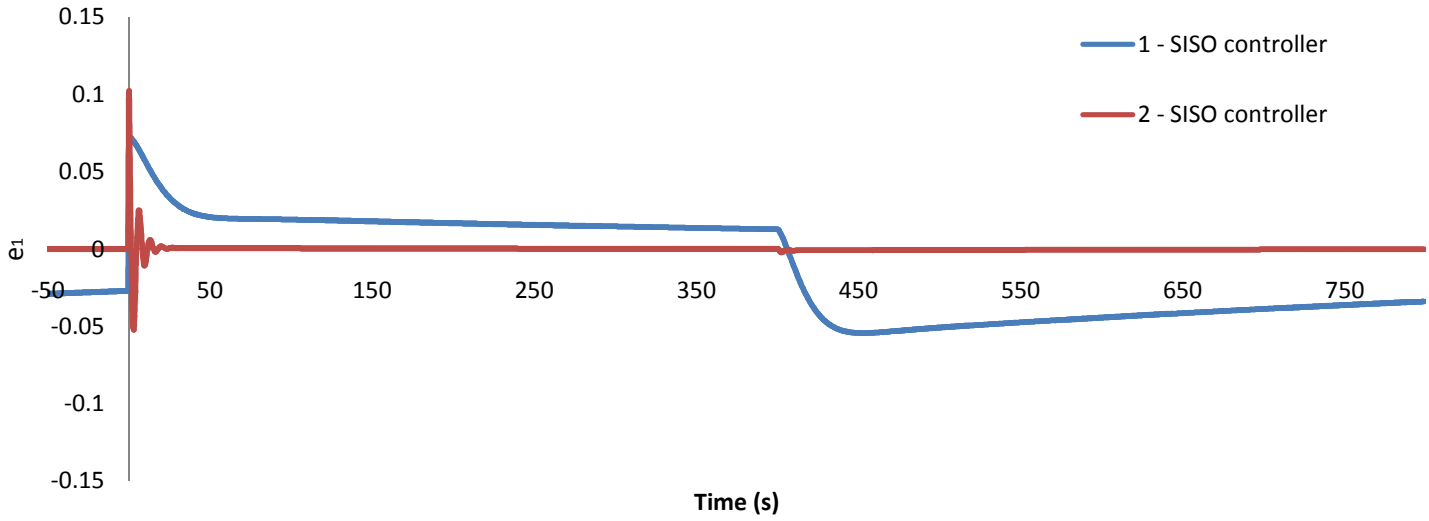

Fig B.1 e_1 vs. Time plot of the SISO controller

In Fig B.2, it's clear that the error due to loop 2 (e_2) of the two points haven't settled yet:

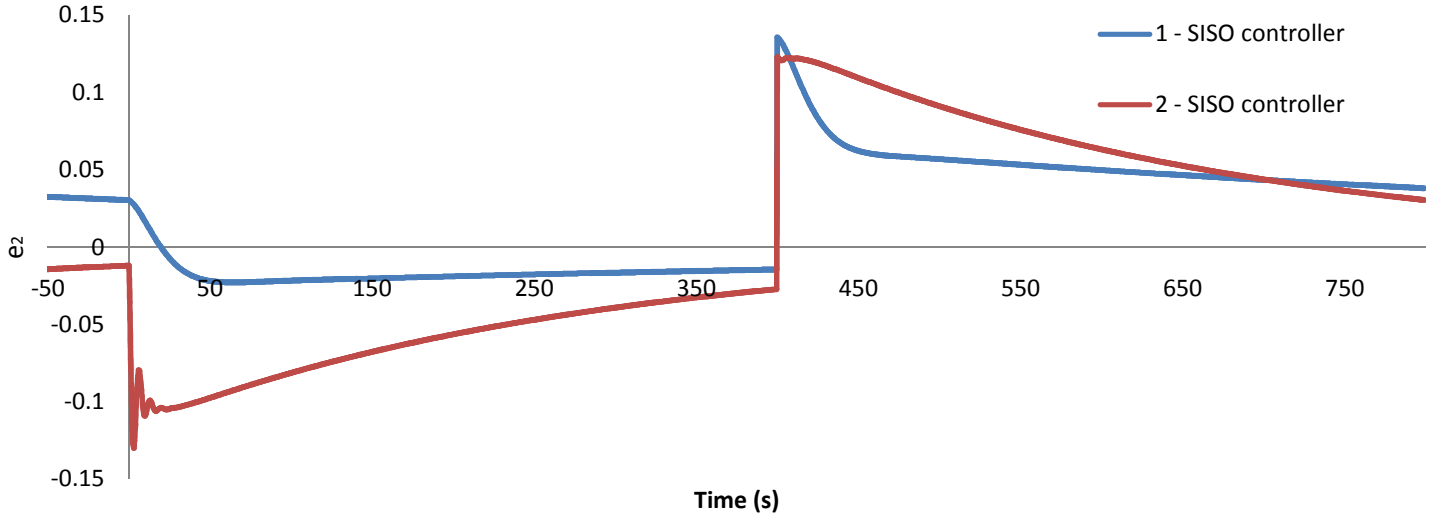

Fig B.2 e_2 vs. Time plot of the SISO controller

From Fig B.3 and Fig B.4, it's clear that the inputs of the two points didn't settle before the setpoints are step again.

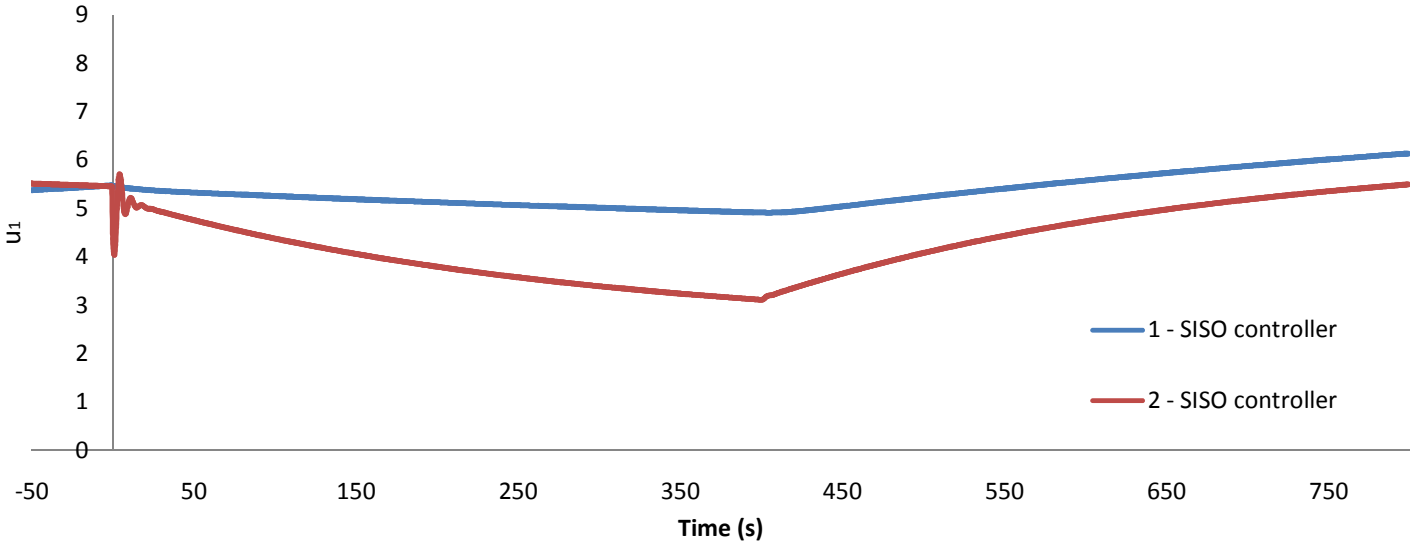

Fig B.3 u_1 vs. Time plot of the SISO controller

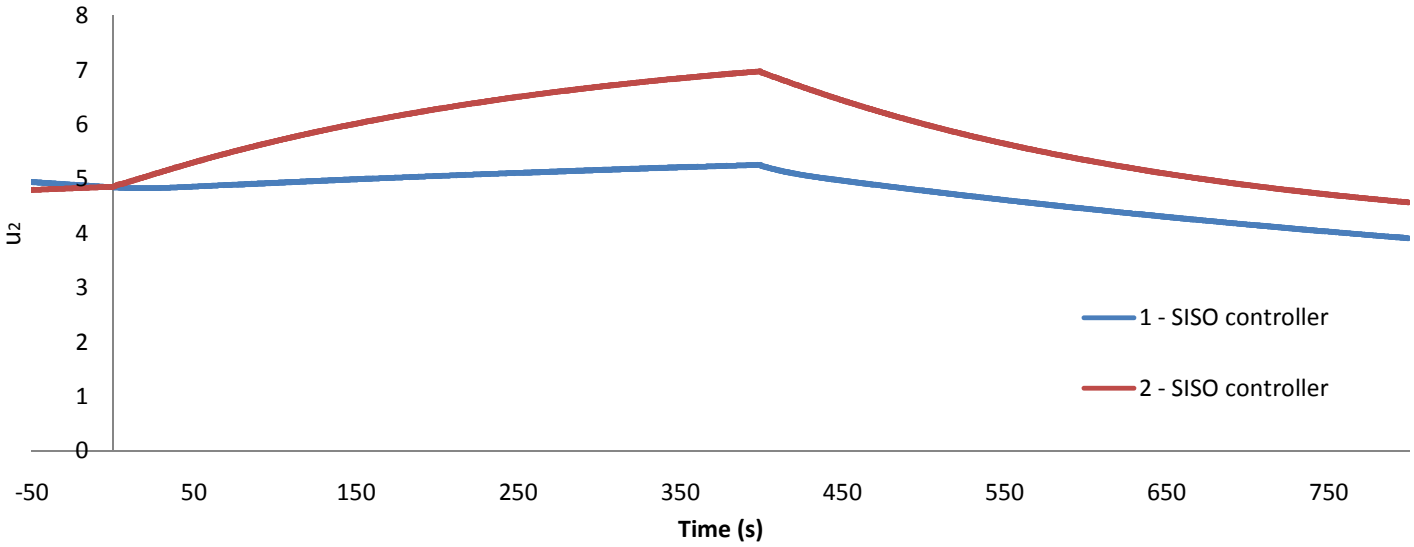

Fig B.4 u_2 vs. Time plot of the SISO controller

In Fig B.5, it's clear that point 2 hasn't settled yet:

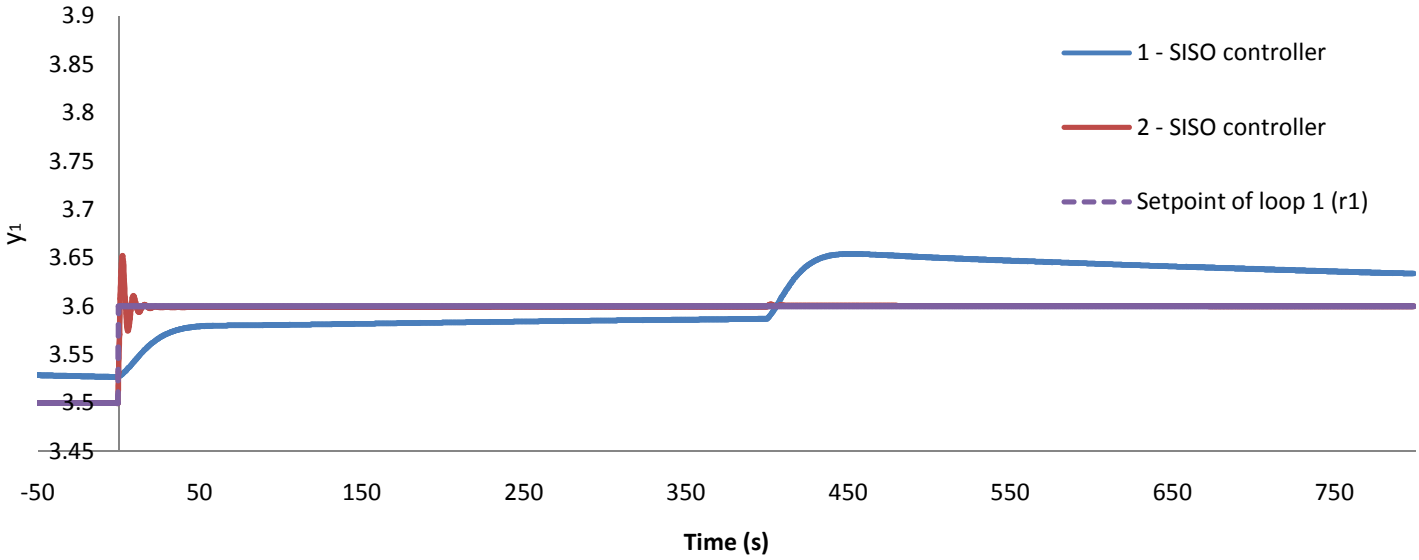

Fig B.5 y_1 vs. Time plot of the SISO controller

In Fig B.6, it's clear that both points haven't settled yet:

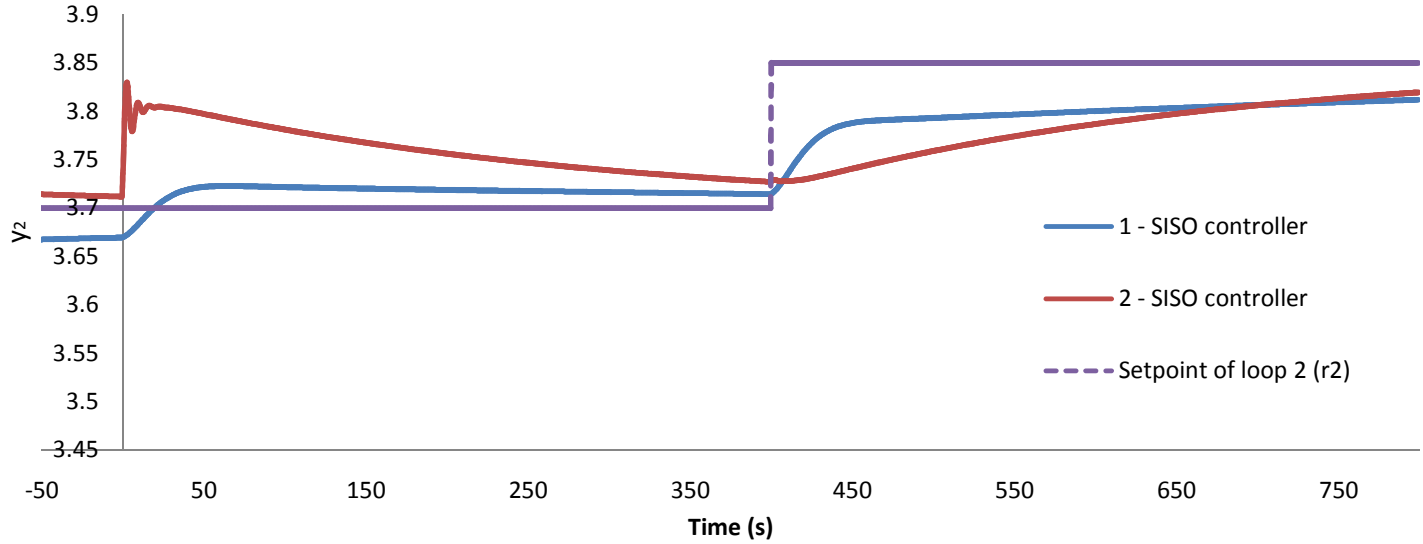

Fig B.6 y_2 vs. Time plot of the SISO controller

The above illustrate that it's important to define a Region of Interest, in order to exclude controller designs that have not settled within the given time interval.

Appendix C

The same experimental test problems are applied on the Pareto front simulation of this thesis, and the result are below in Fig C.1 and Fig C.2.

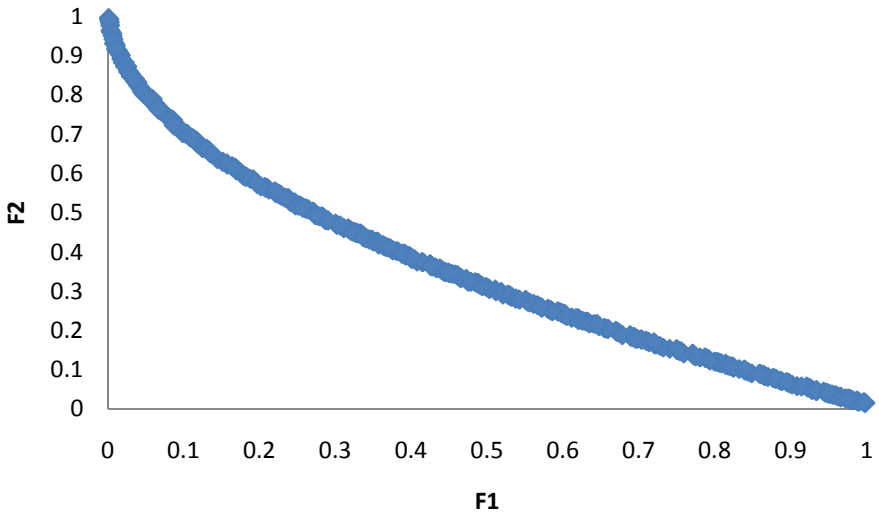

Fig C.1 Experimental Test Problem 1

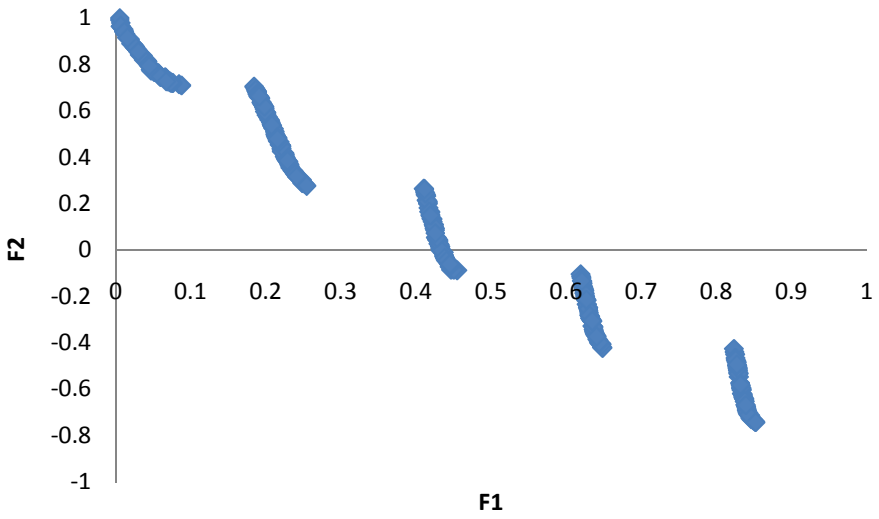

Fig C.2 Experimental Test Problem 2

The result of the two experimental test problems are the same as the one in [Abbass 2001], therefore it illustrated that the Pareto front simulation of this thesis do work correctly.

REFERENCES

Abbass,H.A. (2001), Sarker,R. and Newton,C., PDE: A Pareto–frontier Differential Evolution Approach for Multi-objective Optimization Problems, In Proceedings of the 2001 Congress on Evolutionary Computation, 2, IEEE Piscataway, NJ, USA. ISBN 0-7803-6657- 3, 971 – 978.

Africa,A (2006) and Braae,M. An advanced analogue display for virtual instrumentation. Elektron, p46-48, February.

Bader,J. (2008) and Zitzler,E, HypE: An algorithm for fast hypervolume-based manyobjective optimization. Tik report, 286.

Belanger, P.R. (1995), Control Engineering: A Modern Approach, Saunders College Publishing.

Blasco,X. (2008), Herrero,J. M., Sanchis,J. and Marnez,M., A new graphical visualization of n-dimensional pareto front for decision-making in multiobjective optimization. Information Sciences: an International Journal, 178:3908-3924, October.

Braae,M. (1994a), Design of Multivariable Systems, Course Notes, DeptElec.Eng, U.C.T, Rondebosch.

Braae,M. (1994b) Control Theory for Electrical Engineers, UCT Press, Rondebosch.

Brockho,D. (2007), Zitzler,E. and Thiele,L., The Hypervolume Indicator Revisited: On the Design of Pareto-compliant Indicators Via Weighted Integration. In S. Obayashi et al., editors, Conference on Evolutionary Multi-Criterion Optimization (EMO 2007), volume 4403 of LNCS, pages 862–876, Berlin, Springer.

University of Cape Town

Emmerich,M. (2005), Beume,N. and Naujoks,B., An EMO Algorithm Using the Hypervolume Measure as Selection Criterion, In Springer-Verlag Berlin Heidelberg 2005, C. A. Coello Coello et al. (Eds.): EMO 2005, LNCS 3410, pp. 62–76.

Fleming,P.J. (1998) and Fonseca,C.M., Multiobjective Optimization and Multiple Constraint Handling with Evolutionary Algorithms–Part II: Application Example, In Systems, Man and Cybernetics, Part A: Systems and Humans, IEEE Transactions.

Gambier,A. (2008), MPC and PID control based on Multi-Objective Optimization. In American Control Conference, 2008, pages 4727 – 4732.

Graebe,S. (1994), Robust and Adaptive Control of an Unknown Plant: A Benchmark of New Format, Automatica, 30(4):567-575.

Hamane,H. (2010), Matuki,K., Hiroki,F. and Miyazaki,K., Thermal MIMO Controller for Setpoint Regulation and Load Disturbance Rejection. Department of Mechanical Systems Engineering, Kogakuin University, Japan.

Ibrahim.D. (2006), Microcontroller Based Applied Digital Control. John Wiley & Sons, Ltd.

Lee,K.H. (2010), Tamayo,E.C., Huang,B., Industrial Implementation of Controller Performance Analysis Technology. The Department of Chemical and Materials Engineering, University of Alberta, Edmonton, Alberta, Canada T6G 2G6

Liu,G. P. (2002), Yang, J. B. and Whildborne,J. F., Multiobjective Optimization and Control. Research Studies Press LTD.

Maciejowski, J.M. (1989), Multivariable Feedback Design, Addison – Wesley, Wokingham.

University of Cape Town

Moore,D. (2010). Optimal Controller Comparison using Pareto Fronts. MSc. University of Cape Town.

Olsson,D.M. (1975) and Nelson,L.S., The Nelder-Mead Simplex Procedure for Function Minimization, Technometrics, VOL. 17, NO. 1, February.

Purshouse,R.C. (2007) and Fleming,P.J., On the Evolutionary Optimization of Many Conflicting Objectives, IEEE Transaction on Evolutionary Computation, Vol. 11, No. 6.

Rapson.M. (2007), Pareto Analysis of Controller Design Methodologies for Integrator plus Dead Time Processes. EUROCON 2007 The International Conference on "Computer as a Tool", Warsaw, September 9-12.

Rosenbrock,H.H. (1974), Computer – Aided Control System Design.

While,L. (2006), Hingston,P., Barone,L. and Huband,S., A faster algorithm for calculating hypervolume. IEEE Transactions on Evolutionary Computation, 10(1):29-38.

Zitzler,E. (1999), Evolutionary Algorithms for Multiobjective Optimization: Methods and Applications, PhD Thesis, Swiss Federal Institute of Technology Zurich.

Zitzler,E. (2003), Thiele,L., Laumanns,M., Fonseca,C. and da Fonseca,V. G., Performance Assessment of Multiobjective Optimizers: An Analysis and Review, IEEE Trans. Evol. Comput., 7:117 - 132, April.

University of Cape Town